

12

AD A116422

OFFICE OF NAVAL RESEARCH

Contract N00014-79C-0795

Project No. NR SRO-009/7-30-79 (472)

TECHNICAL REPORT NO. 1

CORROSION AND PASSIVATION STUDIES OF IRON
AND FERROUS ALLOYS

by

Gholamabbas Nazri, Ernest Yeager and B. D. Cahan

Prepared as part of the Ph.D. thesis of G. Nazri
in Chemistry at Case Western Reserve University
June, 1981

Case Center for Electrochemical Sciences
and The Chemistry Department
Case Western Reserve University
Cleveland, Ohio 44106

DTIC
SELECTE
JUL 6 1982

A

15 December 1981

DTIC FILE COPY

Reproduction in whole or in part is permitted for
any purpose of the United States Government

*This document has been approved for public release
and sale; its distribution is unlimited

REPORT DOCUMENTATION PAGE		READ INSTRUCTIONS BEFORE COMPLETING FORM
1. REPORT NUMBER 1	2. GOVT ACCESSION NO. ADA-116 422	3. RECIPIENT'S CATALOG NUMBER
4. TITLE (and Subtitle) Corrosion and Passivation Studies of Iron and Ferrous Alloys		5. TYPE OF REPORT & PERIOD COVERED Technical Report #1
		6. PERFORMING ORG. REPORT NUMBER
7. AUTHOR(s) Gholamabbas Nazri, E. Yeager and B. D. Cahan		8. CONTRACT OR GRANT NUMBER(s) N00014-79C-0795
9. PERFORMING ORGANIZATION NAME AND ADDRESS Case Center for Electrochemical Sciences Case Western Reserve University Cleveland, OH 44106		10. PROGRAM ELEMENT, PROJECT, TASK AREA & WORK UNIT NUMBERS NR SRO-009/7-30-79 (472)
11. CONTROLLING OFFICE NAME AND ADDRESS Office of Naval Research Chemistry Program - Chemistry Code 472 Arlington, Virginia 22217		12. REPORT DATE 15 December 1981
		13. NUMBER OF PAGES 133
14. MONITORING AGENCY NAME & ADDRESS (if different from Controlling Office) 1		15. SECURITY CLASS. (of this report) Unclassified
		15a. DECLASSIFICATION/DOWNGRADING SCHEDULE
16. DISTRIBUTION STATEMENT (of this Report) This document has been approved for public release and sale; its distribution is unlimited.		
17. DISTRIBUTION STATEMENT (of the abstract entered in Block 20 if different from Report)		
18. SUPPLEMENTARY NOTES		
19. KEY WORDS (Continue on reverse side if necessary and identify by block number) passivation, iron, ferrous alloys, corrosion, electrochemical interfaces, electron microscopy, Raman		
20. ABSTRACT (Continue on reverse side if necessary and identify by block number) Corrosion and passivation of iron and ferrous alloys is an important subject in many disciplines from both theoretical and practical points of view. Corrosion and particularly passivation, however, is poorly understood despite extreme efforts. The purpose of this work is to understand the mechanism of passivation film formation and reduction, also the structure of passive film. The <u>in-situ</u> electrochemical techniques such as combined cyclic voltammetry and rotating ring disk electrode have been used in different pH of borate. (over)		

DD FORM 1473
1 JAN 73EDITION OF 1 NOV 65 IS OBSOLETE
S/N 0102-LF-014-6601

Unclassified

SECURITY CLASSIFICATION OF THIS PAGE (When Data Entered)

20.

buffer solution. Both cyclic voltammetry and potential pulse techniques showed that during passive film formation, the ferrous ions enter into the metal solution interface, which causes a formation of a deposited over-layer on surface of the passive film. Most of the problems during passivation studies in the past are related to the existence of this deposited over-layer which serves as the traps for water molecules and also anions. In this respect, a structural model for passive film with deposited over-layer is developed.

▽ In-situ Raman spectroscopy has been used to elucidate the structure of the passive film on iron. The Raman spectra of this film showed several peaks at low frequency (200-800 cm^{-1}) which is not the same as any known stoichiometric iron oxides or oxy-hydroxides. In addition, Raman spectroscopy for air oxidized iron-chromium alloys also has been used. The result showed that this technique can be used to study the dry corrosion as well as wet corrosion.

Transmission electron microscopy of the passive film on iron showed that the passive film on iron has crystalline structure and also there are some epitaxial relationships between oxide and iron substrate. In addition, the thickness of passive films on each crystallographic plane is not the same. In this regard, a structural model for passive film on poly-crystalline iron is developed. The composition of passive film in this condition is believed to be $\gamma\text{-Fe}_2\text{O}_3$ with a compact mosaic type structure.

Accession For	
NTIS GRAM	<input checked="" type="checkbox"/>
ERIC TAB	<input type="checkbox"/>
U.S. GOVERNMENT	<input type="checkbox"/>
OFFICE OF	<input type="checkbox"/>
TECHNICAL SERVICES	<input type="checkbox"/>
Dist	SP

DTIC
COPY
INSPECTED
2

A

TABLE OF CONTENTS

	page
REPORT DOCUMENTATION PAGE	ii
TABLE OF CONTENTS	iv
LIST OF FIGURES	vii
LIST OF TABLES	x
CHAPTER I	1
I. Introduction	1
II. Background	3
1. Film Theory	4
2. Adsorption Theory	5
A. Structure and Composition of Passive Film on Iron and Ferrous Alloys	6
B. The Structure of the Passive Film on Ferrous Alloys	20
REFERENCES	24
CHAPTER II THE FORMATION AND REDUCTION OF PASSIVE FILM IN ALKALINE AND ACID SOLUTION	31
I. Introduction	31
II. Experimental Procedures	32
A. Reagents	32
B. Electrode and Cell Design	33
C. Instruments	35
III. Results	37
IV. Discussion	58
V. Conclusion	63
REFERENCES	66

	page
CHAPTER III IN-SITU LASER RAMAN SPECTROSCOPY OF ANODIC PASSIVE FILM ON IRON AND AIR OXIDIZED IRON AND IRON-CHROMIUM ALLOYS	68
I. Introduction	68
II. Theory of Surface Raman Spectroscopy	69
III. Experimental Procedures	70
A. Reagents	70
B. Electrode and Cell Design	70
C. Alignment	73
IV. Results and Discussion	76
1. The Raman Spectrum of Borate Buffer Solution (pH 8.4)	76
2. Raman Spectrum of the Cathodically Protected Iron Surface	76
3. Raman Spectrum of the Passivated Iron Electrode	78
4. Raman Spectrum After Reduction of the Passive Layer	78
V. Conclusion	86
Raman Spectroscopy of Air Oxidized Fe and Fe-Cr Alloys	91
REFERENCES	100
CHAPTER IV ELECTRON DIFFRACTION STUDIES OF PASSIVE FILM ON IRON AND IRON-CHROMIUM ALLOYS	101
I. Introduction	101
II. Experimental	102
III. Results	105
REFERENCES	122

	page
CHAPTER V. RESULTS AND DISCUSSION	123
1. Dissolution and Passivation of Iron	123
2. <u>In-Situ</u> Raman Spectroscopy of Passive Film	125
3. Electron Microscopy of the Passive Film on Iron	125
DISTRIBUTION LIST	134

LIST OF FIGURES

CHAPTER I	page
Fig. I-1. Typical anodic assivation curve of iron and iron-chromium alloys	4
Fig. I-2. Possible arrangement of combination of two dioxy or di-hydroxy chain species to form a tetramer	17
Fig. I-3. Structure of passive film according to Okamoto	18
CHAPTER II	
Fig. II-1. Rotating disk-ring electrode	34
Fig. II-2. Schematic diagram of the electrochemical cell	36
Fig. II-3. Anodic voltammogram of iron electrode in borate buffer	38
Fig. II-4. Voltammetry curve of iron electrode in borate buffer	39
Fig. II-5. Voltammetry of gold electrode in borate buffer	40
Fig. II-6. Current potential curve of iron electrode in borate	42
Fig. II-7. Current potential curve of the iron electrode in borate buffer	43
Fig. II-8. The cyclic voltammetry of iron electrode in borate buffer	45
Fig. II-9. RRDE measurement of iron electrode in borate buffer solution using potential step techniques	46
Fig. II-9a. Passivation and reduction of iron electrode by potential pulse technique	47
Fig. II-9b. Cathodic reduction of the passivated iron after passivation in borate buffer (pH 8.4) at different potentials for 2 min.	48

	page
Fig. II-10. Reduction curves of the passivated iron electrode at different rotation rates	50
Fig. II-11. Reduction of the passivated iron disk electrode in borate buifer (pH 8.4) under force convection	52
Fig. II-12. Window opening experiment of the iron electrode in borate buffer	56
Fig. II-13. Passivation and reduction of iron disk in the presence of EDTA in borate buffer (pH 8.4)	57
Fig. II-14. Structural model for a passive film and deposited overlayer	65
 CHAPTER III	
Fig. III-1. Optical electrochemical cell and its attachment for <u>in-situ</u> laser Raman spectroscopy	72
Fig. III-2. Beam path in Spex Ramalog spectrometer	74
Fig. III-3. Raman spectrum of borate buffer (pH 8.4)	77
Fig. III-4. Raman spectra of passive film formed on iron in borate buffer	79
Fig. III-4a. Raman spectroscopy (<u>in-situ</u>) of passive film on pure iron in borate buffer	80
Fig. III-5. Raman signal of deposited ferris oxyhydroxy	82
Fig. III-6. Raman signal of $\alpha\text{-Fe}_2\text{O}_3$	83
Fig. III-7. Raman signal of Fe_3O_4	85
Fig. III-8. Raman signal of 1-10 orthophenanthroline in borate buffer (pH 8.4) without iron ion present	87
Fig. III-9. Raman signal of 1-10 orthophenanthroline in borate buffer (pH 8.4) in the presence of 10^{-4}FeSO_4	88

	page
Fig. III-10. Variation of the Raman band (2751) intensity of the 1-10 orthopenanthroline at iron-solution interface due to the electrode potential change from -0.4 V up to 0.1 V	89
Fig. III-11. Raman signal of air oxidized Fe-0.5 Cr % at 500°C for 1 hour	94
Fig. III-12. Raman signal of the air oxidized Fe-1% Cr at 500°C in air	95
Fig. III-13. Raman signal of air oxidized Fe-2% Cr at 500°C	96
Fig. III-14. Raman signal of air oxidized Fe-8% Cr at 500°C (1 hour)	97
Fig. III-15. Raman signal of air oxidized Fe-11.6% Cr at 500°C (1 hour)	98
Fig. III-16. Raman Signal of air oxidized Fe-24% Cr at 500°C (1 hour)	99
CHAPTER IV	
Fig. IV-1. Schematic of jet polishing apparatus	103

LIST OF TABLES

	page
Table III-1. Comparison of Raman frequencies (cm^{-1}) of passivation film <u>in-situ</u> formed at 1.0 V vs. RHE in borate buffer (pH 8.4) and film formed on air oxidized iron-chromium alloys at 500°C (1 hour) with published data for iron oxides and oxy-hydroxides.	84
Table III-2. Composition of iron-chromium alloys	92

CHAPTER I

I. INTRODUCTION

The corrosion of ferrous metals is a very substantial problem on a global bases. The annual cost for corrosion and its prevention in the U.S.A. alone has been estimated to be \$70 billions.¹ Corrosion and corrosion control have been studied for more than three centuries, still there is not a good understanding of corrosion science, particularly passivation, localized corrosion, stress cracking corrosion and fatigue corrosion. For each of these phenomena there are many ambiguities and fallacies. In this regard Marcel Pourbaix noted:²

"Corrosion was often considered as a calamity, a necessary evil, an unavoidable to which we had to submit, without being able to control or even understand it."

Of most importance in controlling corrosion is the phenomenon of passivity. Already in the day of Michael Faraday³ it was recognized that the formation of a film was involved, believed by most workers to be an oxide blocking the surface.

Passivation is an extraordinarily important phenomena because it prevents or minimizes corrosion without the need to apply a protective coating such as a paint, galvanizing or electrodeposited layer. Passivation, however, is poorly understood despite very extreme efforts. Part of the problem is that the study of this phenomenon requires background from many disciplines including inorganic and surface chemistry, metallurgy and solid state physics.

The objective of this study has been the development of better understanding of passivation, particularly of iron and ferrous alloys. The emphasis has been on the following aspects of passivity:

- 1) Structural and electrochemical formation of the passivation film.
- 2) Mechanism for formation of the passive film.
- 3) Reduction of the film.

Most of the work has been directed to pure iron and a few iron-chromium alloys in neutral and acid electrolytes. The formation and reduction of the film have been studied by linear sweep voltammetry, pulse techniques and rotating disk-ring electrode techniques. The studies of the passivity layer on iron have also been complemented with studies of the Fe/Fe(II) and Fe(II)/Fe(III) couples on gold and platinum electrodes. Effects of complexing agents such as ethylenediamine tetraacetic acid (EDTA) and 1-10 ortho phenanthrolyne have also been investigated.

The structural properties of the passive film and air oxidized iron-chromium alloys have been studied by in-situ Raman.

Transmission electron microscopy has been used to investigate the structure of passive films at different potentials. Selected area diffraction patterns have been obtained to examine the crystallinity and possible epitaxy. Finally models for dissolution-deposition of iron and passive film have been developed.

II. BACKGROUND

The passivity of metals was first established by M.N. Lomonosov in 1739.⁴ Many other scientists have reported on the existence of passivity.⁵⁻¹² However, Michael Faraday³ was the first to give a proper definition of passivity. He observed the passivity as a phenomenon of iron in concentrated nitric acid and interpreted due to an oxide film which was formed during passivation and said:

"My strong impression is that the sample is oxidized..."

Many definitions have been given for passivity.¹³⁻¹⁷ Passivation of both a chemical and electrochemical type can be defined as the inhibition of the corrosion of metals or alloys in certain potential regions by the formation of a film even though active corrosion would be expected on the basis of thermodynamics.

Typical anodic passivation of metals and alloys can be represented as is shown in Fig. I-1.

In spite of extensive efforts in the study of passivation phenomenon the mechanism of formation and the structure of passive film are still not fully understood. Various in situ techniques such as electrochemical measurements,¹⁷⁻²² Mössbauer,²³⁻²⁵ infrared,²⁶ electroreflectance spectroscopy,^{27,28} ellipsometry,²⁹⁻³⁴ and radio-tracer methods^{35,36} have been used to investigate the structure of passive film. In addition various ex situ techniques such as x-ray and electron diffraction,^{38,39} scanning and transmission electron

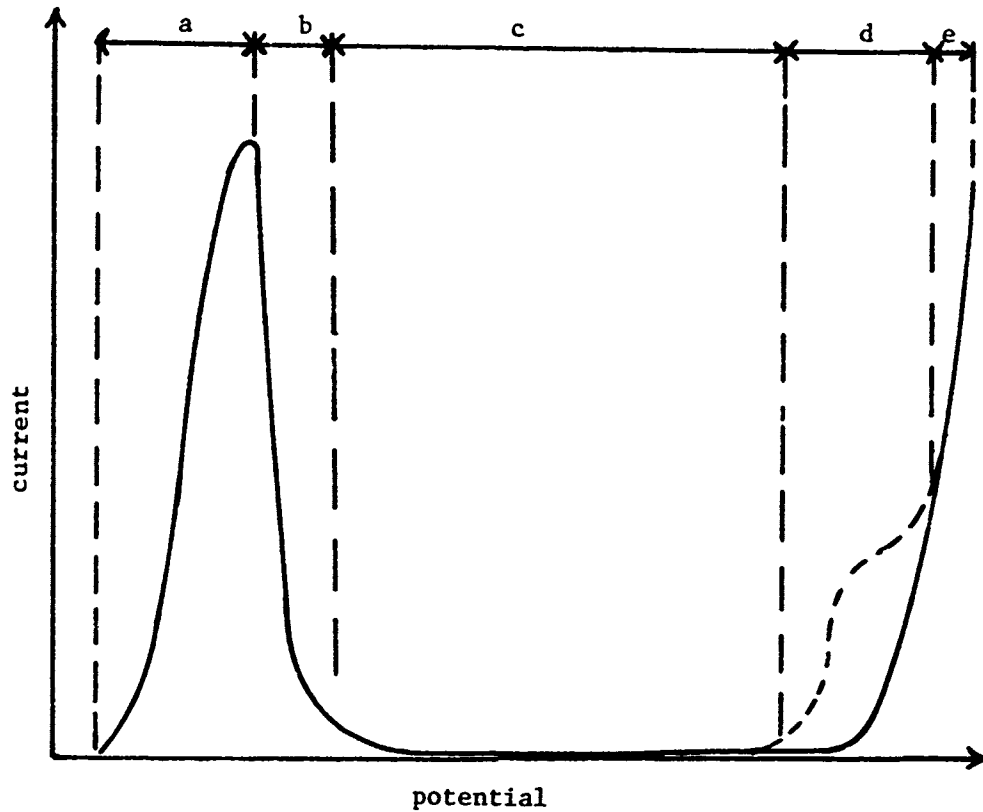


Fig. I-1. Typical anodic passivation curve of iron(—) and iron-chromium alloys. a - active region, b - prepassive region, c - passivation region, d - transpassive region (secondary passivation region -----), e - transpassive region.

microscopy,⁴⁰⁻⁴⁶ electron spectroscopy (i.e., ESCA, AES),⁴⁷⁻⁵³ ion spectroscopy (SIMS, ISS)^{54,55} and glow discharge⁵⁶ have also been used to examine the structure of passive films.

Two well defined theories for passive film formation have been developed:

1) - The Film Theory:

The majority of electrochemists support, in one form or another,

the film theory of passivity. According to this theory a very thin (10-100 Å) invisible film covers the surface of the metals and protects the surface. Many in situ¹⁷⁻³⁶ and ex situ³⁷⁻⁵⁶ experiments have proved the existence of such a film on the surface during passivation.

The structure of this film is highly controversial. On the basis of thermodynamic arguments and experimental studies, some workers have indicated that the passive film on iron is a sandwich-like structure such as Fe/Fe₃O₄/Fe₂O₃,⁵⁷⁻⁶⁵ where the magnetic oxide Fe₃O₄ is interposed between the iron and an outer layer of Fe₂O₃. On the other hand evidence for a single isotropic oxide layer has been reported by other scientists for iron under the same passivation conditions. In both cases it is believed that film has a highly defective and nonstoichiometric structure.⁶⁶⁻⁶⁹ The crystallinity of the passive film is also open to question. Various workers have obtained evidence that the film is amorphous on Fe-Cr alloys at high Cr concentrations but also believe the film, even on pure iron, to be amorphous.

2) - Adsorption Theory:

The adsorption theory has been developed by Frumkin,⁷⁰ Kabanov,⁷¹ Kolotyркин⁷² and Uhlig.⁷³⁻⁷⁶ In this theory it is believed that adsorption of a monolayer of oxygen or oxygen containing species is responsible for passivity. The active surface sites such as edges, kinks, steps and corners preferentially bond with the adsorbed oxygen species. It is believed that the coverage of these

active sites is sufficient to protect the metal from dissolution.⁷⁷⁻⁷⁹

Kolotyrkin⁷² and Kabanov⁷¹ propose that adsorbed oxygen atoms on the surface of the metal together with the metal atoms form dipoles due to partial ionization of the atoms (metal-atom dipoles) with the positive end of these dipoles on the metal and the negative end in the solution. This changes the potential distribution across the interface in such a way as to reduce the potential difference during the kinetics of dissolution and causes pronounced inhibition of the dissolution.

In the early phases of the oxide film on metal such as iron, the adsorption of oxygen or oxygen containing species are believed to play an important role. The adsorbed layer is the first step in the formation of a thicker oxide layer. Therefore oxide film and adsorption theories do not contradict but rather supplement each other in overall perspective.

The weight of the evidence is that for metals such as iron, ferrous alloys and nickel, the passivation involves an oxide film with a thickness substantially greater than that of an oxygen monolayer (typically 10 to 100 Å thick).⁷⁷⁻⁸¹

A. Structure and Composition of Passive Film on Iron and Ferrous

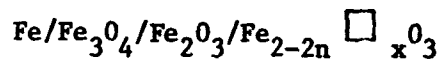
Alloys:

The structure of the passive film has been studied extensively by various techniques but still there is significant disagreement between experimental results. The main problem in the study of

passive film is related to its very small thickness. Usually in situ experiments for passivation studies give indirect information which is influenced by a variety of other phenomena; therefore their interpretation is not always certain. On the other hand, ex situ experimental results are also questionable due to the probability of degradation and dehydration of the film and valency changes of ions in the film during the ex situ measurements.

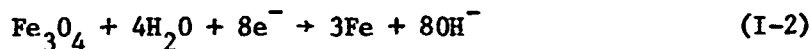
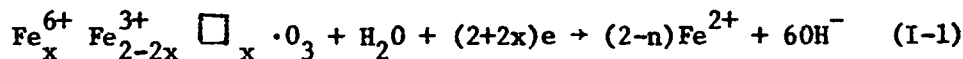
In recent years complementary techniques have been used together to collect simultaneously several types of data needed to gain insight into the structure of the films.⁸¹⁻⁸³ In this regard we shall illustrate some of the milestone experiments which have been carried out over the past two decades.

Nagayama and Cohen^{84,85} have studied the structure of passive film on iron by cathodic reduction and electron diffraction techniques. The cathodic reduction process for the passivated iron in borate buffer solution (pH = 8.4) shows three arrests or two waves. The inflection points for these arrests appear at -550, -920 and -1000 mV vs. SCE respectively. The change from the first wave to the second wave becomes more clear as the potential and time of passivation increase. Based upon this observation Nagayama and Cohen postulated the following sandwich layer for the passive film:



where n and x are integers and potential dependent and \square represents a lattice vacancy. The following equations are also given for the

arrests:



The first step (I-1) corresponds to the reduction of ferric oxide to ferrous, which is believed to dissolve into the solution. The second step in the reduction process corresponds to the reduction of Fe_3O_4 , the only oxide present at the potential of the second step. At the third step, H_2 evolution occurs simultaneously with the iron deposition. Furthermore when the passive layer forms in the presence of ferrous ion, the outer layer is reported to be FeOOH with some inclusion of borate of the buffer in the film.

The potentiodynamic reduction of passive film (cathodic potential sweep) has been carried out by Ogura and Sato.⁸⁶ They found two reduction peaks around -0.55 and -1.02 V vs. SCE at pH = 9 in phosphate-borate buffer. They observed that the first peak in the voltammetry curve is almost independent of the potential scan rate, whereas the second peak is very sensitive to the potential scan rate. Furthermore the potential of the first peak is extremely pH sensitive, but the potential of the second peak is almost independent of pH. The results are interpreted on the basis that the first peak during cathodic reduction is a charge transfer without diffusion being involved. However, reduction at the second peak is probably

controlled by diffusion. It is important to mention that the second peak is always associated with some degree of hydrogen evolution.

Chen et al.¹⁰⁴ studied the film formed on iron in borate buffer (pH 8.4) by ESCA. In the low potential region (0.35-0.65 V vs. RHE)* it is found that the thickness of the passive film is smaller than the escape depth of electrons without loss of energy. Therefore, the ESCA spectra showed a shoulder at 706.6 eV indicating a metal iron peak even when the surface had not been sputtered. For the passive film formed at more anodic potentials (1.05 and 1.35 V), however, the thickness of film becomes greater than the escape depth of the electrons, as is evidenced by the disappearance of the metal iron peak.

The $\text{Fe}2\text{P}_{3/2}$ peak of the passive film in the whole range of anodic potential was broad, which is interpreted as due to the existence of several valancy states of iron with the Fe(III) species predominant. The $0\text{ }1\text{s}$ spectrum showed two clear peaks around 530 eV for the surfaces passivated at low potential. The intensity of the peak at higher energy decreases as one goes to more anodic potentials. Chen et al. interpreted these results as evidence for two types of oxygen (OH^- and O^-) in the film. During their studies these researchers found that the amount of boron in the film strongly depended on the rinsing before transfer of the specimens from the electrochemical system to ESCA instrument.

Seo et al.⁸⁷ studied the passive film by Auger electron spec-

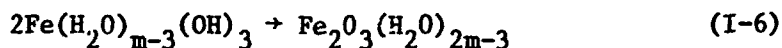
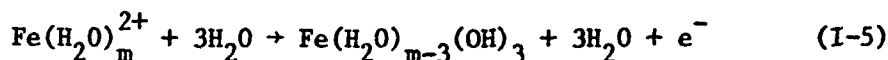
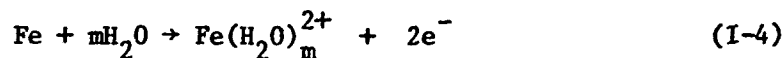
*The reversible hydrogen electrode.

troscopy (AES). Depth profiling by argon ion sputtering and measuring the peak heights ratio of O (510 eV) and Fe (703 eV) lines produce evidence in support of the sandwich model, with a nonstoichiometric oxide in each layer. The inner layer has an excess of iron and the outer layer an excess of oxygen. The MVV transition line indicated that the chemical state of iron in the film changes when one moves from the outer layer toward the metal/passive film interface. Argon ion sputtering, however, is known to change the chemical composition of the film and therefore this work by itself is not conclusive evidence for the sandwich model.

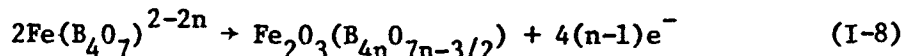
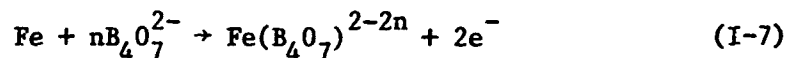
van Diepen et al.⁸⁸ studied the composition of passive films on iron powder by Mössbauer spectroscopy, x-ray diffraction and magnetization measurement. They found a concentration gradient of Fe^{2+} from the metal passive film interface toward the outer layer surface. van Diepen did his experiments with cylindrical iron particle with 400 Å average diameter produced by reduction of needle like $\alpha\text{-FeOOH}$. The passive film on such a sample conformed with the $\text{FeO}/\text{Fe}_3\text{O}_4/\gamma\text{-Fe}_2\text{O}_3$ model.

Using water containing tritium (H^*) for passivation, Yolken⁸⁹ found that there is H^* in the film with the amount dependent on the potential and thickness of passive film. The amount of H^* in the film decreased as the potential was increased to more anodic value. Yolken postulated the existence of H^* in the film as $\gamma\text{-FeOOH}$ and not as a bound H_2O molecule as Sato⁹⁰ and Nagayama⁹¹ had postulated.

K. Ogura⁹² studied the passive film on iron in borate buffer solution. He found boron in the passive film. This evidenced that $B_4O_7^{2-}$ participates in the passive film during its formation and growth, and he proposed the following reactions:



and



Seo et al.⁹³ also found boron in the film by using Auger electron spectroscopy (AES) but the concentration of B is small.

Chen et al.¹⁰⁴ also studied passive film formation and reduction by in situ automatic ellipsometry. During film formation at a given potential, they found that optical constant above a critical thickness (10-15 Å) remain constant. However, in earlier stages of growth ($t < 1$ s) a linear relation exists between thickness and the charged passed. The changes of the apparent complex refractive index ($\hat{n} = n + ik$) at this stage ($d < 10-15$ Å) were believed to be due to continuous changes in the growing film. These authors further indicated from their studies that the reduction of the passive film occurred in the following stages:

In the first stage involving 5 to 10% of the total charge required for complete reduction the effective thickness (d) remains constant, but n and k show changes. On the other hand, as the reduction proceeds further up to 1/3 of the total charge the film parameters including d (thickness) as well as n and k showed a drastic change. Finally, during the last 2/3 of the reduction process, the thickness changed linearly with respect to the charge, but the optical constant remained almost constant. This has been interpreted by Chen et al. as follows:

First stage: Reduction of Fe^{4+} to Fe^{3+} occurs accompanied by introduction of proton into the film or loss of oxygen. This interpretation is supported by rather constant thickness (d), while changes in n and k occur.

Second stage: The reduction of Fe^{3+} to Fe^{2+} with the oxygen is expected to occur when the concentration of Fe^{4+} has been decreased to a sufficiently low value. This process has been associated with the dissolution of Fe^{2+} into the solution until local saturation is reached.

Third stage: The interface of the ferrous outer layer and ferric inner layer moves toward the metal oxide interface. Formation and dissolution of Fe^{2+} probably start at the edge and spread out over the surface of the passive film. At the end of this stage, $Fe(OH)$ is believed to cover the entire surface.

Fourth stage: The reduction of Fe^{2+} to the metallic phase

starts and highly non-uniform iron dendrite-like growth may occur. However, there may still be ferric species in some parts of the film.

Fifth stage. The reduction of solution phase Fe^{2+} produced in earlier stages takes place.

Sixth stage: Continued reduction of Fe^{2+} to metallic phase takes place until the film is entirely reduced.

Seventh stage: Reduction of solution phase Fe^{2+} to Fe metallic and hydrogen discharge from the electrolyte occurs.

Chen et al. have examined the passive film in borate buffer with automatic ellipsometer and obtained the optical complex dielectric constant as a function of wave length. The spectra showed a peak in E_2 at 2.2 eV and a more pronounced broad peak at 3.6 eV.

On the basis of the Lorentz oscillator model (which has been used to analyze the spectrum of $\alpha\text{-Fe}_2\text{O}_3$) the authors predicted another optical transition at higher energies beyond the range of the experiments (> 3.6 eV). The existence of such transitions, e.g., $0\ 2p\text{-Fe}\ 4s$, have been predicted by Goodenough to occur at 5.5 eV or above. The minor peak at 2.2 eV was attributed to be a d-d transition and the peak at 3.6 eV to the charge transfer transition ($0\ 2p \rightarrow \text{Fe}\ 3d$). The broadening of the intense peak at 3.6 eV can be due to the defects and proton in the film.

Akimov studied the passivation of iron in different environments with electrochemical technique, x-ray electron spectroscopy (XPS) and automatic ellipsometry.^{94,95} Akimov during his ellipsometric studies found the formation of the passive film with a potential step to involve three stages. In the first stage ($t_0 \rightarrow t_1$), he proposed that islands of Fe_3O_4 form and that this process is fast. In the second stage the islands of Fe_3O_4 spread out following a logarithmic growth law, ($t_1 \rightarrow t_2$). The third stage involves the growth of the film under an inverse logarithmic law, based upon Hauffe-Ilschner⁹⁶ and Cabrera-Mott⁹⁷ model.

Akimov et al.¹⁷ studied the passivation of iron in neutral solution using XPS with layer-by-layer removed with argon ion sputtering. He concluded that the passive film is a two layer film such as Fe_3O_4/Fe_2O_3 . The chemical shift ΔE_b for the $Fe 2P_{3/2}$ peak decreased showing that the degree of oxidation of iron changes with depth in the passive film. In the outer layer ΔE_b was 4.2 eV which corresponds to Fe^{3+} ion or the Fe_2O_3 oxide on the surface. However, with sputtering away of the oxide, ΔE_b decreases to a typical value for FeO or Fe_3O_4 . The structure of passive film in this experiment is modeled as $[(FeO)_n \cdot (Fe_2O_3)_m]$ where $n > m$. Because of the question of partial reduction of the film during ion bombardment, Akimov measured the emission of electron, emitted at different angles with a variable angle spectrometer. He found that the decrease of ΔE_b for $Fe 2P_{3/2}$ is real and is due to the structure of passive film. Furthermore, Akimov claimed that the complex refractive index \hat{n} measured with an automatic ellip-

someter correspond to the $[(\text{FeO})_n \cdot (\text{Fe}_2\text{O}_3)_m]$. The XPS data also support this model. On the basis of the ellipsometer measurements, Akimov concluded that with a rapid change in potential (i.e., a potential step), the change in n and m lags behind the potential. Therefore a nonuniform defective multilayer oxide film is formed and its refractive index changes with each layer.

Ebiko et al.⁹⁸ studied the structure of the passive film on iron in various solutions using ex situ infrared and ex situ Mössbauer spectroscopy. While he obtained the infrared reflectance spectra, these spectra do not show any peak structure and were not particularly useful. The Mössbauer spectroscopy of the anodic passive film were run at room temperature and showed 12 clear peaks (6 peaks for Fe and 6 peaks for oxide film). In this experiment the back scattering mode was used. The peaks for passive film were relatively broad. In contrast the film formed on iron in concentrated nitric acid showed sharp Mössbauer peaks. Ebiko et al. concluded that the film is close to $\tau\text{-Fe}_2\text{O}_3$.

Recently, O'Grady⁹⁹ studied the Mössbauer spectroscopy of electrodeposited iron passivated in borate buffer (pH 8.4) both in situ and ex situ. In these experiments the in situ Mössbauer spectrum of passive film did not match with any known stoichiometric iron oxides or hydroxides. It was close to $\alpha\text{-FeOOH}$ and $\delta\text{-FeOOH}$. The differences with these two oxide-hydroxides were that $\alpha\text{-FeOOH}$ does not have quadrupole splitting and the quadrupole splitting of $\delta\text{-FeOOH}$ is not the

same as for the passive film on iron. The isomer shift (0.70 mm/sec) and quadrupole splitting (1.02 mm/sec) of the passive film were found to be in the range of octahedral high spin ferric iron oxide. Furthermore, the isomer shift and quadrupole splitting for the passive film is more characteristic of the amorphous oxide with Fe octahedrally coordinated to 6 O's with different local bonding. O'Grady proposed that the passive film is amorphous and polymeric in nature consisting of FeO_6 octahedrons in a chain-like structure with di-oxy and di-hydroxy bridging bonds. These chains are supposed to be linked with each other by water molecules. O'Grady found that the Mössbauer spectrum of the dried passive film was not the same as for wet passive film. During drying chemically bound water is believed to be lost. The important point in this experiment is that the dehydration of the passive film is a reversible process if the passive film is not dried for longer than five hours. During the dehydration process two water molecules from each iron are removed. Because of the reversible process of hydration-dehydration it is assumed that the structure of passive film is like a hydrolized iron sol with four octahedrally coordinated irons that are bounded together with oxy-bridging and water as shown in Fig. I-2.

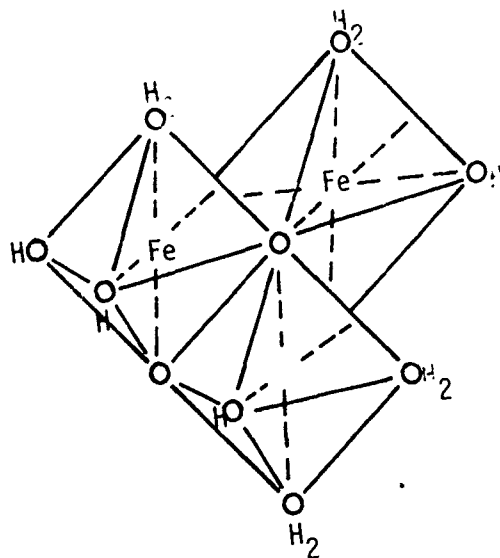
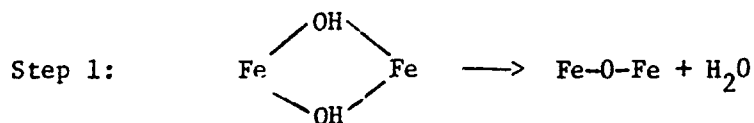
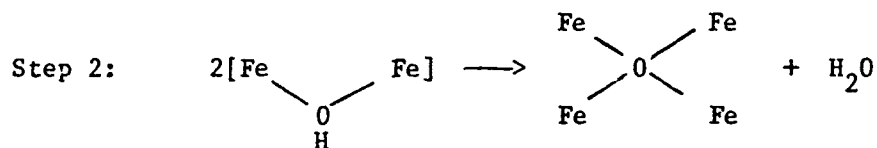


Fig. I-2 Possible arrangement of combination of two dioxy or di-hydroxy chain species to form a tetramer (ref. 25).

The structure of dry passive film is proposed to become $\gamma\text{-Fe}_2\text{O}_3$ through the following process:

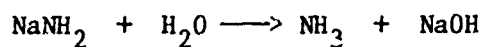


After five hours of dehydration, the passive film is changed as follows:

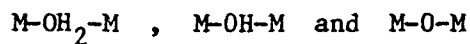


The existence of water in the passive film also has been reported by many other corrosion scientists. Saito et al.¹⁰⁰ propose that the water in the film plays an important role in the corrosion inhibition. Colorimetric titration method has been used to determine the amount of water in the passive film. In this experiment the released

water reacts with NaNH_2 as follows:



The NH_3 was determined colorimetrically. Based upon this experiment, Saito et al. proposed that the passive film consists of polymeric hydrous metal oxides including various forms of bridges between metal ions such as the following .



depending on the degree of dehydration. Okamoto¹⁰¹ also concluded that passive film in a hydrated gel-like oxide with three types of different bridges depending on loss of proton by aging or changing of the potential. He postulated the following model for passive film.

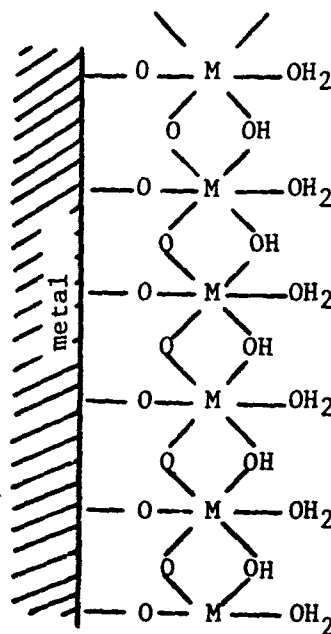


Fig. I-3 Structure of passive film according to Okamoto (Ref. 101).

ESCA studies of passive film on iron formed in borate buffer (pH 8.4) have shown two different binding states in terms of the O 1's peaks, one at 532.2 eV for M-OH or M-O-OH and a second at 530.7 eV for the M-O type bond. The peak height for the M-OH bond decreases with increasing anodic potential for passivation. Sato et al.¹⁰² have also studied the anodic passivation of iron in borate solution while the film was heated in vacuo to desorb water. They gave evidence for two types of water in the passive film with the ratio of one half. They reported that as the pH is increased, the amount of water in the passive film increased as well. Bloom and Gold¹⁰³ also reported two types of water in the passive film, an inner layer with $\text{Fe}_3\text{O}_4 \cdot 0.2\text{H}_2\text{O}$ and an outer layer with $\text{Fe}_2\text{O}_3 \cdot 1.8\text{H}_2\text{O}$.

Cahan et al.^{106a,b} have studied the passive film on the surface of iron extensively by various techniques such as automatic ellipsometry, ESCA, AC-electroreflectance, impedance measurements and the pulse interruptor technique. Recently Cahan et al.^{106c} developed a new model for passive film on the basis of their experimental results as well as other literature data. According to this model there is a concentration profile of Fe^{2+} in the passive film extending from the metal passive film interface to the passive film-solution interface. This concentration profile of Fe^{2+} is dependent on the electrode potential. As the potential across the passive layer is increased with increasing anodic potential, the Fe^{2+} concentration at the outer surface will decrease so as to maintain a constant electrochemical potential for this species within the film. These workers also propose the Fe(IV)

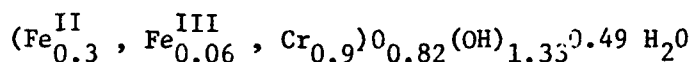
rather than Fe(VI) is formed at more anodic potentials, starting first at the outer surface of the film, and then extending into the film.

The authors believe that this model can interpret the behavior of passive film much better than any other earlier developed models. In addition, deviation of Mott-Schotky plot ($\frac{1}{C^2}$ vs. E) at low and high potential and also the existence of oxygen evolution on the surface of the passive film at high anodic potentials can be explained by this model on the basis of dynamic nature of the passive film over the entire range of passivation. Cahan et al. have concluded that the passive film is not a sandwich layer and does not behave like an intrinsic semi-conductor with well defined band gaps.

Cahan et al.^{106c} used a new term for passive film and called it a "chemi-conductor". They define the term of the chemi-conductor as a material "whose stoichiometry can be varied by oxidative and/or reductive valency state changes".

B. The Structure of the Passive Film on Ferrous Alloys:

The structure of the passive film on the surface of alloys also has been studied extensively. Asami et al.¹⁰⁷ studied the structure of the passive film on the surface of iron-chromium alloys by XPS. From data analysis of Cr $2P_{3/2}$, Fe $2P_{3/2}$ and O 1s, the composition of passive film on the surface of Fe-12.5% Cr and Fe-50% Cr was proposed to be as follows:



for Fe-12.5% Cr and $\text{CrO}_x(\text{OH})_{3-2x} \cdot n\text{H}_2\text{O}$ for Fe-50% Cr. n and x changed with alloy composition and the potential of passivation.

Hara and Sugimoto¹⁰⁸ also studied the passive film on Fe-Cr alloys by in situ electromodulation reflectance spectroscopy.⁵ The modulation reflectance spectra of Fe-Cr alloys (5-40 w% Cr) in 1M Na_2SO_4 (pH 2) have been obtained. The spectra for alloys containing less than 10% Cr are close to that for pure iron. At the beginning of the passive range, these workers proposed that the film contains both Fe^{2+} and Fe^{3+} ions which, with increasing positive potential, the concentration of Fe^{3+} increases. The spectra for the film on pure iron formed at quite anodic potentials have a broad peak at 3.2 eV and shoulders at 4.2, 4.1 eV. However, the spectra for film formed at low potential (up to 0.4 V vs. S.C.E.) have two large broad peaks at 2.4 eV and one small peak at 4.0 eV. On the other hand, Fe^{2+} oxides usually do not show any strong characteristic absorption bands in the visible region but a strong absorption band in the UV at 4.8 eV (due to charge transfer phenomenon). However, Fe^{3+} has strong absorption bands in the visible (due to charge transfer) at 2.4 and 3.0 eV. Based upon this comparison one should be able to consider the change of Fe^{2+} to Fe^{3+} in the film. The modulated reflectance spectra of passive film on iron-chromium are compared with spectra of Cr^{3+} and Cr^{6+} in other compounds. It has been found that Cr^{3+}

compounds in weak ligand fields have absorption peaks at 2.2, 3.1 and 4.8 eV and in strong fields the peaks position are at 6.9 and 3.6 eV. The Cr^{6+} absorption peak appeared at around 3.7 eV. The results showed that in the potential region (0.00-0.80 V vs. SCE) most of the passive films for Fe-Cr alloys with higher than 10% Cr are Cr^{3+} and Fe^{3+} oxide-oxy-hydroxide. However, at the starting point for the $\text{Cr}^{3+} \rightarrow \text{Cr}^{6+}$ changes (0.8 + 1.0 V) the composition of the passive film might be Fe^{3+} , small amounts of Fe^{2+} , Cr^{3+} and Cr^{6+} . The Fe-Cr alloys show a secondary passivation region at high anodic potentials. In the transition region between the initial and secondary passivation region the current passes through a maximum. In the secondary passivation region up to the transpassive region, the composition of the passive film is postulated to be Fe^{3+} and a small amount of Cr^{3+} and Cr^{6+} . For Fe-Cr alloys with higher than 30% Cr in the secondary passive region, the surface roughening (due to dissolution) is so high that it is difficult to get accurate modulated reflectance spectra. Because of the dissolution of Cr^{6+} in the secondary passive region, the composition of passive film in this region is more or less the same as that for the passive film on pure iron.

The composition of the passive film on ferritic stainless steel has been studied by AES.¹⁰⁹ Mo was not detected by AES on the surface or near the surface. However, Mo has been detected by gas discharge spectroscopy (GDS) and secondary ion mass spectroscopy (SIMS) in 4% Mo ferritic steel.¹¹⁰ Hashimoto et al.¹¹¹ using ESCA were able

to find Mo on the surface of the passive film as a hexavalent species on the surface of amorphous Fe-Mo alloys.

REFERENCES

CHAPTER I

1. National Bureau of Standards. Special publication 511-1, Economics of Metallic Corrosion in the United States (1978).
2. M. Pourbaix, Proc. 5th. Cong. Metallic Corrosion (NACE, p. 17, 1972)
3. M. Faraday, Experimental Researches in Electricity, Vol. 2, pp. 234-250, New York, Dover Pub., Reprinted 1965.
4. M.N. Lomonosov, Collected Works I. Moscow, Academy of Science, 1950.
5. J. Kier, Phil. Trans. 80, 359 (1790).
6. C. Schöbein, Progg. Ann. 37, 390 (1830).
7. A. Russel, Nature 115, 445 (1925).
8. R.S. Lillie, Science 67, 593 (1928).
9. C. Wenzel, Handbuch der Anorganischen Chemie, Gmelin, Teil 59A, p. 313, Berlin (1929).
10. N. Tamoshov, Theory of Corrosion and Protection of Metals, (Translated by B.H. Tytell, I. Geld and H.S. Preiser), New York, The Macmillan Co. (1966).
11. F. Balaha, Nature 166, 607 (1950).
12. F. Flade, Z. Physik. Chem. 76, 513 (1911).
13. H.H. Uhlig (ed.) Corrosion Handbook, New York, John Wiley and Sons (1948).
14. K.J. Vetter, Electrochemical Kinetics Theoretical and Experimental Aspects (translated by Scripta Technica) New York, Academic Press (1967).
15. L. Young, Anodic Oxide Films, London, Academic Press (1961).
16. T.P. Hoar, Corrosion Sci. 7, 341 (1967) and C. Wagner, Corrosion Sci. 5, 751 (1965).

17. U.R. Evans, Metallic Corrosion, Passivity and Protection, New York, Longmans, Green (1948), and O. Kuba Schewski and B.E. Hopkins, Oxidation of Metals and Alloys, New York, Academic Press (1953).
18. I. Epelboin, C. Gabrielli, M. Keddan, J.C. Lestrade and H. Takenouti, J. Electrochem. Soc. 119, 1632 (1972).
19. R.P. Frankenthal, J. Electrochem. Soc. 116, 580 (1969) and R.P. Frankenthal, Electrochim. Acta 16, 1845 (1971).
20. M. Fleischman and H.R. Thirsk, J. Electrochem. Soc. 110, 688 (1963).
21. A. Pigeand, J. Electrochem. Soc. 122, 80, (1975).
22. N. Sato, M. Cohen, J. Electrochem. Soc. 111, 519 (1964).
23. W.E. O'Grady, J. Electrochem. Soc. 127, 555 (1980).
24. H. Ebiko, H. Yamato, W. Suetaka and S. Shimodaria, Proceeding of the Fifth Congress on Metallic Corrosion, p. 285 (1972).
25. A.M. Van Diepen, H.J. Vledder and C. Langereis, Appl. Phys. 15, 163-166 (1977).
26. H. Ebiko, H. Yamato, W. Suetaka and S. Shimodaria, Proceeding of the Fifth Congress on Metallic Corrosion (NACE), p. 285 (1972).
27. D.J. Wheeler, B.D. Cahan, C.T. Chen and E. Yeager, Passivity of Metals (Eds. R. Frankenthal and J. Kruger) Princeton, p. 546 (1978), The Electrochemical Society, Inc.
28. N. Hora and K. Sugimoto, J. Electrochem. Soc. 126, 1328 (1979).
29. J. O'M. Bockris, M.A. Genshaw, V. Brusica and H. Wroblowa, Electrochim. Acta 16, 1859 (1971).
30. V. Brusica, Ph.D. Thesis, University of Pennsylvania (1971).
31. C. Chen, Ph.D. Thesis, Case Western Reserve University (1979).
32. J. Kruger and J.P. Calvert, J. Electrochem. Soc. 114, 43 (1967), and reference 29.
33. J.L. Ord, Passivity of Metals (Eds. R.P. Frankenthal and J. Kruger), Princeton, The Electrochemical Soc., Inc. p. 273 (1978).

34. S. Matsuda, K. Sugimoto, and Y. Sawada, ibid, p. 699.
35. B. Agihs and J. Siegka, Proceedings of the Fifth Congress on Metallic Corrosion, p. 228 (1972).
36. J. Siejka, C. Ckerki, Electrochimica Acta 17, 2371 (1972).
37. J.E. Holliday and R.P. Frankenthal, J. Electrochem. Soc. 119, 1190 (1972).
38. J. Yahalom and L.K. Ives, Passivity and its Breakdown on Iron and Iron Base Alloys (USA-Japan Seminars) (Eds. R.W. Staehle and H. Okada) Houston, p. 69 (1976) National Association of Corrosion Engineers.
39. P.B. Sewell, P.F. Mitchell and M. Cohen, Surface Sci. 33, 535 (1972).
40. G.L. Foley, J. Kruger and C.J. Bechtold, J. Electrochem. Soc. 114, 939 (1967).
41. N. Nagayama and M. Cohen, J. Electrochem. Soc. 110, 670 (1963).
42. B. MacDougall and M. Cohen, Passivity of Metals, Eds. R.P. Frankenthal and J. Kruger, Princeton (The Electrochemical Society, Inc., 1978) p. 827.
43. C.L. Mcbee and J. Kruger, Electrochimica Acta 17, 1337 (1972).
44. C.L. Foley, J. Kruger and C.J. Bechtoldt, J. Electrochem. Soc. 114, 995 (1967).
45. S.H. Chen and J.W. Morris, Metallurgical Transactions A. 8A, 19 (1977).
46. B. MacDougall, D.F. Mitchell and J.J. Graham, Israel Journal of Chemistry 18, 125 (1979).

47. C.R. Brundle, Surface Sic. 66, 581 (1977).
48. Konno and M. Nagayama, Passivity of Metals (Ed. R.P. Frankenthal and J. Kruger) Princeton, The Electrochemical Society, Inc. (1978) p. 585.
49. J.R. Ambrose, ibid, p. 740.
50. A.E. Yaniv, J.B. Lumsden, R.W. Staehle, Passivity and Break-down on Iron and Iron Base Alloys, Ed. by R.W. Staehle and H. Okada (Houston; National Association of Corrosion Engineers, 1976) p. 72.
51. S. Shimodaira, ibid, p. 38.
52. K. Tachibana, M.B. Ives, Passivity of Metals, Ed. by Robert P. Frankenthal and J. Kruger (Princeton; The Electrochemical Society, Inc. 1978) p. 878.
53. K. Asami, K. Hashimoto and S. Shimodaira, Corrosion Sci. 16, 387 (1976).
54. K. Hashimoto, M. Naka, K. Asami and T. Masumoto, Corrosion Sci. 19, 165 (1979).
55. H.H. Strehblow, B. Titze, Electrochimica Acta 25, 839 (1980).
56. R. Berneron, J.C. Charbonnier, R. Namdar-Irani and J. Manenc, Corrosion Sci. 20, 899 (1980).
57. M. Nagayama, M. Cohen, J. Electrochem. Soc. 109, 781 (1962).
58. A.G. Revesz, J. Kruger, Passivity of Metals, Ed. by R.P. Frankenthal and J. Kruger (Princeton, The Electrochemical Society, Inc. 1978) p. 137.
59. K. Hashimoto, M. Naka, J. Noguchi, K. Asami and T. Masumoto, ibid, p. 156.
60. J.E.O. Mayne and M.J. Pryor, J. Chem. Soc. 1831 (1949).
61. K.E. Heusler, Z. Electrochem. 66, 177 (1962).
62. M. Nagayama, M. Cohen, J. Electrochem. Soc. 109, 781 (1962).
63. L. Young, D.J. Smith, J. Electrochem. Soc. 126, 765 (1979).
64. A.J. Arvia, J.J. Podesta and R.C.V. Piatti, Electrochimica Acta 16, 1797 (1971).

65. N. Sato and M. Cohen, J. Electrochem. Soc. 111, 512 (1964).
66. M.J. Pryor, J. Electrochem. Soc. 106, 557 (1959).
67. M.C. Bloom and L. Goldenberg, Corrosion Sci. 5, 623 (1965).
68. C. Wagner, Berichte der Bunsen - Gesellschaft 77, 1090 (1973).
69. E.K. Oshe, I.L. Rozenfeld and V.G. Doroshenko, Z. Metallov, 13, 410 (1977) and ibid, p. 38 (1971).
70. A.N. Frumkin, V.S. Bagotskii, Z.A. Jofa and B.V. Kabanov, Kinetics of Electrode Processes (English transl.) (1967).
71. B.N. Kabanov and D.I. Leikis, Z. Electrochem. 62, 660 (1958).
72. Ya.M. Kolotyркиn, Z. Electrochem. 62, 664 (1958).
73. H.H. Uhlig, Passivity and its Breakdown on Iron and Iron Base Alloys (Houston, National Association of Corrosion Engineers, 1976) p. 19.
74. H.H. Uhlig, ibid. p. 21.
75. H.H. Uhlig and P.F. King, J. Electrochem. Soc. 106, 1 (1959).
76. H.H. Uhlig, Corrosion Sci. 7, 325 (1967).
77. N. Sato and M. Cohen, J. Electrochem. Soc. 110, 670 (1968).
78. N. Sato and G. Okamoto, J. Electrochem. Soc. 110, 605 (1963).
79. J. O'M. Bockris, N.A. Genshaw, V. Brusic and H. Wroblowa, Electrochim. Acta 16, 1859 (1971).
80. M.D. Reingeverts, O.S. Andreeva and A.M. Sukhotin, Elektro Khimija 15, 972 (1979).
81. K. Kudo, T. Shibata, G. Okamoto and N. Sato, Corrosion Sci. 8, 809 (1968).
82. M. Cohen, D. Mitchell and K. Hashimoto, J. Electrochem. Soc. 126, 442 (1979).
83. T. Ohtsuka and K.E. Heusler, J. Electroanal. Chem. 100, 319 (1979).

84. M. Nagayama, M. Kohen, J. Electrochem. Soc. 109, 781 (1962).
85. M. Nagoyama and M. Kohen, J. Electrochem. Soc. 110, 781 (1963).
86. K. Ogura and K. Sato, Electrochimica Acta 25, 857 (1979).
87. M. Seo, J.B. Lumsden and R.W. Staehle, Surf. Sci. 42, 337 (1974).
88. A.M. Van Diepen, H.J. Vledder and C. Langereis, Appl. Phys. 15, 163 (1977).
89. H.T. Yolken, J. Kruger, and J.P. Calvert, Corrosion Sci. 8, 103 (1968).
90. H. Saito, T. Shibata and G. Okamoto, Corrosion Sci. 19, 693 (1979).
91. N. Nagayama and M. Cohen, J. Electrochem. Soc. 110, 670 (1963).
92. K. Ogura, J. Electroanal. Chem. 79, 149 (1977).
93. M. Seo, N. Sato, J.B. Lumsden and R.W. Staehle, Spring meeting of the Electrochemical Society, Japan (1975), Ext. Abstr. p. 65.
94. A.G. Akimov, N.P. Andreeva and I.L. Rosenfeld, Elektrokhimiya, 16, 96 (1980).
95. A.G. Akimov, N.P. Andreeva and I.L. Rosenfeld, ibid, 16, 96 (1980).
96. M. Hauffe, Oxidation of Metals, New York, Plenum Press (1965).
97. N.F.J. Mott, Chem. Phys. 44, 172 (1947).
98. H. Ebiko, H. Yamamoto, W. Suhtaka and S. Shimodaira, Proceeding of the Fifth Int. Congress on Metallic Corrosion, p. 258 (1972).
99. W.E. O'Grady, J. Electrochem. Soc. 127, 555 (1980).
100. H. Saito, T. Shibata and G. Okamoto, Corrosion Sci. 19, 693 (1979).
101. G. Okamoto and T. Shibata, Proc. 3rd Int. Congress on Metallic Corrosion, Moscow (1966) p. 396.

102. N. Sato, K. Kudo and T. Noda, Electrochimica Acta 16, 1909 (1971).
103. M.C. Bloom and L. Goldenberg, Corrosion Sci. 5, 623 (1965).
104. C.T. Chen, Ph.D. Dissertation, Case Western Reserve University (1979).
105. D.J. Wheeler, B.D. Cahan, C.T. Chen, and E. Yeager, Passivity of Metals, Ed. by R.P. Frankenthal and J. Kruger, p. 546.
106. a and b) The Nature of the Passive Film on Iron
C.T. Chen and B.D. Cahan, I-Automatic Ellipsometric Spectroscopy Studies.
B.D. Cahan and C.T. Chen, II-AC Impedance Studies, Submitted to J. Electrochem. Soc.
106. c) ibid
B.D. Cahan and C.T. Chen, III-The Chemi-Conductor Model, to be submitted to J. Electrochem. Soc.
107. K. Hashimoto and K. Asami, Corrosion Sci. 19, 251 (1979).
108. K. Asami and K. Hashimoto, Corrosion Sci. 17, 559 (1977).
109. A.E. Yaniv, J. Electrochem. Soc. 124, 490 (1977).
110. R. Berneron, J.C. Chorbonnier, R. Namdor-Irani and J. Manenc, Corrosion Sci. 20, 899 (1980).
111. K. Hashimota, M. Naka, K. Asami and T. Masumoto, Corrosion Sci. 19, 165 (1979).

CHAPTER II
THE FORMATION AND REDUCTION OF PASSIVE FILM
IN ALKALINE AND ACID SOLUTION

I. INTRODUCTION

The dissolution and passivation of iron have been studied extensively over the last two or three decades.¹⁻²⁹ However, there are still a great number of ambiguities in this field. Most of the problems are related to the many internal and external factors which can be involved, and which are often neglected. In this respect many theories and models have been built up such as the adsorption theory⁷⁻¹⁰ and film theory.¹²⁻¹⁵ In addition, the structure of passive film has been proposed to consist of a multi-layer structure involving different iron oxides^{12,16-18} or oxide-oxyhydroxides¹⁹ with an open gel-like outer layer.²² On the other hand, some scientists believe that the passive film is a single isotropic layer.²³ Despite extensive effort, it is not clear whether the passive film is formed by a dissolution-precipitation mechanism or by the direct oxidation of the metal.

The objective of this work is to obtain experimental data which can be used to establish the mechanism of the formation and reduction of passive film. The influence of various factors on the structure of the film has been examined. Three types of electrochemical measurements have been carried out with pure iron:

- 1) Linear sweep cyclic voltammetry, including the effect of sweep rate, voltage range and forced convection.
- 2) Potential step measurements of the formation and reduction of the film.
- 3) Rotating disk-ring electrode studies of the formation and reduction of the film using both the linear sweep and potential step techniques to investigate the introduction of Fe^{II} into the solution.

The measurements have been carried out in borate buffer over the pH range 5.6-9.1 and also in ferrous sulfate-borate buffer solutions. While measurements of these types have been made one at a time by other workers, it is thought that by combined use more insight can be obtained into the nature of the passivation phenomenon.

II. EXPERIMENTAL PROCEDURES

A. Reagents

The $\text{Na}_2\text{B}_4\text{O}_7$, FeSO_4 and ethylenediamine-tetraacetic acid (EDTA) were analytical reagent grade from Fisher Scientific Co. The borate buffers of various pH were prepared by mixing X M H_3BO_3 and Y M $\text{Na}_2\text{B}_4\text{O}_7$ with distilled water, where $0.4 \geq X \geq 0.03$ and $0.2 \geq Y \geq 0.04$. The electrolytes was further purified by preelectrolysis, using for the anode a palladium tube filled inside with pure hydro-

gen and for the cathode a pure gold sheet electrode (2 cm x 2 cm).

B. Electrode and Cell Design

Pure polycrystalline iron (99.999%) from Organic-Inorganic Corporation was used. This pure iron rod was cut with a stress free diamond wheel cutter in the form of a disk (7.6 mm diameter and 5 mm high). This disk was molded in a Teflon tube (press fit) and was joined to the proper stainless steel shaft for external connection as shown in Fig. II-1.

The Pine ring-disk electrode assembly consisted of an epoxy mounted ring without a disk with the space normally occupied by the disk filled with epoxy. This space was then drilled out to provide for a disk with the proper cone shape as shown in Fig. II-1. The disk for this electrode was made from pure iron and was mounted in the center of the ring with a very thin shrinkable Teflon tube between the ring and the disk. The disk electrode would be tightened from the back by a screw. This electrode was used for the major part of this study.

For each experiment the electrode was polished with diamond paste (6 μ , 3 μ and 1 μ) and alumina powders (0.3, 0.4 and 0.05 μ) respectively. After polishing with each grade of the diamond pastes and alumina powders, the electrode was washed with sufficient distilled water and cleaned at least two times in an ultrasonic bath for about 15-20 min. The electrode thus cleaned was then transferred to the electrochemical cell. This electrode was then

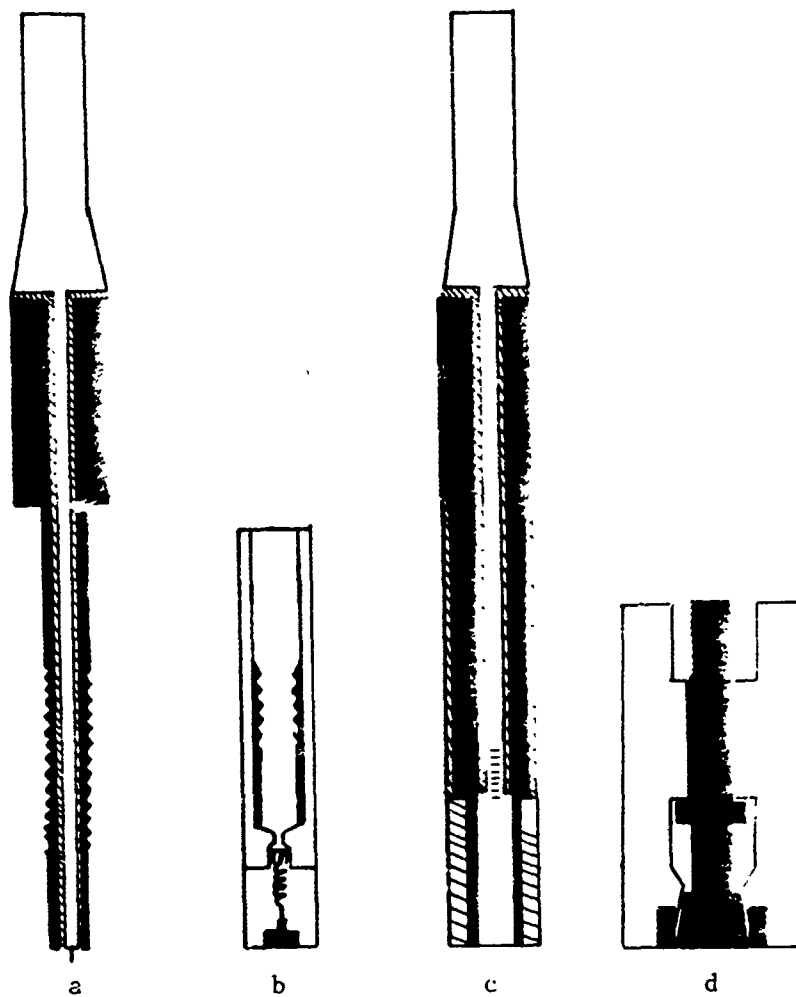


Fig. II-1. Rotating disk-ring electrode.
a - stainless steel shaft, b - disk electrode
c and d - new design for RRDE.

cathodically reduced at -0.4 V vs RHE for 15-20 min to reduce any surface oxide. At this stage the electrode was pushed to the bottom of the cell and the existing electrolyte was sucked out, while the electrode was maintained as long as possible under cathodic potential control. Then fresh and deaerated electrolyte was flowed into the cell, keeping the electrode potential at -0.4 V. This procedure was carried out in a closed system as shown in Fig. II-2. The purpose of this procedure was to remove any ferrous ion which had been produced earlier during the cathodic reduction. In addition, this procedure has the advantage of changing the electrolyte rapidly.

An α -Pd H bead was used as the reference electrode and a platinum wire (4 cm long and $\sqrt{1}$ mm diameter) was used as the counter electrode.

C. Instruments

The Stonehart (BC1200) potentiostat and PARC programmed wave generator (Model 175) have been used for the measurements. The data were recorded by a two-pen Yokogawa recorder. In the case of pulse technique measurements the data were recorded with the same recorder and also a Nicolet storage oscilloscope (Model 201). These data were transferred to the Commodore PET (2001 series) computer and recorded with a printer-plotter (Hemlett-Packard 7245A).

The Pine rotating ring disk drive system has been modified by using extra brush contacts, two for the ring and two for

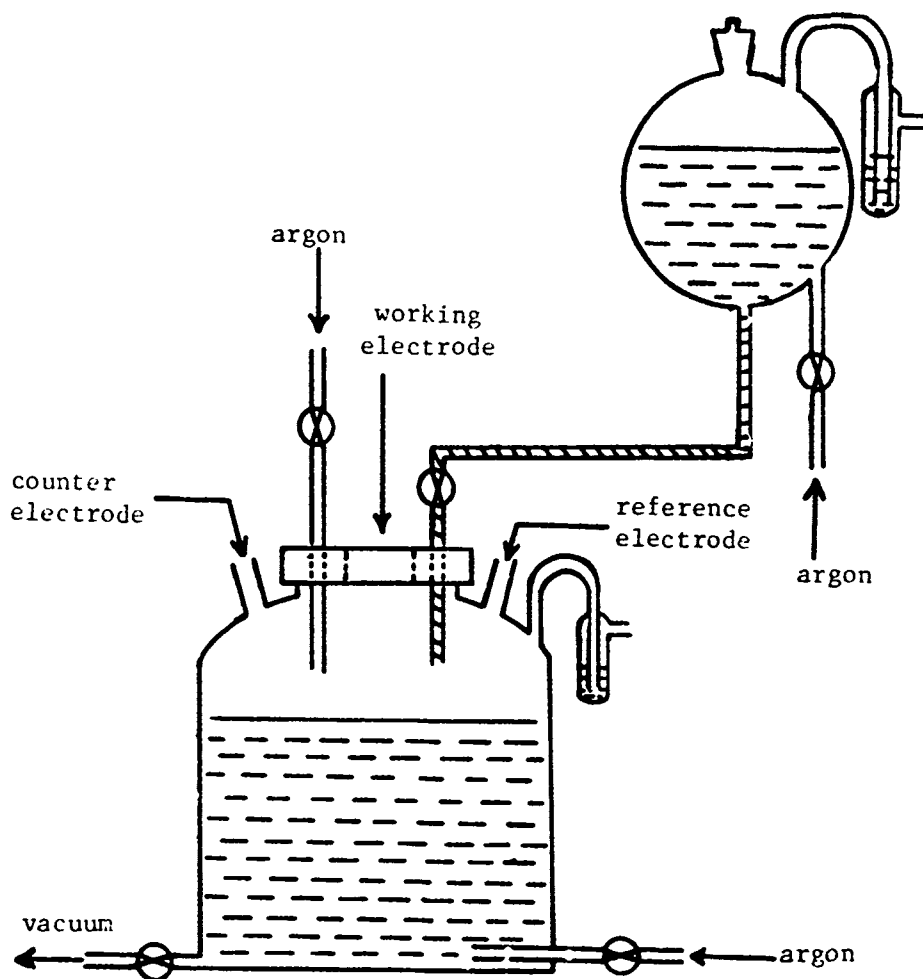


Fig. 11-2. Schematic diagram of the electrochemical cell

the disk connections, to reduce electrical noise.

III. RESULTS

The voltammetry curves of the iron electrode in stagnant borate buffer solution (pH 6.5-9.1) have been obtained (Fig. II-3). The potential of the anodic peak (A_I) due to the dissolution of iron was found to be strongly pH dependent. The anodic current and the symmetry of the A_I peak are also pH dependent. The A_I peak changes from a bell shape to the traditional passivation shape, with increasing acidity of the solution. Figure II-3 shows the shift of the A_I peak to a more positive potential as the acidity of the solution increased. The passivation current which is almost potential independent is greater in a more acidic solution.

The voltammetry curves of the iron electrode with potential scan rates higher than 10 mV/sec showed two clear anodic peaks (A_I and A_{II}) with the second anodic peak A_{II} at higher anodic potential smaller than the A_I peak. The effect of stirring on the A_{II} peak was studied. Figure II-4 shows the effect of rotation on this peak. The peak current decreases by increasing the rotation speed. However, during potential cycling, this peak A_{II} increases. In the presence of ferrous ion in the solution, this peak increases significantly. Figure II-5 shows the voltammetry curve of gold in borate buffer containing 10^{-4} M $FeSO_4$. This experiment shows that the oxidation of solution phase ferrous ion to the ferric state in the oxide form has almost the same potential

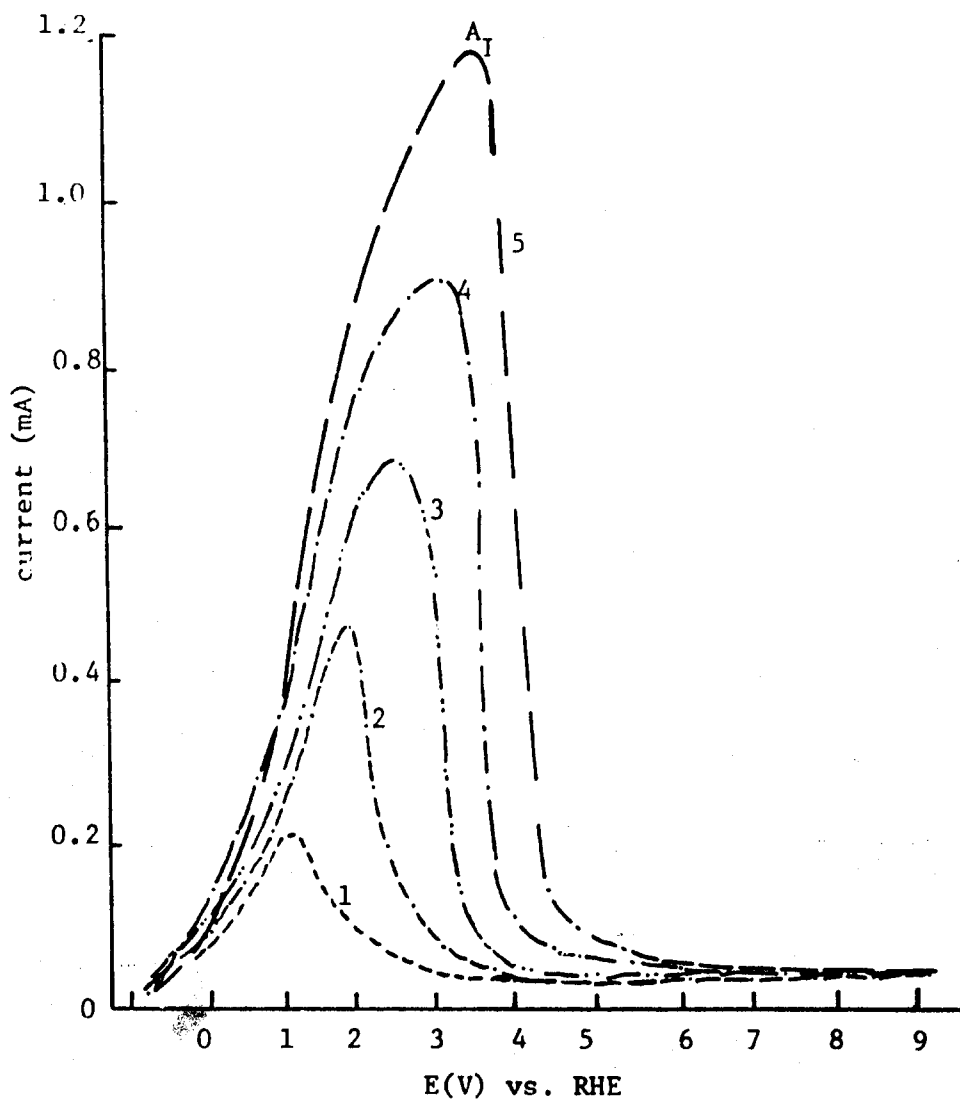


Fig. II-3. Anodic voltammogram of iron electrode in borate buffer at pH = 1 - 9.1; 2 - 7.6; 3 - 7.0; 4 - 6.8; and 5 - 6.4 in stagnant solution. Sweep rate: 100 mV/s. Direction of sweep: anodic electrode area: 0.45 cm².

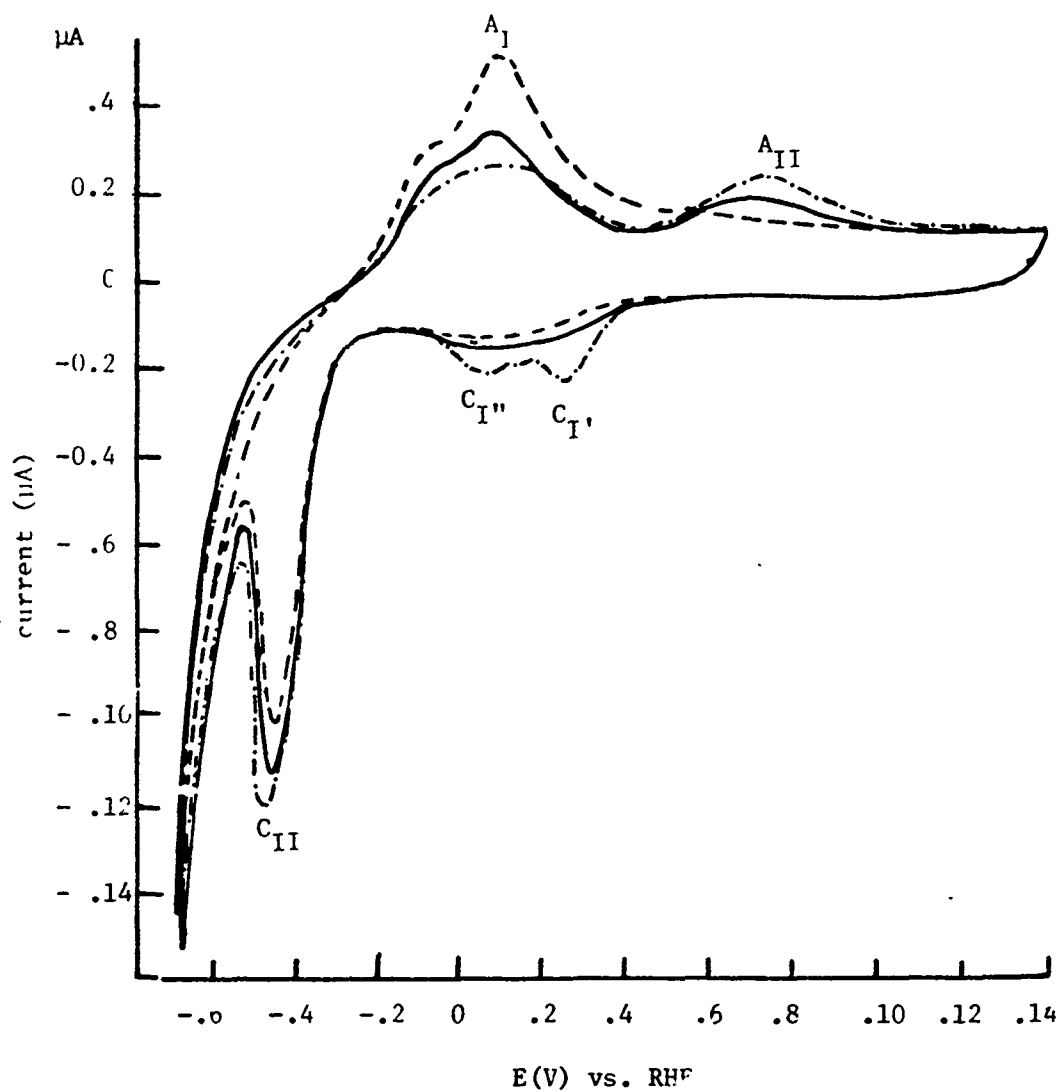


Fig. II-4. Voltammetry curve of iron electrode in borate buffer pH 8.4 (100 mV/s). — first potential sweep, --- effect of rotation, -.-.-. effect of potential cycling. Electrode area: 0.453 cm².

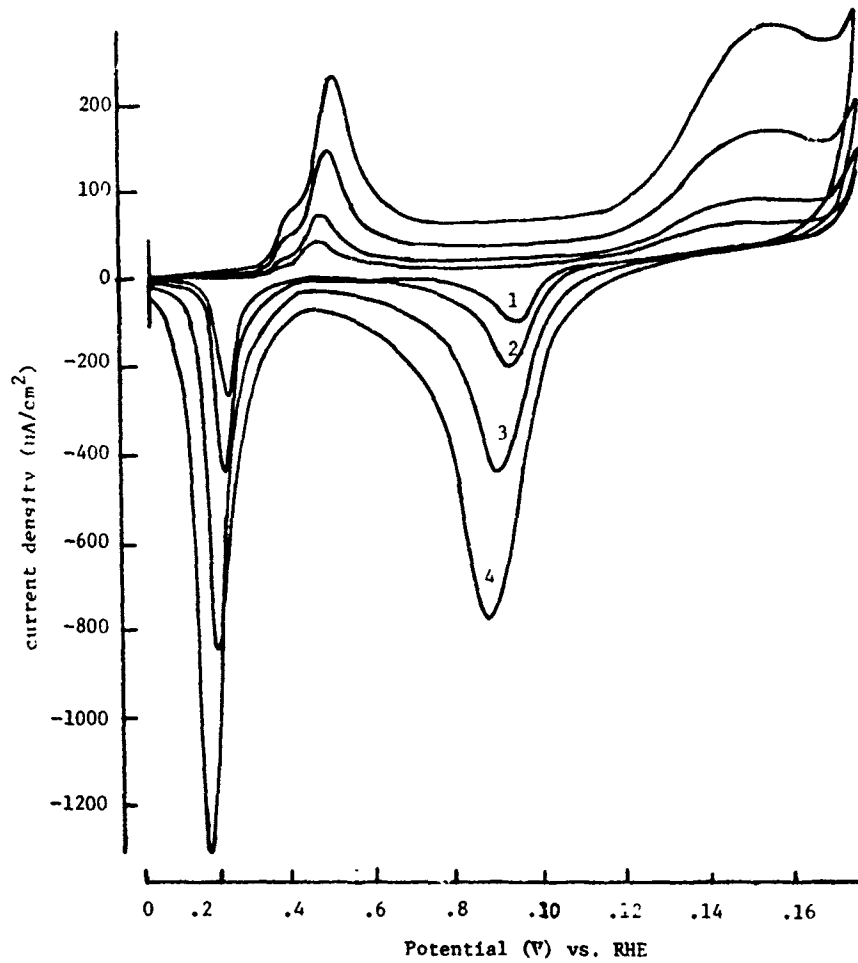


Fig. II-5 Voltammetry of gold electrode in borate buffer (pH 8.4) containing 10^{-4} M FeSO_4 at different potential scan rates, 1-10, 2-20, 3, 50 and 4, 100 mV/s. Electrode area: 0.453 cm^2 .

as the A_{II} peak in the polarization curve for the electrode. The current at potentials in the passive range on iron is many orders greater than that in the absence of ferrous ion in the solution.

The potential of the iron disk, passivated at 1.0 V in pure borate buffer solution (pH 8.4) was shifted to 0.2 V and then 10^{-3} ml M $FeSO_4$ was added to the electrochemical cell containing borate buffer (pH 8.4). To ensure against air oxidation of the $FeSO_4$ solution the whole experiment was carried out in a N_2 filled glove box. After 1 min or less at 0.2 V the potential was then swept in the anodic direction from 0.2 V up to 1.6 V. The current over this potential range, when the electrode is passive, is increased by the presence of the ferrous ion very substantially (Fig. II-6 and Fig. II-7). The measured current is due to the oxidation of Fe(II) to Fe(III) probably with precepitation of the Fe(III) as a hydrated oxide or gel on the passivation film. This also requires sufficient conductivity in the passive film to support the Fe(II) oxidation current.

The RRDE technique was used to examine the dissolution of the iron electrode during passivation and reduction of the film. Both the potential sweep and potential step methods were used. In the case of the potential sweep method, the potential of the disk has been swept from -0.6 up to 1.65 V vs. RHE, at various sweep rates. However, the potential of the Pt ring was held at a constant value (1.0 V), at which Fe(II) should be oxidized on the ring.

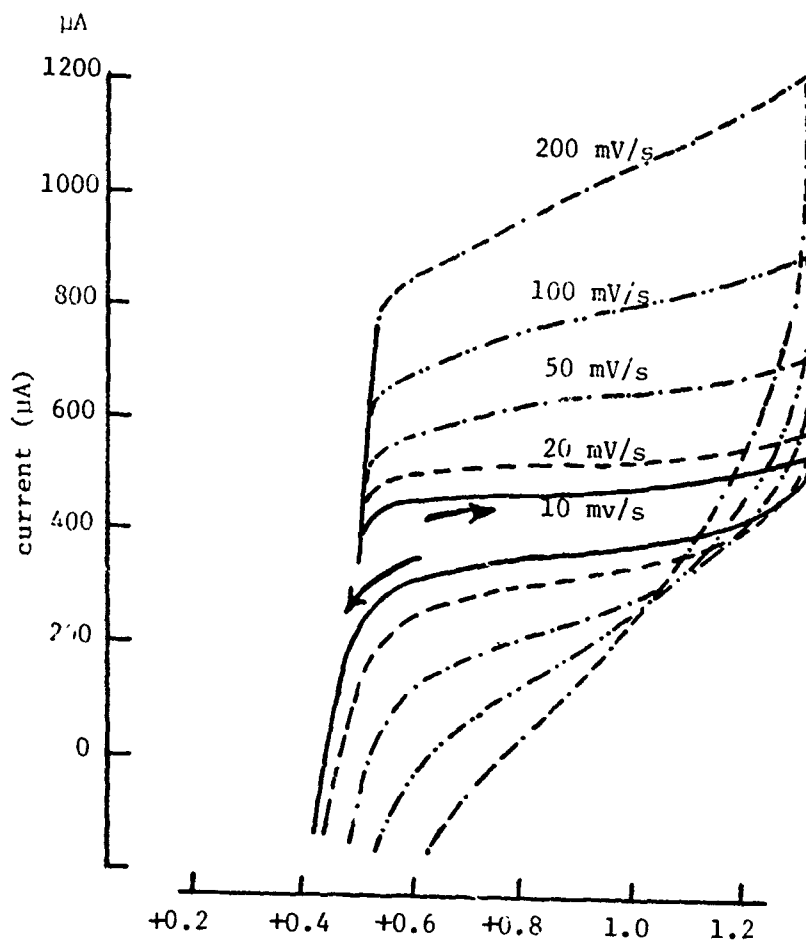


Fig. II-6. Current potential curve of iron electrode in borate (pH 8.4) containing FeSO_4 with different potential scan rates, 10, 20, 50, 100, 200 mV/s. Electrode area: 0.453 cm^2 .

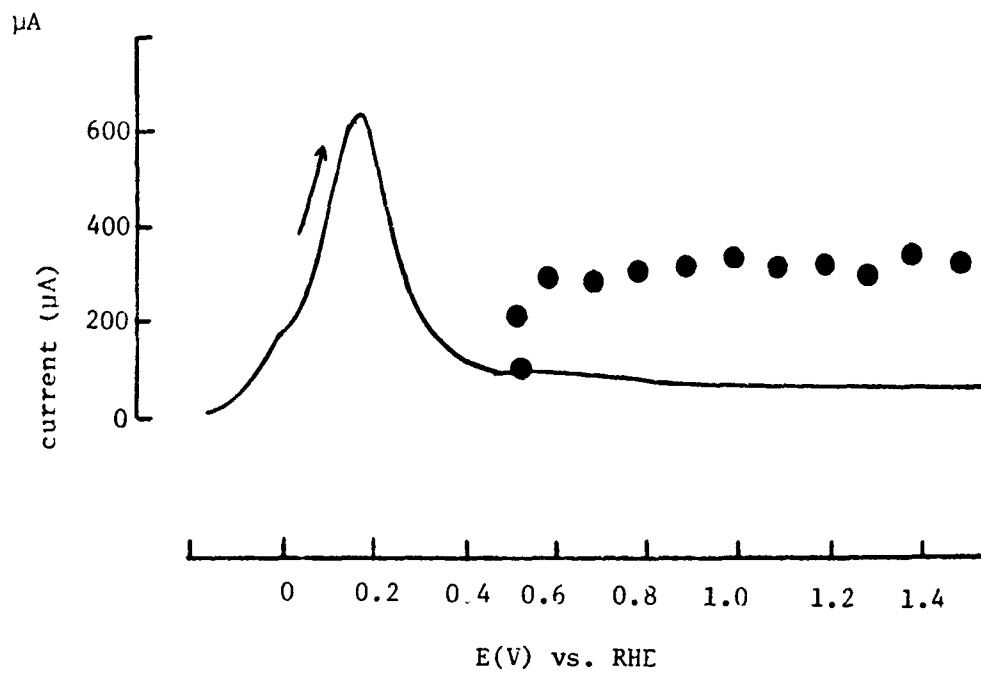


Fig. II-7. Current-potential curve of the iron electrode in borate buffer (pH 8.4). • indicates the current after adding 10^{-4} FeSO_4 in the solution, Scan rate: 10 mV/s; electrode area: 0.453 cm^2 .

The ring current showed that the disk at a potential corresponds to A_I dissolved and ferrous ions under force connection were transported to the ring through the solution. Figure II-8 shows the behavior of the ring current when the potential of the disk was swept from -0.6 up to 1.65 V. These measurements indicate the dissolution to yield ferrous ion at A_I potential.

The magnitude of ring current is low but still reliable. The current on the ring is almost 1% of the disk current. The integration of the peak in the ring current corresponding to A_I yields a charge of $\sim 1 \times 10^{-4}$ C/cm² which is equivalent to $\sim 5 \times 10^{-9}$ moles of Fe(II). If the solution were not transported away by convection, this could result in the precipitation of an oxy-hydroxide layer on the top surface of passive film. The thickness of this precipitated layer in more acidic solution will be greater.

The potential step technique with RRDE also showed the introduction of the Fe(II) into solution when the potential of the disk was stepped from the cathodic to anodic region. The potential was stepped from -0.4 V in the cathodic protection region to progressively more anodic potentials. Figure II-9 shows the ring and disk current due to the potential changes on the disk. The disk current first increased fast and after a few seconds decayed gradually and approached the steady state condition. The ring current and integrated charge indicated that the amount of Fe(II) introduced into the solution decreased as the potential of the disk was stepped

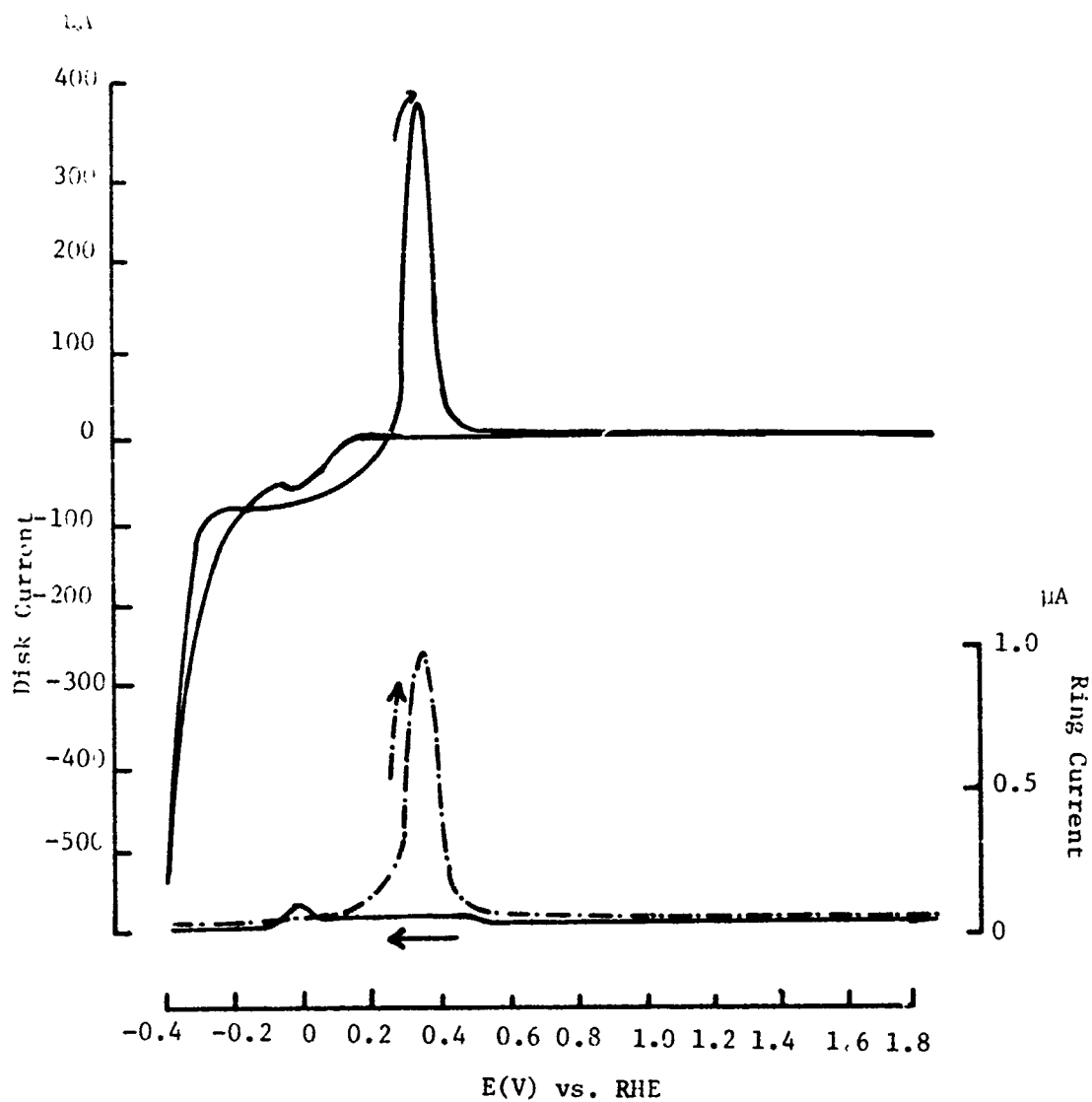


Fig. II-8. The cyclic voltammetry of iron electrode in borate buffer pH 3.4 (1 mV/s) combined with RRDE technique. Disk electrode area: 0.453 cm^2 . Collection efficiency of ring: 0.42. Ring potential: 1.0 V vs. RHE.

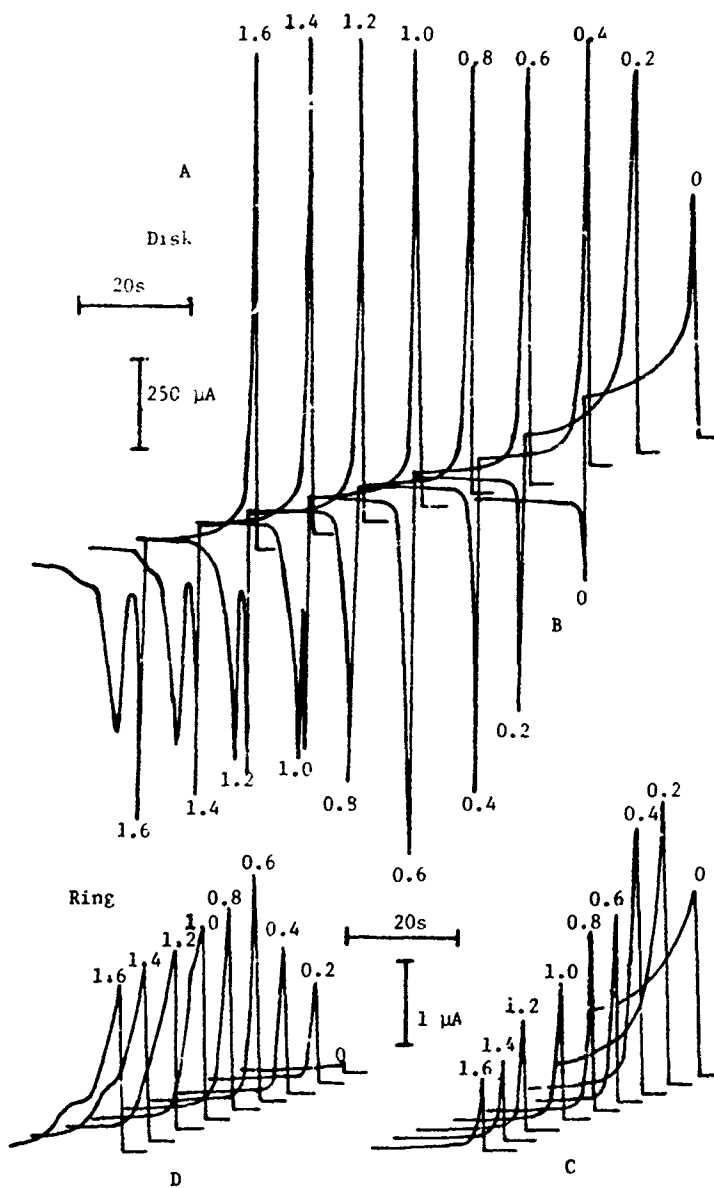


Fig. II-9. RRDE measurement of iron electrode in borate buffer solution using potential step techniques. A. Anodic disk current (stopped from -0.4 V vs. RHE to indicated potential); B. Cathodic disk reduction currents (stepped from indicated potential to -0.4 V); C. Ring currents corresponding to C; D. Ring currents corresponding to B.

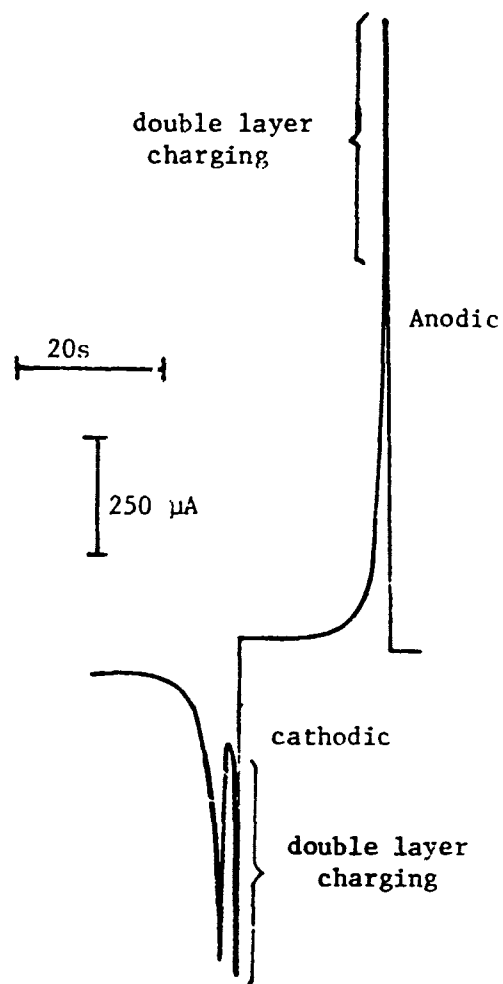


Fig. II-9a. Passivation and reduction of iron electrode by potential pulse technique. The brackets show the section of the current time-curve corresponding principally to double layer charging during the potential step.

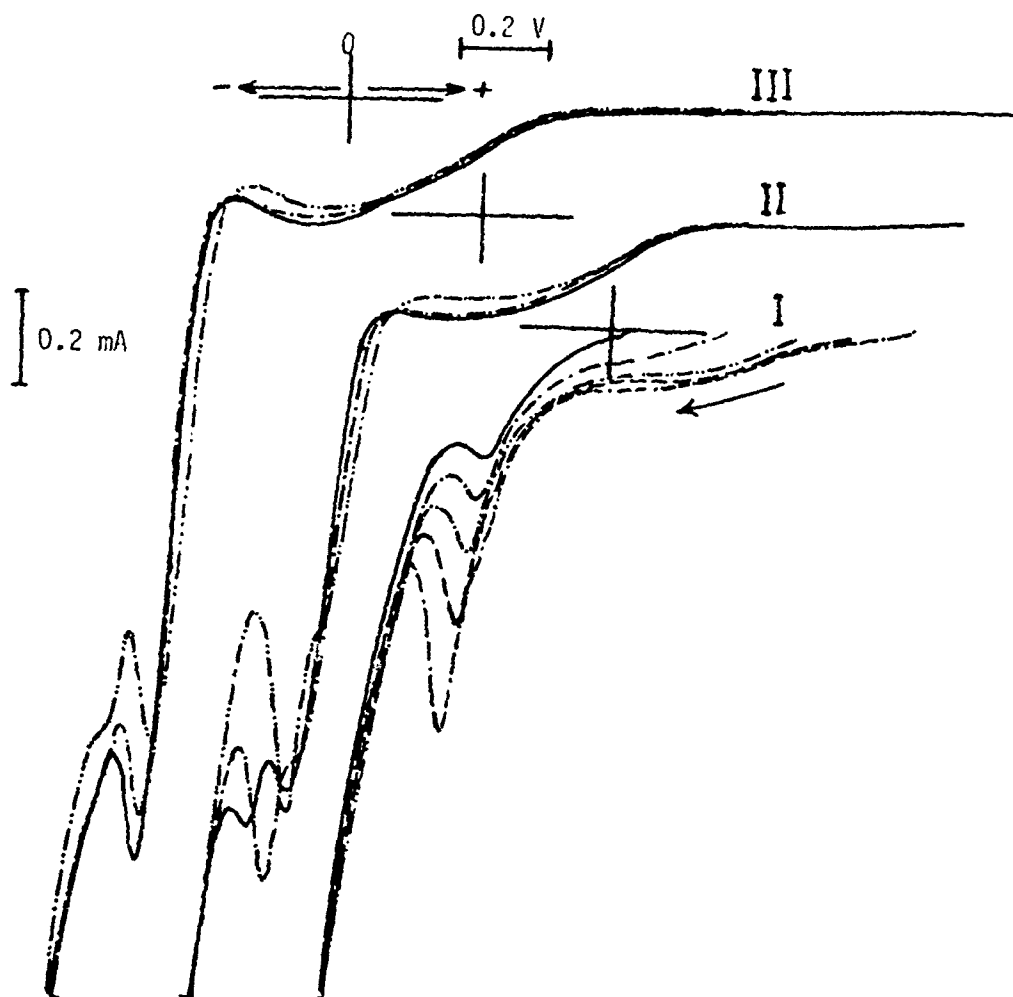


Fig. II-9b. Cathodic reduction of the passivated iron after passivation in borate buffer (pH 8.4) at different potentials for 2 min. Curve I 0-0.8 V, II. 0.8-1.4 V, III. 1.3-1.6 V. Cathodic sweep rate: ≈ 100 mV/s. Electrode area: 0.453 cm^2 .

to more anodic potentials.

The cathodic reduction of the passive film on iron in borate buffer solution show two cathodic peaks (C_I and C_{II}) in the voltammetry curves (Fig. II-4). In some experiments the electrode was prepassivated and the potential then sweep cathodically. In these experiments, the peak currents for C_I and C_{II} were dependent on the passivation time and also the passivation potential at which the electrode was prepassivated. The peak C_I appears more like a shoulder, probably because of the overlap of peak C_{II} and C_I . An attempt has been made to give a qualitative interpretation of this overlap with dotted lines in Fig. II-10. With multiple sweeps, peak C_I increases and separates into two peaks (see Fig. II-4).

For a better understanding of the splitting of the cathodic peak C_{II} , the following experiments were carried out. The passive film was formed on an iron disk at 1.0 V using a potential step and the electrode maintained at this voltage for 2 minutes. The voltage was then swept cathodically at 100 mV/s. In one experiment (Fig. II-10) the disk electrode was rotated during the potential step and for 1.5 min of the total 2 min. The rotation then was stopped during the last 0.5 min and the potential sweep cathodically. The rotation motion essentially stopped during the half minute before the cathodic sweep. In a second experiment (Fig. II-11), the electrode was passivated without rotation and rotation then started one half minute before the cathodic sweep and continued during the sweep. Peak C_I is not affected significantly by the

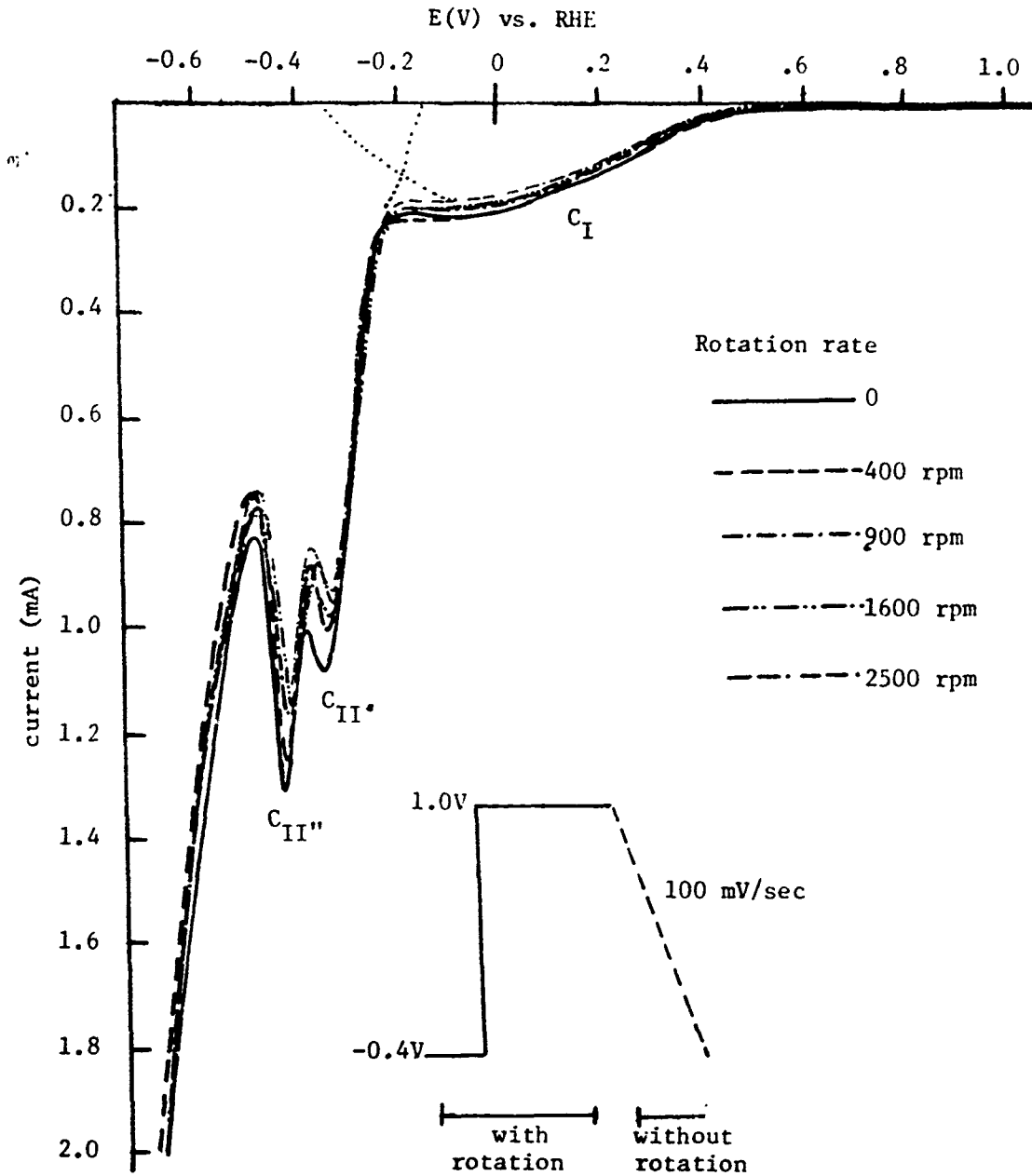


Fig. II-10. Reduction curves of the passivated iron disk electrode in borate buffer (pH 8.4) at different rotation rates.

rotation in either experiment. Peak C_{II} exhibits only minor sensitivity to rotation during passivation prior to the cathodic sweep but was more sensitive to rotation during the cathodic sweep (Fig. II-11). The sub peak C_{II}'' almost disappears at higher rotation rates (≥ 900). The apparent shift and decrease of peak C_{II} , with increasing rotation rate is probably not real but caused by the overlap with peak C_{II}'' . The most simple explanation for the behavior of peak C_{II} is that Fe^{2+} is produced in solution during the reduction peak C_I and then further reduction at peak C_{II} . With strong convection the Fe^{2+} is transported away from the electrode before it can be further reduced at more cathodic potentials.

In the voltage sweep experiments combined with RRDE techniques the reduction of the peak currents for C_I and C_{II} indicates that the ferrous ion dissolves into the solution. The ring current during the reduction process on the disk (scanning the potential through C_I and C_{II}), is highly dependent on the passivation time and passivation potential at which the sample was held. Figure II-8 shows the reduction current on both disk and ring when the potential of the passivated iron electrode is swept to a cathodic potential (-0.6 V) under forced convection.

The reduction of passive film also has been studied with potential step techniques. In this experiment the RRDE has been used to investigate the mechanism of the reduction of passivated iron elec-

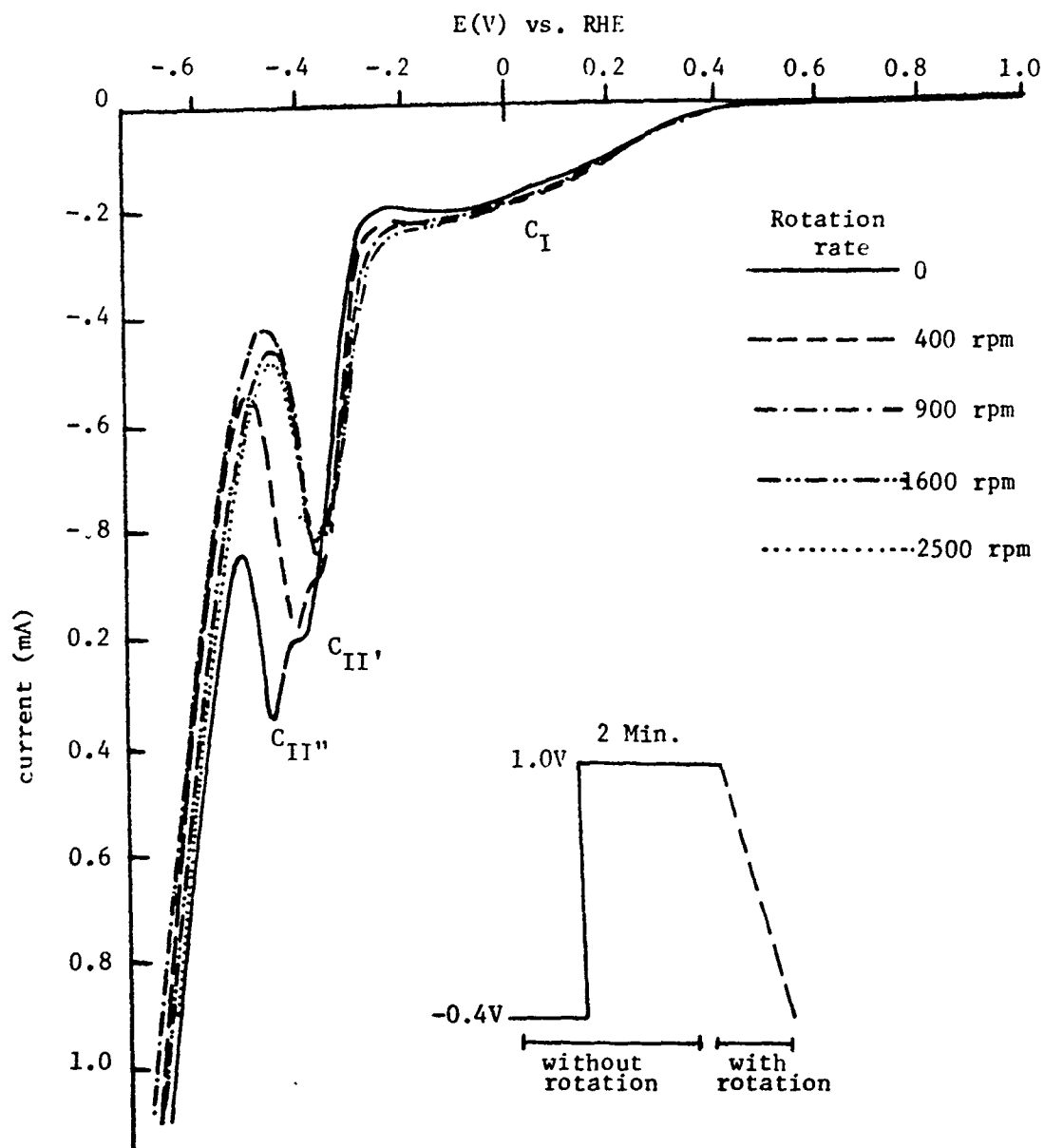


Fig. II-11. Reduction of the passivated iron disk electrode in borate buffer (pH 8.4) under force convection. Electrode area: 0.453 cm^2 .

trode. The iron disk electrode was reduced at -0.4 V for 15-20 min and its potential stepped from -0.4 V to the desired anodic potential (1.0 V). After formation of the passive film with the electrode maintained at this potential for 50 s (single pulse time), the disk potential was stepped to a lower potential (from 1.0 to -0.6 V). The disk and the ring currents were recorded with respect to time during formation and reduction of the passive film (Fig. II-9).

The cathodic current on the disk increased rapidly upon switching back to a cathodic potential (e.g., -0.4 V) from a passivation potential less than $+0.8$ V. The charge (e.g., $1000 \mu\text{C}/\text{cm}^2$ of apparent area) from the integration of the current associated with the sharp cathodic peaks in Fig. II-9, however, is at least one order of magnitude greater than expected on the basis of a simple double layer charge using a capacitance value of $\sim 30 \mu\text{F}/\text{cm}^2$ of apparent area. Even taking into account surface roughness of the film, it is unlikely that the simple double layer charging can account for these peaks.

The spike-like portions at the top of the anodic pulses and bottom of the cathodic pulses are principally due to double layer charging (see Fig. II-9). The major area under the peaks is probably associated with the reduction of an outer portion of the anodic film, but there is some question as to whether the reduction proceeds beyond the Fe^{2+} to Fe^0 because of the irreversibility

of reduction to metallic iron.

For the passive film formed at potentials greater than 0.8 V in Fig. II-9 and Fig. II-9b, the reduction curve splits into two peaks. The fact that the first peak is extremely sharp is probably due to the superposition of the double layer charging spikes. One possible explanation is that the film formed at more anodic passivation potentials has a nonuniform structure. After an outer region has been reduced, the further reduction proceeds more rapidly, thus resulting in an increase in the current at constant applied potential. The outer region that would need to be reduced first would be very thin, perhaps only a few monolayers. This outer region might correspond to the inversion layer described by earlier workers in which higher value states iron species (Fe^{4+} or Fe^{6+}) are being produced because of the extensive band bending. An alternate explanation favored by the author is that the outer region of the layer formed at more anodic potential has a somewhat defect structure, for example, because of differences in the amount of protons in the film. The protons in the film probably play an important role in compensating charges during oxidation and reduction of the film as will be discussed in another section of this thesis.

The window opening experiment (extending the limiting anodic potential for each electrode potential cycle) has been carried out with an iron disk electrode in borate buffer (pH = 8.4). For

each cycle the electrode was held at -0.4 V for 10 min, and then the electrode potential swept (100 mV/s) to the desired potential as shown in Fig. II-12. The curves obtained by sweeping the potential between -0.6 and 0.0 V showed two conjugated peaks (A_I and C_{II}) in the anodic and cathodic sweep (Fig. II-12). When the upper limiting potential was increased to more anodic values $E > 0.25$, a second anodic peak A_{II} appeared which corresponded to the oxidation of ferrous ion in the solution phase on the surface of the passive film. This anodic peak can be related to both the C_I and C_{II} cathodic peaks. The cathodic peak, C_I , is broad and unsymmetric, extending from $+0.45$ to $-.035$ V. It was found that during repeated sweeps (without interruption of the cathodic limit) C_I separated into the two clear peaks (C_I and C_{II}) as is shown in Fig. II-4.

The effect of complexing agents such as ethylene diamine tetraacetic acid (EDTA) on the passivation and reduction of the passive film has been carried out with potential pulse techniques with EDTA at a concentration of 10^{-2} M in borate buffer. The ring current during passivation of the iron and reduction of the passive film was almost two times higher than the ring current in the absence of EDTA (see Fig. II-13). The potential pulse measurement showed that during passive film formation the dissolution of iron to ferrous ion takes place. Figure (II-13) shows that as the potential of the disk was stepped to more anodic potential, the amount of dissolved ferrous ions decreased, but it did not become negligible. The integrated

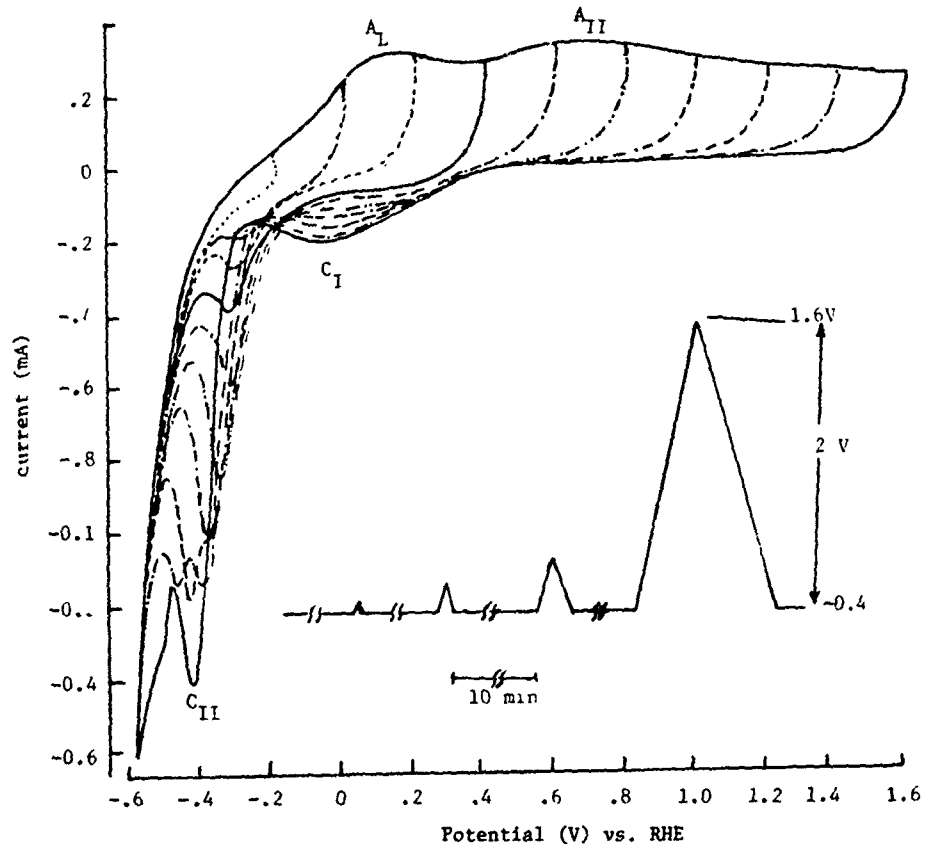


Fig. II-12. Window opening experiment of the iron electrode in borate buffer (pH 8.4). Sweep rate: 100 mV/s, electrode area: 0.453 cm². Electrolytic stagnant.

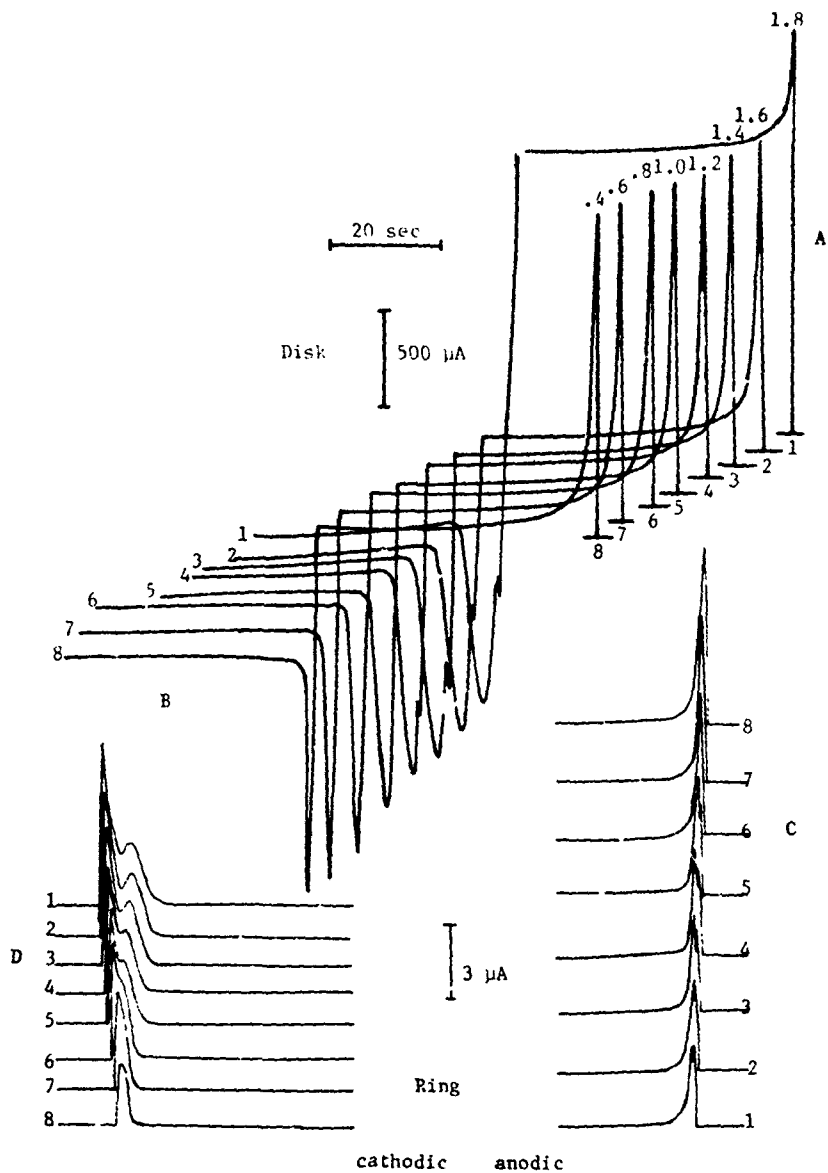


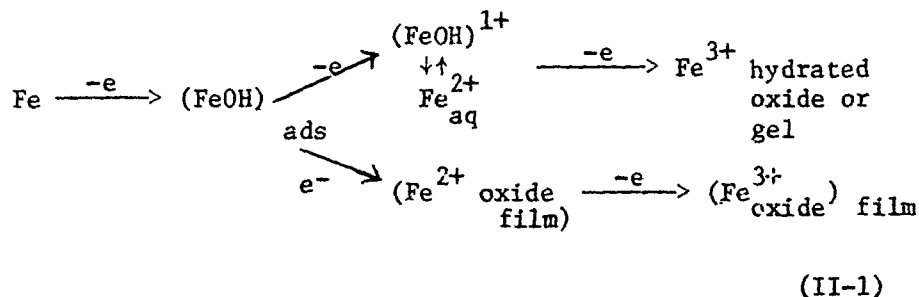
Fig. II-13. Passivation and reduction of iron disk in the presence of EDTA in borate buffer (pH 8.4). Rotation rate: 1000 rpm. A. disk current (potential stepped from -0.4 V to indicated potential); B. Cathodic disk current (potential stepped from indicated values to -0.4 V); C. Ring current corresponding to A; D. Ring current corresponding to D.

charge and currenting due to the oxidation of Fe(II) to Fe(III) indicates that ferrous ion at the interface during passive film formation is enough to form only a few monolayers of a deposited hydrated Fe(III) oxide on the surface of the passive film.

IV. DISCUSSION

The anodic dissolution of an iron electrode is highly pH dependent. Figure II-13 shows the anodic current corresponding to the dissolution of iron which is greater in more acidic medium. As pH decreases the passivation potential and the maximum of the first anodic peak shift to more anodic potential as shown in Fig. II-13. These phenomena can be explained in terms of the higher solubility of ferrous ion and the greater tendency of passive film to dissolve in the more acidic solution.

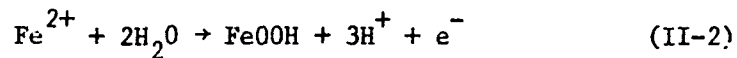
The iron metal dissolution mechanism is believed to be a multi-step reaction, which schematically can be represented as follows:



This scheme is similar to that proposed by Heusler and Schwabe³⁰ except for the $\text{Fe}^{2+} \longrightarrow \text{Fe}^{3+}$ oxide film step.

The process of the dissolution-passivation can follow two pathways as shown in eq. II-1. The ferrous ion which dissolves at

the interface (reaction pathway 1) at a higher anodic potential than the active dissolution region can be deposited to form an outer layer of oxy-hydroxide such as FeOOH, but this is not the passive film. This process can proceed as follows:

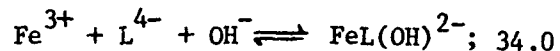
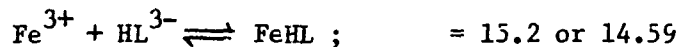
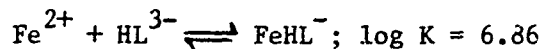


This process is believed to take place at more anodic potentials ($E > E_{A_I}$) in the linear sweep voltammograms. The ferrous species in solution is produced through iron dissolution at less anodic potentials during the anodic sweep. Further evidence for this deposition (eq. II-2) is that the peak potential A_{II} in Fig. II-12 is close to the formation of FeOOH or an equivalent hydrated Fe^{3+} oxide. In addition, the A_{II} peak in Fig. II-12 is highly stirring sensitive which is in good agreement with the postulation of the deposition of Fe(II) from the solution to form hydrated Fe(III) layers on top of the passive film. The layer may have a gel like structure. A similar layer has been proposed by other workers. The thickness of this deposited layer in the presence of stirring is smaller than without stirring. The reason is that the concentration of ferrous ion at the interface at potentials greater than A_I decreases as the rotation speed increases.

Using potential step techniques rather than voltage sweep for passivation, one can decrease the thickness of this deposited overlayer significantly. During the potential pulse the thickness of

the deposited layer is strongly dependent on the potential at which the sample is being passivated. For an iron surface passivated at more anodic potentials (using the potential step) the thickness of the deposited layer is expected to become smaller, since less ring current and Fe^{2+} enters into the solution phase. At low anodic potential the electric field at electrode solution interface is not sufficient to prevent dissolution and subsequent deposition of the ferrous ion occurs. Therefore the thickness of the deposited layer is dependent on the passivation potential.

The addition of the complexing agent EDTA at pH 8.4 can result in the formation of complexes with both Fe^{2+} and Fe^{3+} ions at pH 8.4. EDTA should exist principally in the form of LH^{3-} according to literature data. These equilibrium constants are listed as follows:

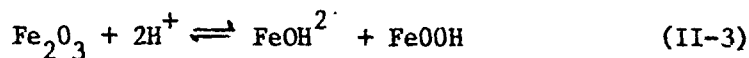


On this basis in a 10^{-2} M EDTA solution one would expect complexing with any Fe^{2+} and Fe^{3+} intermediate in the solution.

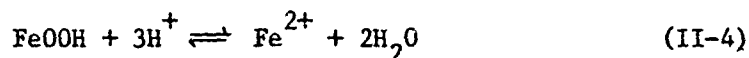
The reduction of the passive film on iron which exhibits two cathodic peaks (C_I and C_{II}) can be described as follows:

First stage: The film which can be concluded to be a ferric

oxide or ferric oxy-hydroxide, is reduced first to a ferrous state at the C_I peak (Fig. II-12). This reduction is actually a solid state process. The dissolution rate of this ferrous state, formed on the surface of passive film, is significant and much greater than the dissolution rate of the ferric oxide in the borate buffer. Therefore the reduction is accompanied with the dissolution of ferrous ion. If the potential of passivated electrode is held at the C_I peak potential, the whole film will eventually be reduced to the Fe(II) state. The reduction at the potential C_I can be represented as follows:



or



The evidence for such a process is that the C_I potential is not stirring sensitive. Therefore the reduction process at C_I does not involve solution phase reactant iron species and is a surface reaction. The dissolved ferrous ion at C_I potential was observed in both the potential sweep and potential step measurements using the rotating ring-disk technique. As we mentioned earlier, the C_I peak is a broad peak with the reduction of the solution precipitated Fe(III) over layer also taking place at the more cathodic part of this C_I peak. Evidence for this is the observation that the potential for the reduction of the Fe(III) layer deposited on Au from solutions

containing Fe(II) ions is the same as that for the more cathodic peak of C_I . In addition, as we mentioned earlier, during repetitive potential cycling the two conjugated peaks (A_{II} and the lower part of C_I) increase with each potential cycle. This is because ferrous ion increases during any one cathodic sweep or anodic sweep and is precipitated in the form of Fe(III) hydrated oxide over-layer and thus is more available to produce Fe^{2+} in successive sweeps. Therefore, the peaks corresponding to the redeposition and reduction of this deposited layer are enhanced with each potential cycle.

The broadness of the C_I may be caused by the defect structure of passive film and also overlapping of two peaks, one from the reduction of passive film from ferric state to ferrous state and the other corresponds to the reduction of the deposited layer from Fe(III) to Fe(II) state. As discussed earlier, the second cathodic reduction peak C_{II} corresponds to the reduction of a ferrous oxide in the film as well as in the Fe(II) solution. The redeposition of ferrous ion to form the metallic state changes the roughness of the electrode because the deposition and growth of this deposited iron are not uniform. Dendrite-like iron deposit may grow on the surface of the iron electrode.

The process of reduction of ferrous ion to metallic iron is accompanied by some hydrogen discharge.

V. CONCLUSION

Evidence exists that the passive film formed on iron with the potential sweep method is covered with a deposited overlayer of an Fe(III) oxy-hydroxide. Such an overlayer may also form during the potential step measurements with the thickness of the overlayer strongly dependent on the potential of passivation and the pH of the solution. At higher anodic potentials and pH 8.4 the thickness of this deposited overlayer would be at the most only a few monolayers and may not form at all since much less Fe(II) enters into the solution.

The author believes that some of the problems and ambiguities in the field of passivation studies are related to the existence of this deposited overlayer. The majority of corrosion scientists have either not taken into account the existence of this deposited overlayer or have considered it as a part of the passive film. This deposited layer on top of the passive film, however, is a foreign layer and is not part of the protective passive film.

A number of ambiguities and apparent contradictions concerning the properties of the passive film on iron can be explained in terms of the proposed deposited Fe(III) overlayer. These include the following observations reported by various workers:

1. The passive film has a sandwich or multilayer structure with the composition of the layers different.
2. There are several types of bonded water molecules in the passive film.

3. The passive film contains anions which are incorporated in the film, but are mostly found on the outer surface of passive film, and highly dependent on the rinsing procedure.
4. The structure of passive film is amorphous and after aging or dehydration crystallizes to a fine grain crystalline structure.

Each of these reported observations is compatible with the proposed deposited overlayer. Such a deposited overlayer is expected to have gel-like structures. In the case of iron, this deposited layer is probably FeOOH .

The open structure of the deposited layer can serve as a trap for water molecules and anions such as borate. The water molecules and anions can be bonded through hydrogen bonding in the open void structure of FeOOH . Figure II-14 shows a schematic representation of the passive film and foreign deposited overlayer containing water molecules and borate anions.

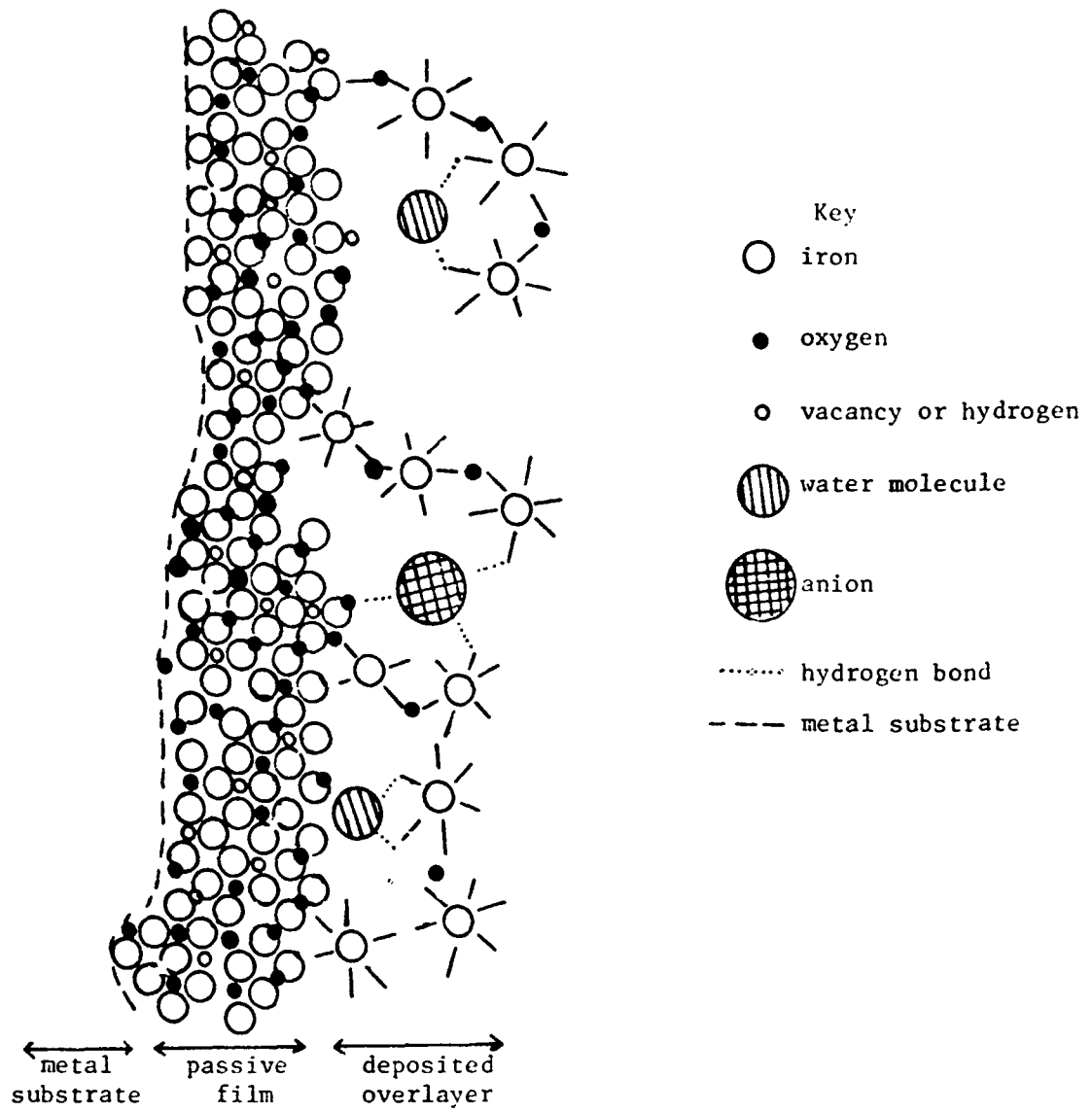


Fig. II-14. Structural model for a passive film and deposited overlayer.

REFERENCES

CHAPTER II

1. N. Sato and M. Cahen, J. Electrochem. Soc. 111, 512 (1964).
2. Ibid, p. 519.
3. W.J. Lorenz, G. Eichkorn and C. Mayer, Corrosion Sci. 7, 357 (1967).
4. B. Kabanov, R. Burstein, and A.N. Frumkin, Discussions Faraday Soc. 1, 259 (1947).
5. T.P. Hoar and J. Holliday, J. Appl. Chem. 3, 502 (1953).
6. T.P. Hoar and T.W. Farrer, Corrosion Sci. 1, 49 (1961).
7. V.M. Novakovskii and Y.M. Kolotyркиn, Zash. Met. 8, 283 (1972).
8. H.H. Uhlig, Electrochem. Acta 16, 1939 (1971).
9. L. Germer and A. Macrae, Proc. National Acad. Sci., U.S. 48, 997 (1962).
10. H.H. Uhlig, Passivity and Its Breakdown on Iron and Iron Base Alloys (Houston, National Association of Corrosion Engineers, 1976) p. 19.
11. H. Gerischer, Electrochim. Acta 2, 1 (1960).
12. V. Bruslic, Ph.D. Thesis, University of Pennsylvania (1971).
13. K.J. Vetter, Electrochemical Kinetics Theoretical and Experimental Aspects (Trans. by Scripta Technica), New York, Academic Press, 1967.
14. U.R. Evans, J. Chem. Soc. (London) 1020 (1927).
15. N. Sato, K. Kudo and T. Noda, Electrochim. Acta 16, 1909 (1971).
16. Masa-ichi Nagayama and M. Cohen, J. Electrochem. Soc. 110, 670 (1963).
17. B. Agius and J. Siejka, J. Electrochem. Soc. 120, 1019 (1973).

18. K. Asami, K. Hashimoto and S. Shimodaira, Corrosion Sci. 18, 151 (1978).
19. L. Øjefors, J. Electrochem. Soc. 123, 1691 (1976).
20. J. O'M. Bockris and D. Drazic, Electrochim. Acta 7, 293 (1962).
21. J. O'M. Bockris and H. Kita, J. Electrochem. Soc. 108, 676 (1961).
22. H. Saito, T. Shibata and G. Okamoto, Corrosion Sci. 19, 693 (1979).
23. M. Fleischmann and H.R. Thirsk, J. Electrochem. Soc. 110, 688 (1963).
24. E.J. Kelly, J. Electrochem. Soc. 112, 124 (1965).
25. G. Eichkorn, W.J. Lorenz, L. Albert and H. Fischer, Electrochim. Acta 13 183 (1968).
26. J.A. Harrison and W.J. Lorenz, Electrochimica Acta 22, 205 (1977).
27. R.S. Schrebler Guman, J.R. Vilche and A.J. Arvia, Electrochimica Acta 24, 359 (1979).
28. K.A. Christiansen, H. Hoeg, Kirsten Michelsen, G. Bech Nielsen and H. Nord, Acta Chem. Scand. 15, 300 (1961).
29. W. Allgaier, K.E. Heusler, J. Appl. Electrochem. 9, 155 (1979).

CHAPTER III
IN-SITU LASER RAMAN SPECTROSCOPY OF ANODIC
PASSIVE FILM ON IRON AND AIR OXIDIZED IRON
AND IRON-CHROMIUM ALLOYS

I. INTRODUCTION

In view of the importance of the anodic oxide film a great number of experimental techniques have been used to elucidate the structure and composition of the anodic film. Many of the ex-situ techniques for surface studies do not have great potential for use in anodic film studies. The reason is that the majority of ex-situ techniques require high vacuum. The preferred methods in surface electrochemistry are those which can be used to examine the surface of the electrode in-situ while the electrode is under potential control. However, there are only a few in-situ techniques available to study the structure of anodic film. Optical reflectance spectroscopy including attenuated total reflectance (ATR) and ellipsometry as well as Mössbauer have been used by various workers for this purpose. Recently Raman spectroscopy has been employed as a powerful in-situ tool in the field of surface electrochemistry with metal electrodes such as Ag.

In the present studies this technique has been used to investigate the structure of the anodic passive film on iron electrode as well as oxides formed on iron-chromium alloys at high temperature.

While other workers have attempted to obtain in-situ Raman

spectra for the passive film on iron, to the best of our knowledge the spectra presented in this chapter are the first obtained for this film.

To facilitate the interpretation of the Raman spectra of the passive film additional spectra have been obtained for iron oxides such as $\alpha\text{-Fe}_2\text{O}_3$ and Fe_3O_4 and also the spectra of the electrochemically deposited oxy-hydroxide on the surface of passive film.

II. THEORY OF SURFACE RAMAN SPECTROSCOPY

Since the early report by Fleischmann et al.¹ of high intensity Raman signals for adsorbed pyridine on the surface of silver, extensive efforts have been made to explain the mechanism of this unexpected but important intense Raman signal. Van Duyne et al.² and others^{3,4} calculated the intensity ratio of Raman lines of some molecules such as pyridine on the surface of silver electrodes. The intensity of adsorbed pyridine is about 10^6 times greater than the intensity for the pyridine in the bulk of solution. Several theories and models have been developed to explain the behavior of this surface enhanced Raman spectroscopy (SERS).

Van Duyne² explained the phenomena of SERS on the basis of the image dipole model. The induced dipole in the adsorbed molecule results in an image dipole in the metal whose field further increases the induced dipole in the absolute. The induced dipole in this theory is presented as follows

$$\mu = \alpha_z (E + E_{\text{image}}) \quad (\text{III-1})$$

where α_z is the component of the polarization of the molecule on the surface which is a function of the distance of the molecule from the electrode surface. The enhancement is due to the perpendicular component of the dipole on the surface.

Otto et al.⁵ has proposed that the enhancement in the Raman signal is related to the scattering processes in the metal rather than in the adsorbed molecule. In this model the electrons at or near the surface (conduction band electrons) oscillate with the vibration of the adsorbed molecule, and the reflectance of the metal surface therefore is modulated at the frequency of vibrating molecules. This gives rise to side bands in the scattered light.

Several other explanations for this phenomena (SERS) also exist such as a collective resonance Raman process for the adsorbent-adsorbate system. Even the classical model for light scattering on a highly conducting metal leads to considerable enhancement, according to Meitue and Eforma.⁶ SERS has generally been observed only on the surface of metals such as silver which have a certain degree of controlled roughness. Kötzt and Yeager⁷ produced roughening of silver by cycling the potential over an appropriate range. They found that the intensity of the enhanced Raman is dependent on the number of cycles. After a certain number of potential sweeps, the intensity essentially reaches a limit. Unfortunately the surface enhancement is very large ($> 10^4$) for only a few metals such as Ag, Cu and Au, but is still substantial (10^2 - 10^3) for a number of other metals such as nickel and probably including iron.

III. EXPERIMENTAL PROCEDURE

A. Reagents

The purified borate buffer (pH 8.4) mentioned in Chapter II has been used. This electrolyte was saturated with pure argon gas for 12 hours. Ferrous sulfate (analytical grade) was obtained from the Fisher Scientific Company. Pure iron oxides (Fe_3O_4 and $\alpha\text{-Fe}_2\text{O}_3$) were obtained from Harshaw Chemical Company. 1-10 orthophenanthroline was obtained from

B. Electrode and Cell Design

In this experiment a rectangular quartz cell with optical windows has been used. An iron (99.999%) electrode (8 mm x 15 mm) obtained from Organics-Inorganics Co. was used as a working electrode. $\alpha\text{Pd-H}$ electrode was used as a reference and platinum wire as a counter electrode.

For each experiment the iron electrode was polished with diamond pastes of grades 5,3,1,.3,.1 and 0.05 μm . After polishing with each diamond paste, the electrode was cleaned in distilled water in an ultrasonic bath and further rinsed with distilled water. The optical electrochemical cell was attached to the mounting shown in Fig. III-1 which provided three degrees of movement with micrometers to facilitate alignment.

For control of the potential, the PARC potentostat and programmer were used. The electrochemical cell and its electrodes were tested separately, using voltammetry and the potential step technique. The results of these tests were exactly the same as

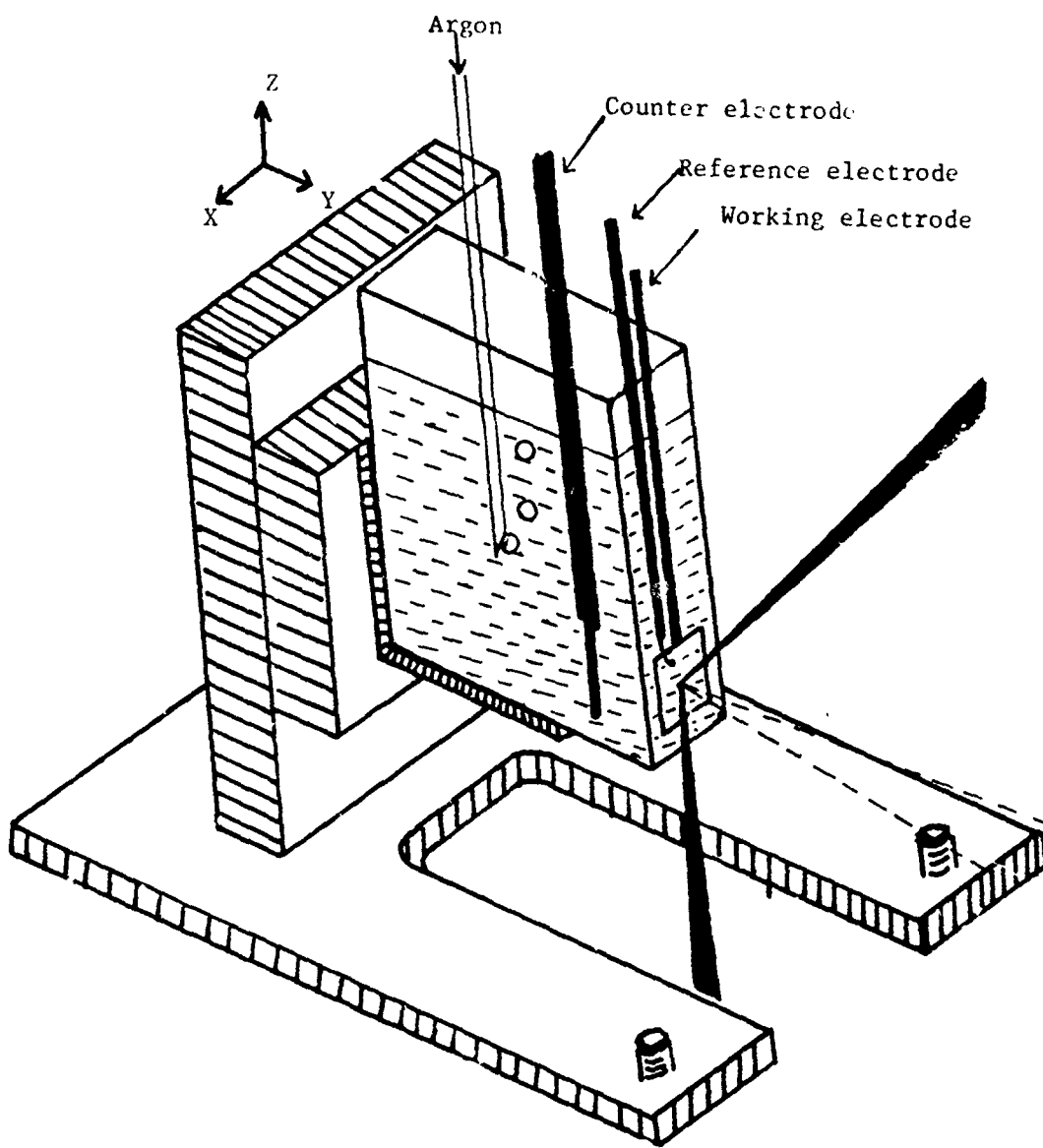


Fig. III-1. Optical electrochemical cell and its attachment for in-situ laser Raman spectroscopy.

those reported in the second chapter.

C. Alignment

Proper alignment is very important for Raman spectroscopy.

The following alignment procedure has been carried out.

- a. The incident laser beam is focused at the focus point A for the collecting lens L_2 (see Fig. III-2). This produces the maximum intensity of the laser beam. At this stage the laser beam is perpendicular to the surface of the Ramalog spectrometer table and a symmetric cone shape beam passes through the focusing lens L_1 (Fig. III-2). This part of alignment can be achieved by tilting the lens (L_1).
- b. The power of the laser beam is checked with a power meter placed at a position above A (Fig. III-2) so as to intercept the whole beam without the cell in place. The power was recorded before each experiment to check the stability of the laser plasma tube.
- c. The electrochemical cell with connections to the potentiostat already in place was positioned on the base M (see Fig. III-2). The laser beam passed through the electrochemical cell and reflected from the surface of the electrode. The angle of the electrode surface relative to the incident beam was about 65° , which insures that the specular reflectance beam from the electrode did not enter the collection lens.

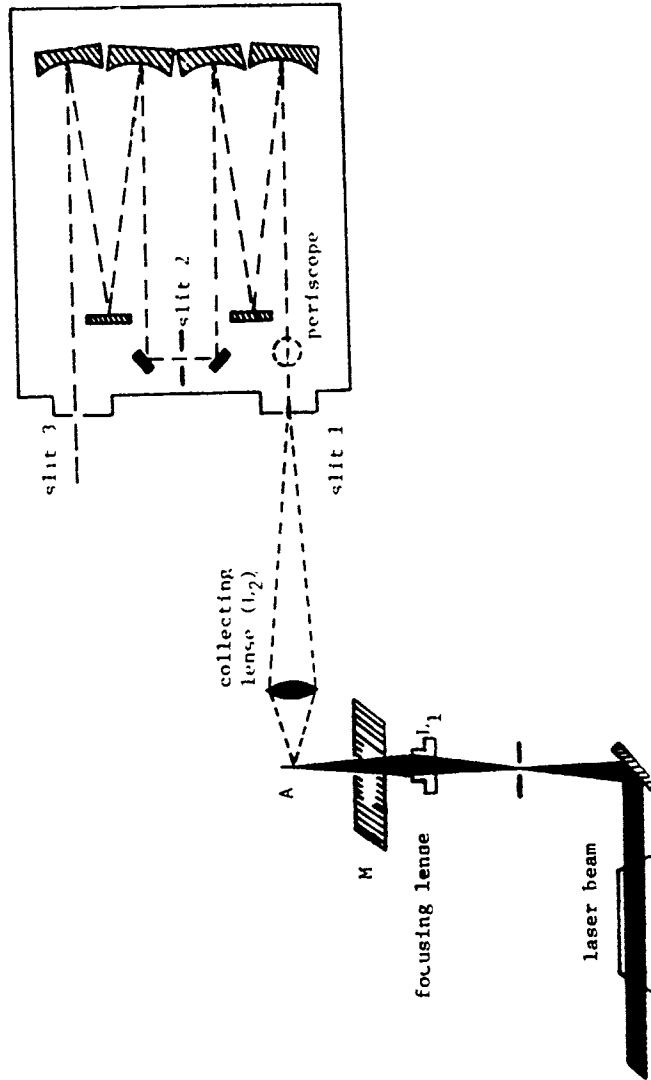


Fig. III-2. Beam path in Spex Ramlog spectrometer.
A - iron electrode surface; M - mounting platform for cell.

prism

- d. The scattering light was collected and focused on the first entrance slit of the spectrometer by the collecting lens (L_2). This part of the alignment can be done by adjusting lenses L_1 and L_2 and also the location of the electrode. The proper alignment at this stage can be obtained by viewing the slit and source by using a periscope alignment optical system which is a part of the Spex Ramalog system and is located beyond the entrance slit of the double monochromator. This periscope permits one to view the region from which the light is collected by lens L_2 . With the electrode in place and properly aligned, one sees a greatly magnified image of the electrode surface in sharp focus.
- e. After alignment the periscope mirror is removed from the beam and the light allowed to pass through the spectrometer. Further optimization can be achieved by slightly changing the position of L_2 with the micromovement controls for this lens (L_2). This optimization for giving a strong Raman signal sample can be accomplished by adjusting the collection lens for a maximum intensity of a particular Raman band. However, for an unknown sample it is difficult to obtain optimum conditions and the periscope system itself must be aligned sufficiently well relative to

the collection point for L_2 to give very close to optimum Raman signal strength. The angle of the incident laser beam on the sample also has a strong effect on the Raman signal strength. For most flat specimens an angle of incidence for the laser beam of 60-70° is optimum.

After proper alignment, the spectrometer-detector system is adjusted to give the desired wave number, range, scan rate and integration time.

IV. RESULTS AND DISCUSSION

The following spectra have been obtained using 514.5 nm (green light) as the incident laser beam.

1. The Raman Spectrum of Borate Buffer Solution (pH 8.4)

Figure III-3 shows the Raman spectrum of the electrolyte which has a rather sharp Raman peak at about 875 cm^{-1} due to the borate buffer.

2. Raman Spectrum of the Cathodically Protected Iron Surface

First the optically polished electrode was reduced cathodically for 15 mins and then to remove the ferrous ion from solution the electrolyte was replaced with fresh electrolyte, saturated with argon gas. The potential of the electrode during the changing of the electrolyte was kept constant at -0.4 V vs. RHE. Then the electrode potential was changed to -0.35 V to lower the hydrogen discharge on the surface of the electrode which caused bubble form-

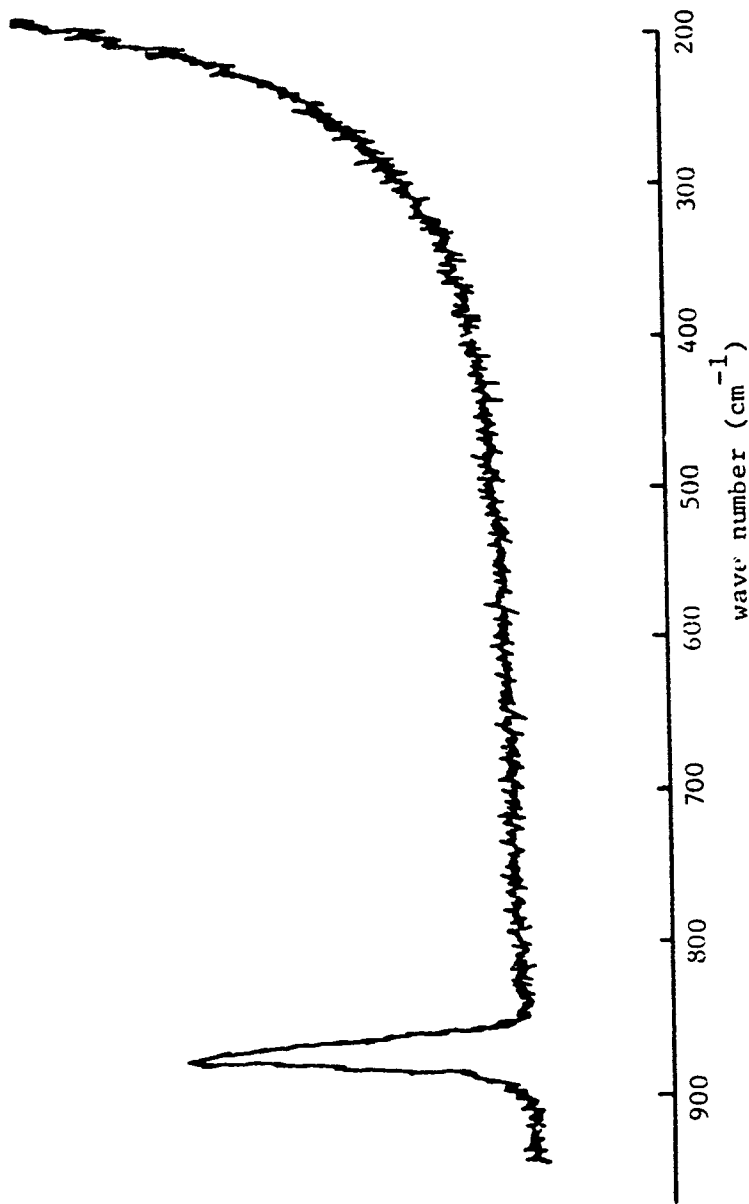


Fig. III-3. Raman spectrum of borate buffer (pH 8.4). Laser beam 514.5 nm. Slits 400/400/400. Full scale 1K (CPS).

ation. The Raman spectrum of the cathodically protected iron surface at this potential (-0.35 V) was then recorded over the range of 200 to 900 cm^{-1} (Fig. III-4). This Raman spectrum showed only one peak associated with the borate in the solution at 875 cm^{-1} .

3. Raman Spectrum of the Passivated Iron Electrode

After cathodic treatment of the iron electrode the potential was stepped to the desired passivation potential and held constant for half an hour with the laser beam blocked from impinging on the electrode surface. The Raman spectrum was then recorded. Figure III-4 shows the Raman spectrum of the passive film formed at different potentials. The spectra were recorded from 200 to 900 cm^{-1} . Because of the low signal and high noise level, the integration time was long (20 s/count). Each spectrum required about 3 hours to be recorded.

4. Raman Spectrum After Reduction of the Passive Layer

The potential of the passivated iron electrode was then stepped to the cathodic potential (-0.4 V) and maintained at this potential for 20 min. The Raman spectrum of electrode was then recorded. Figure III-4 shows that the Raman peaks disappeared at this potential. This result provides evidence that the Raman peaks obtained at the passivation potential do correspond to the structure of the passive film. Reducing the film at the cathodic potential caused them to disappear.

The Raman measurements show that the spectra from 0.8 V up to 1.4 V are almost the same but the intensities for more anodic

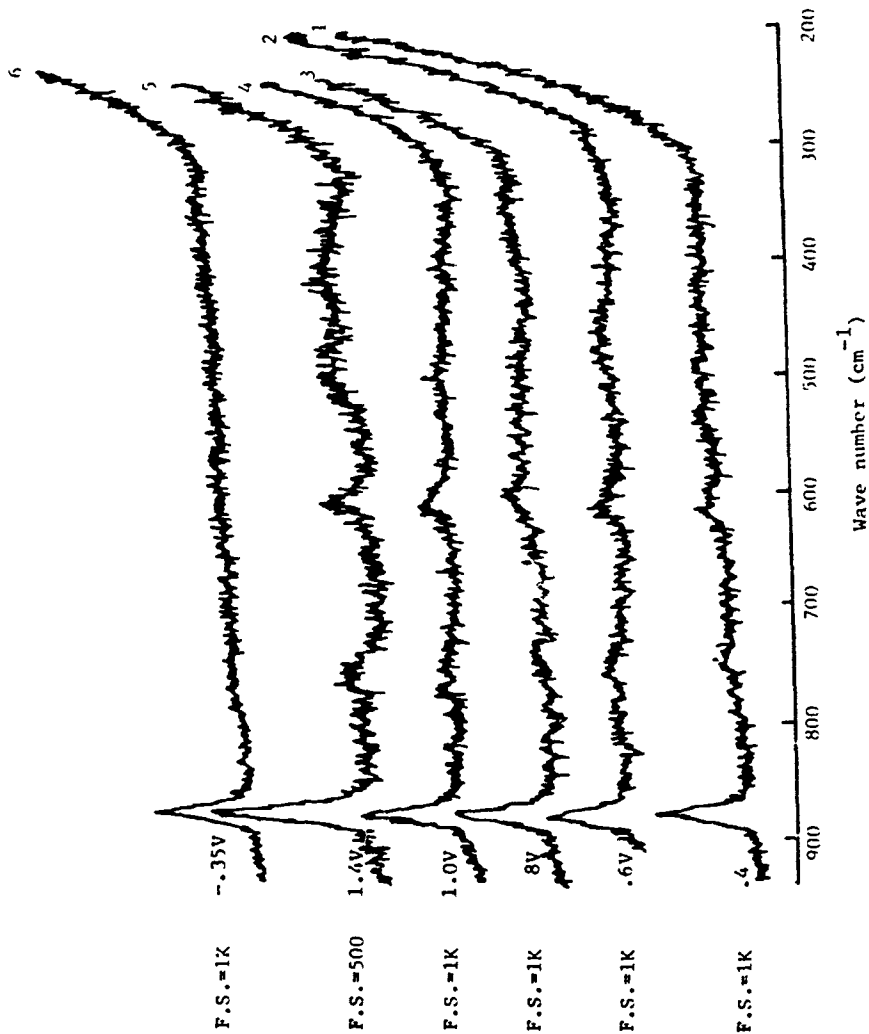


Fig. III-4. Raman spectra of passive film formed on iron in borate buffer (pH 8.4) at 0.4, 0.6, 0.8, 1.0, 1.4 V. Full scale (1.2, 3, 4.6) = 1K CPS; F.S. (5) = 500 CPS.

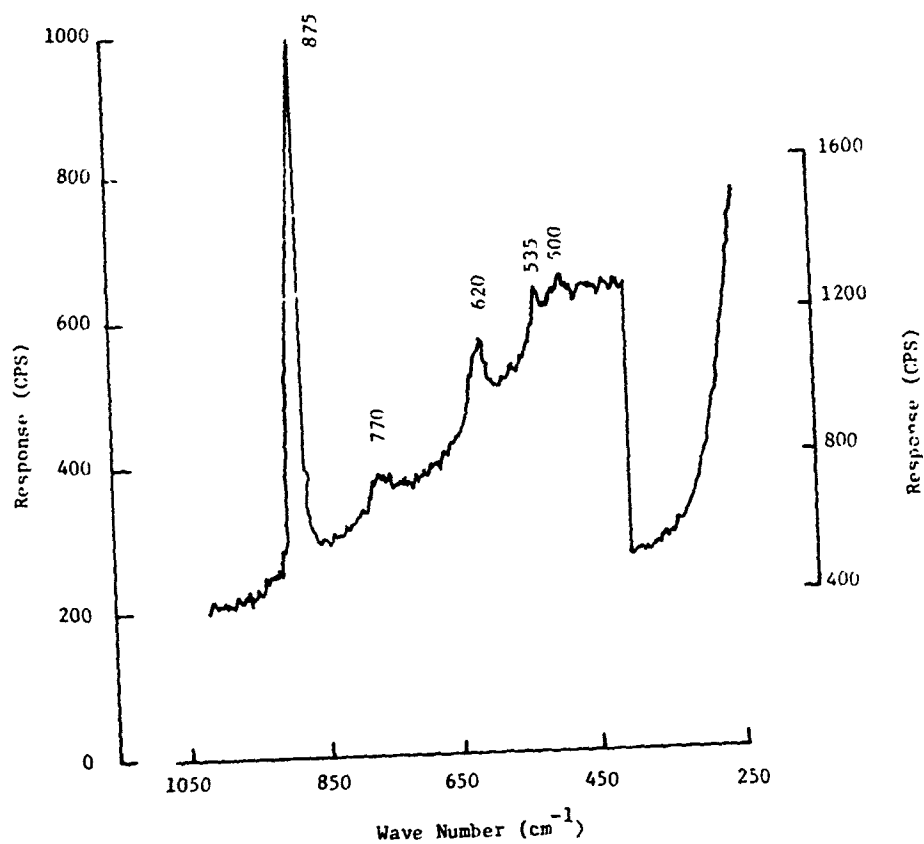


Fig III-4a. Raman spectroscopy (*in-situ*) of passive film on pure iron in borate buffer (pH = 8.4) at 25°C. Passivation time prior to scan 0.50 hrs, scan time: 3.5 hrs., with increasing wave number. $\lambda_o = 514.5$ nm.

potentials are higher. With the exception of the peak at 875 cm^{-1} , all peaks between 200 and 800 cm^{-1} are due to the passive film.

To facilitate the interpretation of this spectrum the following complementary experiments have been done.

The iron electrode was passivated at 1.0 V in 10^{-4} M FeSO_4 plus borate buffer (pH 8.4) for 30 min. In this experiment the ferrous ion is oxidized on the surface of the electrode and deposited in the Fe(III) state, probably as a hydrated oxide. The thickness of this film is much greater than that of the passive film. To obtain the Raman spectrum of this film, the electrolyte was replaced with a borate buffer solution free from ferrous sulfate. The reason for this was to prevent the overlap of the Raman peak of ferrous sulfate and that of the oxide film on the surface of the electrode. Figure III-5 shows the Raman spectra of this deposited layer. Based upon literature data of Keisers *et al.*⁸ this in-situ spectrum appears to correspond to the $\gamma\text{-FeOOH}$ iron oxy-hydroxide run ex-situ

The Raman spectra of iron oxide powder (Fe_3O_4 and $\alpha\text{-Fe}_2\text{O}_3$) were also obtained. In this case the iron oxide powders were pressed into a disk (1 cm diameter and 0.3 cm height) without any binder or matrix. These samples were mounted in the rotating sample holder of the Spex Ramalog spectrometer and rotated at $\sim 1000\text{ rpm}$ while the Raman spectrum was recorded. The rotator was used to minimize beam heating or any physical or chemical changes associated with heat or photochemical effects. The spectra is given in Fig. III-6 and 7.

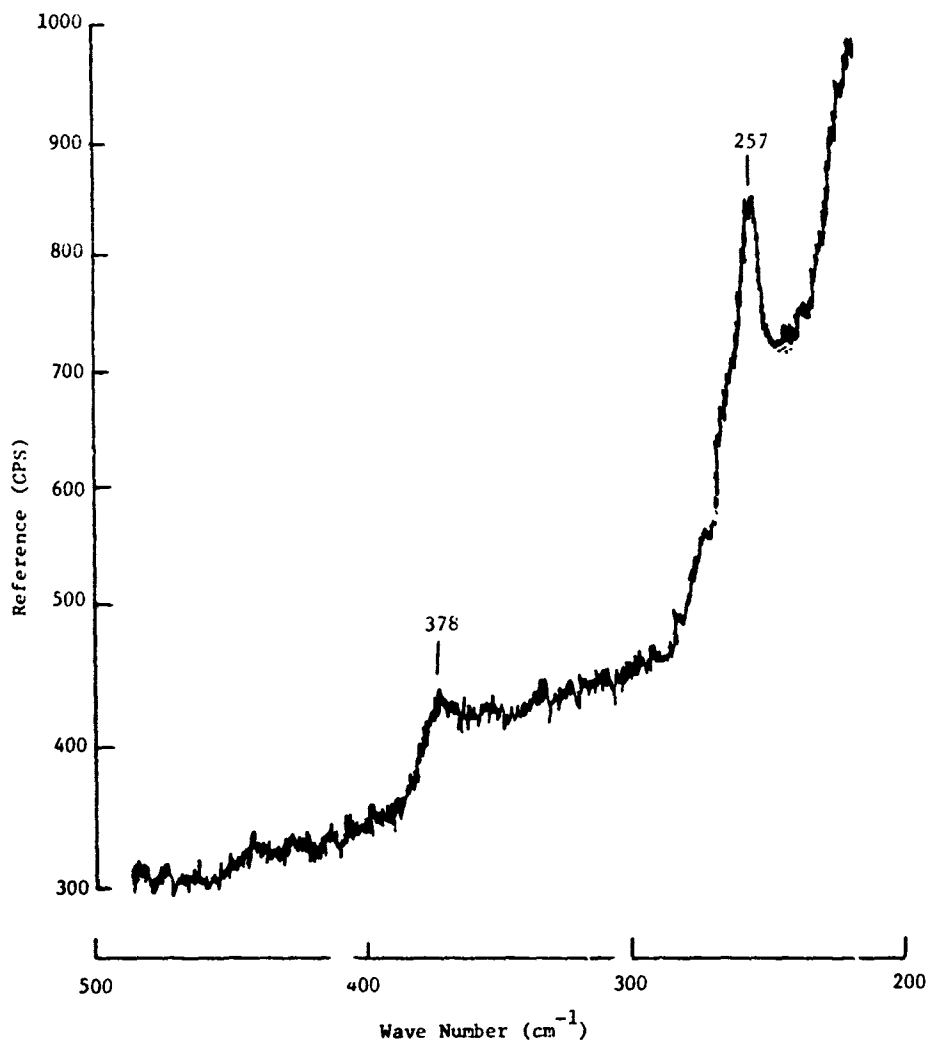


Fig. III-5. Raman signal of deposited ferris oxy-hydroxide (FeOOH) $\lambda = 514.5$ nm

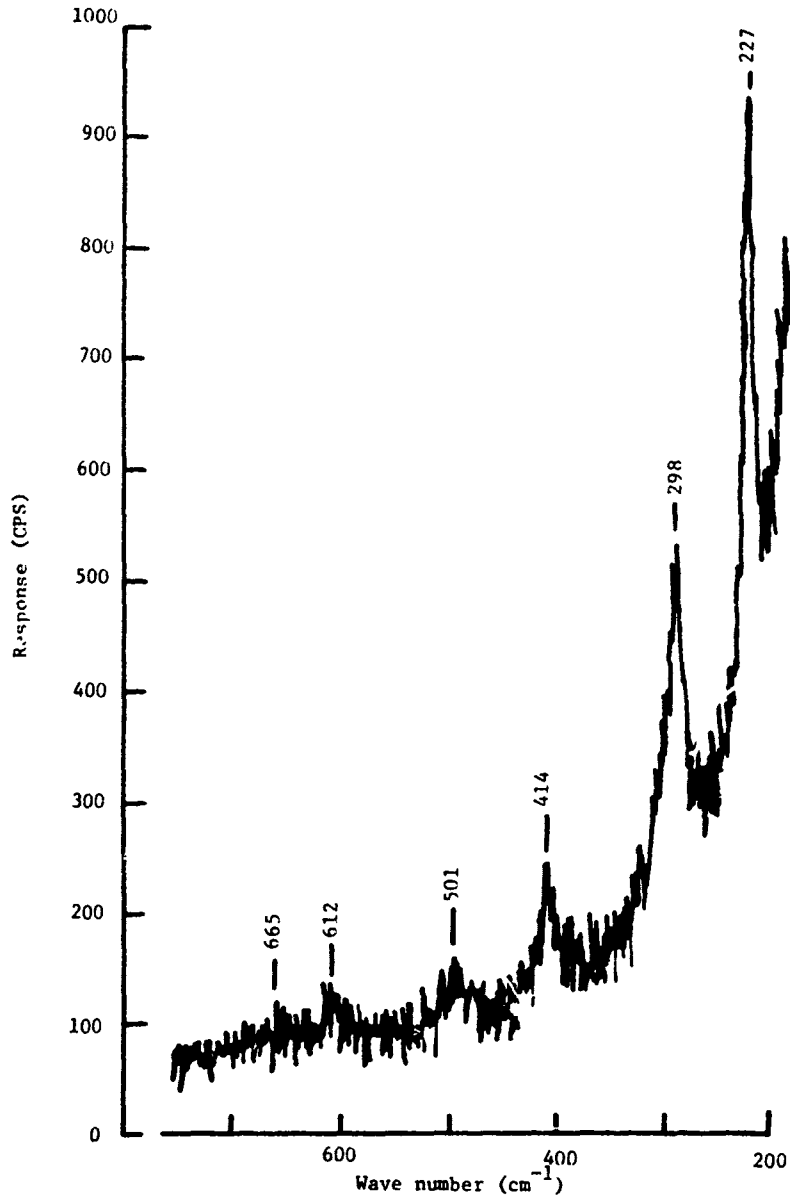


Fig. III-6. Raman signal of $\alpha\text{-Fe}_2\text{O}_3$ (Harshaw Chemical Co.) in the form of pressed disk: examined in air, $\lambda_0 = 514.5 \text{ nm}$.

Table III-1: Comparison of Raman frequencies (cm^{-1}) of passivation film (in-situ) formed at 1.0 V vs. NHE in borate buffer (pH 8.4) and film on air oxidized iron-chromium alloys at 500°C (1 hour) with published data for iron oxides and oxy-hydroxides

Literature Data		Present work									
Fe_3O_4 (O_h) ^a	$\alpha\text{-Fe}_2\text{O}_3$ (O_d) ^b	FeO c,c	Fe_3O_4 c,c	$\alpha\text{-Fe}_2\text{O}_3$ c	r-FeOOH c	$\alpha\text{-FeOOH}$ c	$\alpha\text{-Fe}_2\text{O}_3$ c	Fe_3O_4 buff	Air oxidized 500°C 1 hr	Passive film in-situ	Deposited ferric layer
	613 cm^{-1} E_g	663 cm^{-1}	663 cm^{-1}	612 cm^{-1}	380 cm^{-1}	550 cm^{-1}	665 cm^{-1}	667	673	700 cm^{-1}	257
550 T_{2g}	498 A_{1g}	616	616	501	252	474	612	612	613	620	378
420 T_{2g}	412 E_g			414		414	501	425	501	535	
320 E_g	299 E_g			298		397	414		412	500	
298 T_{2g}	293 E_g			293		298			245		
	247 E_g			245		277			245		
	225 A_{1g}			227					225		

Uns. Magnon: 472

Two Magnons: 1320

^aT.R. Hart, H. Temkin and S.B. Adams, "Light Scattering in Magnetite Fe_3O_4 " in Proceedings of the Third International Conference on Light Scattering in Solids, M. Balkanski, R. Leite and S. Porto, eds., Flammarion Sciences, Paris, 1976, pp. 254-8.

^bT.R. Hart, S.B. Adams and H. Temkin, "Raman Scattering from Phonons and Magnons in $\alpha\text{-Fe}_2\text{O}_3$," loc. cit., pp. 259-263.

^cR.J. Thibau, C.W. Bron and R.H. Heidersbach, Applied Spectroscopy 12, (1978) 532.

^dDeposited ferric oxide-hydroxide

^eThibau et al. report the same frequencies for both FeO and Fe_3O_4 . This is surprising and implies that at least the surface layers have the same structure for both specimens.

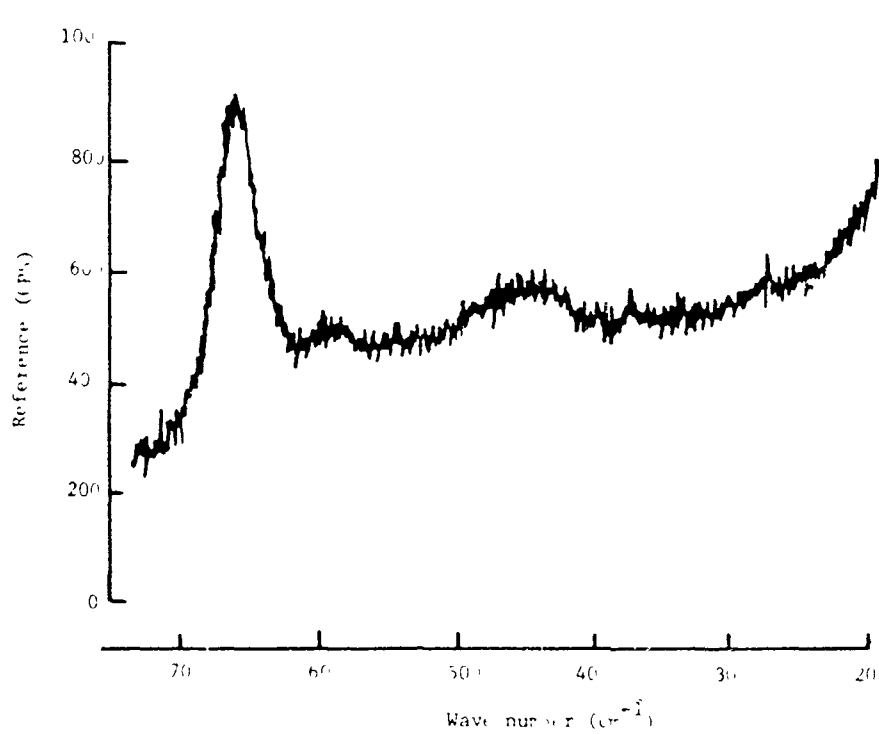


Fig. 117-11. Kramér signal of Fe₃O₄ (Garslow Chemical Co.) in the form of pressed disc; examined in air, $\lambda = 514. \text{m}\mu$.

Raman spectroscopy has also been used to follow the introduction of Fe into the solution from an iron electrode during potential sweeping. For this work the complexing agent, 1-10 orthophenanthro line was added to the solution in a concentration of 10^{-4} M. The electrode surface was oriented parallel to the laser beam and the beam focused within ~ 1 mm from the surface. The spectrum in the absence and presence of iron added as 10^{-4} M FeSO_4 is shown in Figs. III-8 and 9. It is not clear whether the Fe complex is in only the II valence state. Most likely the $(\text{OHP})_3\text{Fe(II)}$ and $(\text{OHP})_3\text{Fe(III)}$ complexes are present. In any event the complexing of (OHP) with either results in the loss of the 2751 cm^{-1} peak. This peak then was monitored when the iron electrode was swept anodic at 1 mV/s from -0.4 to 0.1 V, the latter of which is in the active range. The marked decrease on the signal in Fig. III-10 indicates the introduction of the Fe into the electrolyte. The valence state is most likely II but this measurement will not necessarily discriminate between the two valence states. Unfortunately it was not possible to detect any further change in signal strength at more anodic potential.

V. CONCLUSION

The Raman spectrum of the passive film on the surface of iron shows several Raman peaks which correspond to the structure of passive film. The peaks do not match well with any peaks in the oxide and oxy-hydroxides of known structures. The closest match is that for the 620 cm^{-1} peak in the passive film and the $612\text{-}613 \text{ cm}^{-1}$

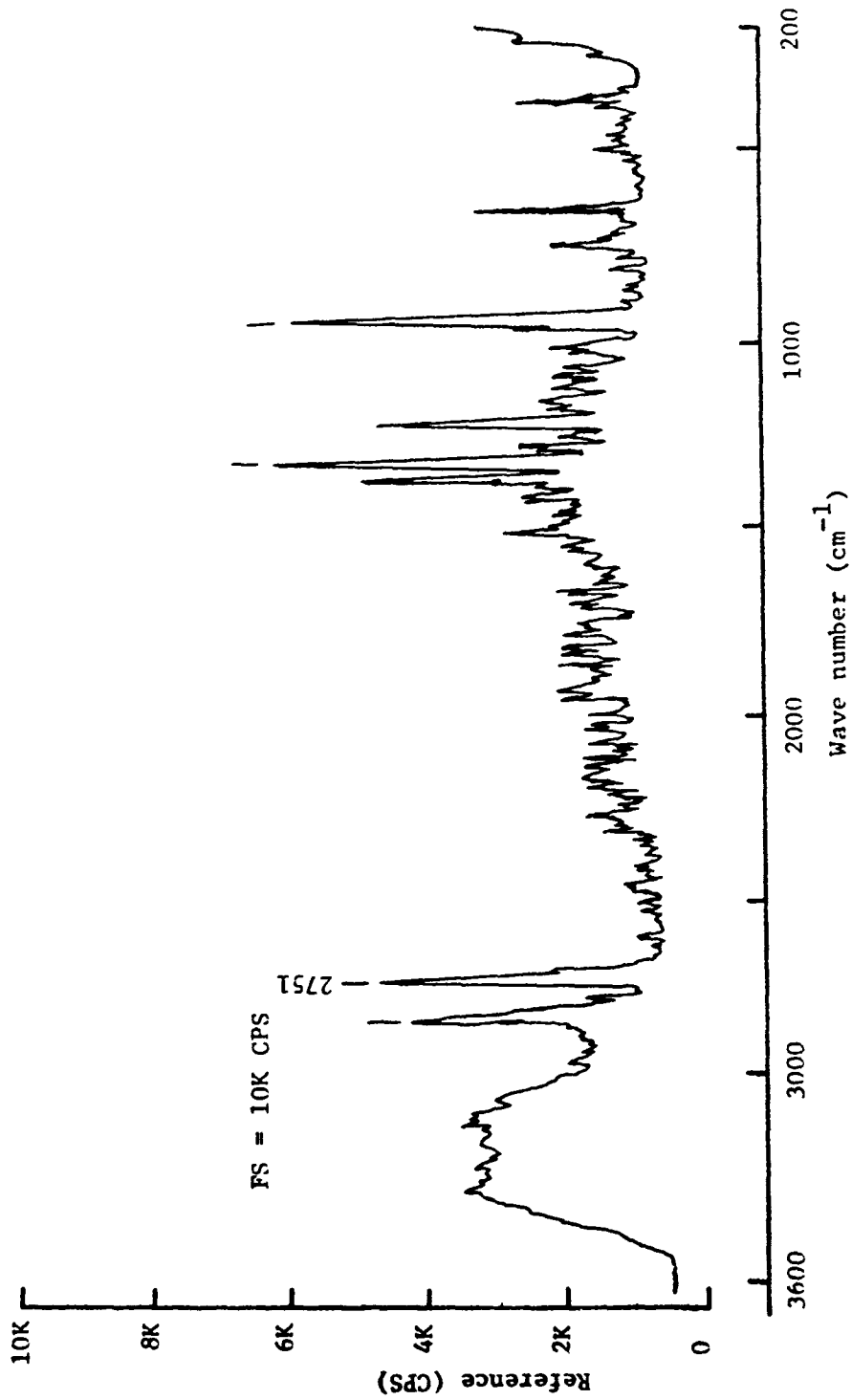


Fig. III-8 . Raman signal of 1-10 orthophenanthroline in borate buffer (pH 8.4) without iron ion present, $\lambda = 514.5 \text{ nm}$

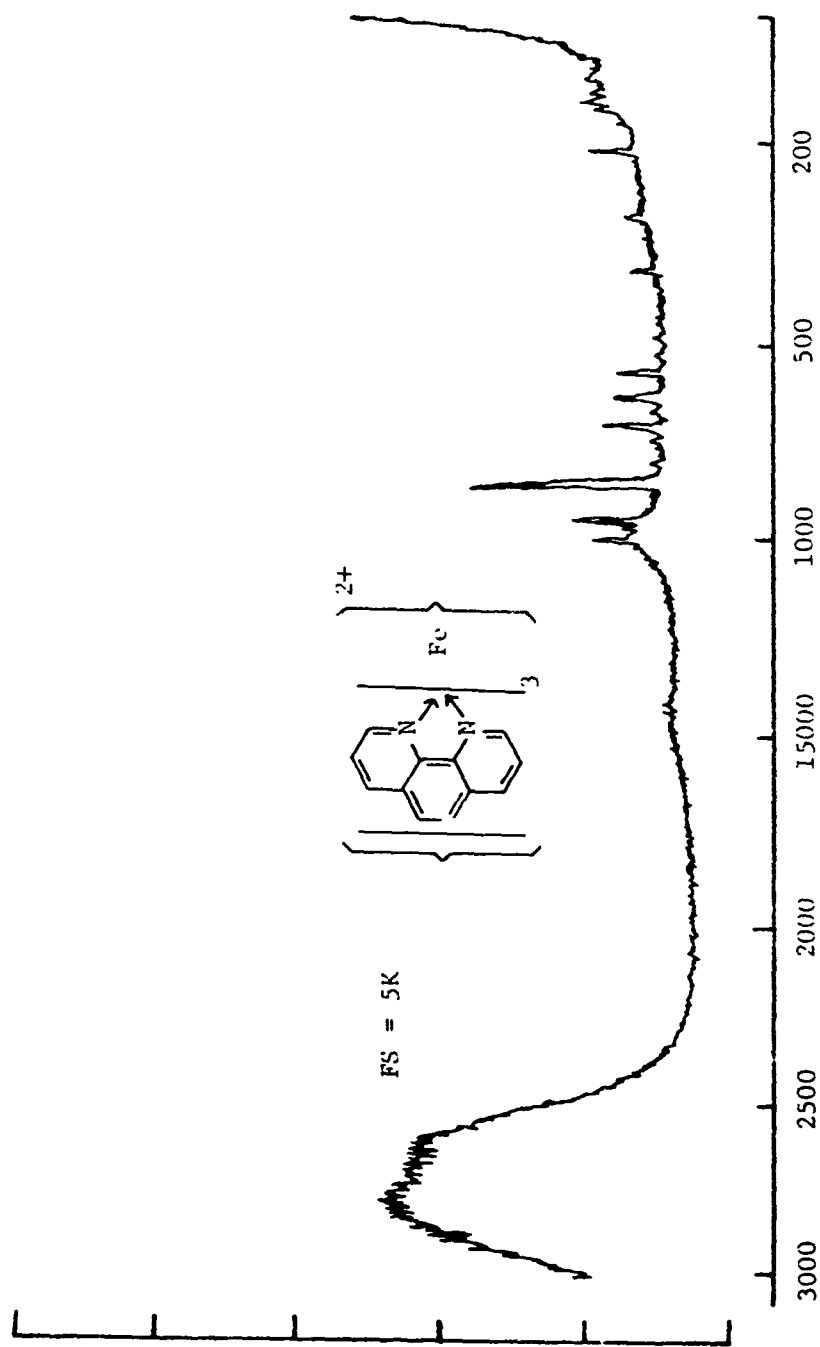


Fig. III-9. Raman signal of 1-10 orthophenanthroline in borate buffer (pH 8.4) in the presence of 10^{-4} FeSO_4 .

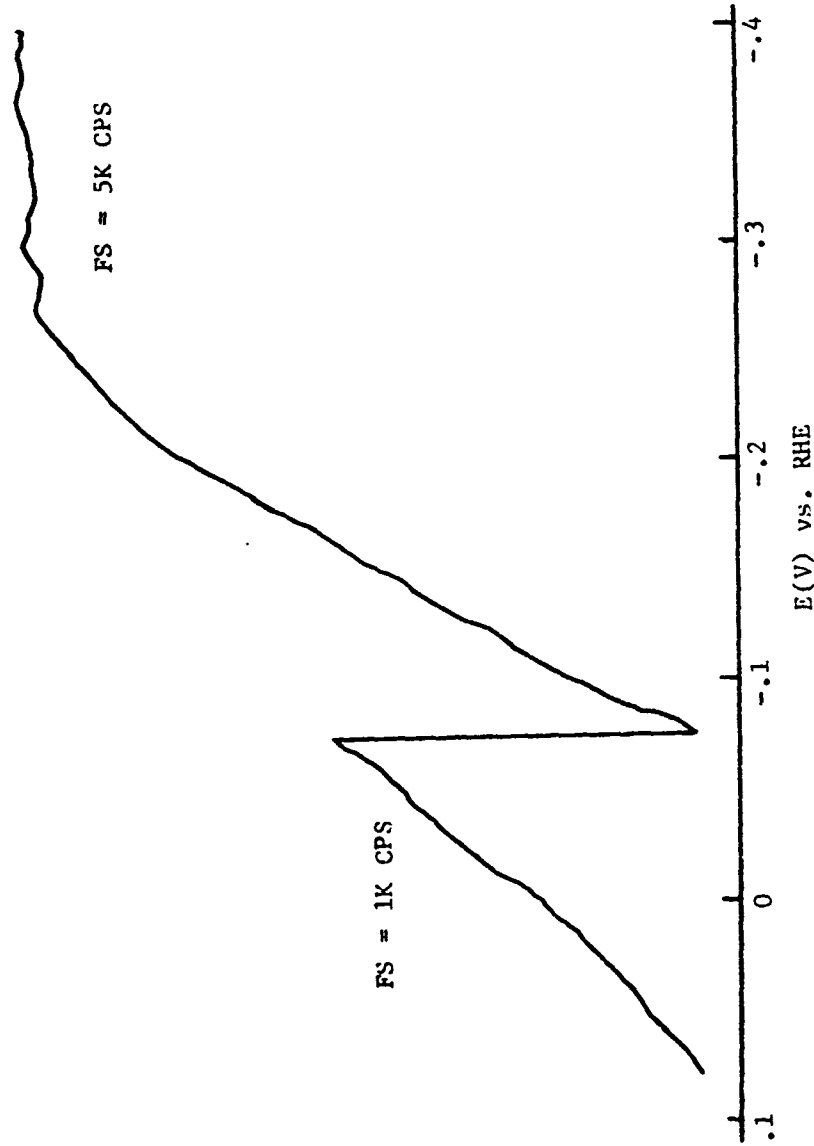


Fig. III-10. Variation of the Raman band (2751) intensity of the 1-10 orthopenanthroline at iron-solution interface due to the electrode potential change from -0.4 V up to 0.1 V

peak in the α - Fe_2O_3 , the 616 cm^{-1} peak in the FeO and Fe_3O_4 . Other spectral features, however, are lacking. The passive layer is believed by most workers to be γ - Fe_2O_3 and hence it would be more appropriate to compare the in-situ passivation spectrum with that for a sample of γ - Fe_2O_3 .

Heidersback et al.⁹ have reported the Raman spectra for a sample of γ - Fe_2O_3 prepared synthetically. They claim that Raman spectra to be similar to that for Fe_3O_4 but this is questionable on the basis of their reported spectra. The γ - Fe_2O_3 exhibits only one very broad peak centered at 720 cm^{-1} while Fe_3O_4 has a sharp peak at 663 cm^{-1} .

The thickness of passive films in this experiment should not be greater than $\sim 50 \text{ \AA}$; therefore, the intensity of the Raman peak would be expected to be smaller than that observed in this experiment. There are several possibilities for such a strong signal. Iron may, and probably does, exhibit some SER but this enhancement would occur only a short distance from the iron surface into the oxide (e.g. $\sim 10 \text{ \AA}$). The oxide may also exhibit a resonance Raman or preresonance Raman enhancement; the latter is more likely.

Such is to be expected if the laser frequency approaches that for an electronic transition in the oxide as may be possible. An alternate explanation is that the laser beam promotes the growth of a much thicker layer because of chemical and/or photochemical effects. Further work is necessary to establish whether the laser beam promotes the growth of a thicker or modifying film and is

planned as part of the ongoing research at Case.

The in-situ Raman peaks are at relatively low frequency (800-500 cm^{-1}). No other peaks were detected over the frequency range from 200 to 4000 cm^{-1} except for a water band. In addition to localized soft deformation modes, this frequency range of 800 to 500 cm^{-1} encompasses that where lattice modes and magnon modes may occur. It is impossible to make any assignment at this time. Raman polarization measurements are worthwhile making, but may not prove particularly helpful if the film is not highly oriented or crystalline. The peaks are relatively sharp in the passive film spectra. The slit widths were such that instrument peak widths should be 5 cm^{-1} . The observed peak width is 15 to 20 cm^{-1} for the 620 cm^{-1} peak. Such line widths are comparable with either crystalline or amorphous structures if localized vibrational modes are involved.

Raman Spectroscopy of Air Oxidized Fe and Fe-Cr Alloys

The Raman spectrum of the scale formed on the surface of iron-chromium alloys has been obtained to illustrate the use of Raman spectroscopy in atmospheric corrosion studies as well as wet corrosion.

The experiments have been done for Fe-Cr alloys. The procedure for preparing the specimens were the same as for the wet corrosion studies through the ultrasonic cleaning procedure. Compositions of the specimens are given in Table III-2.

The samples were put in the oven in air for 1 hour at 500°C

TABLE III-2. Composition of Iron-Chromium Alloys

Material Number	Percentage by weight							
	C	Mn	P	S	Si	Cu	Ni	Cr
1	0.15	1.3	0.011	0.037	0.22	0.09	0.12	0.5
2	0.14	1.3	0.010	0.025	0.21	0.09	0.03	1.0
3	0.16	1.4	0.010	0.022	0.22	0.09	0.03	2.0
4	0.17	1.5	0.012	0.027	0.19	0.09	0.06	8.0
5	0.17	1.5	0.012	0.020	0.18	0.09	0.08	11.6
6	0.7	1.68	0.020	0.004	0.51	-	8.48	18.32

and then cooled to room temperature. The Raman spectra of these oxidized samples were taken from 200 to 900 cm^{-1} using 514.5 nm for laser radiation. In order to minimize beam heating, the samples were rotated at 1000 rpm while collecting the Raman spectrum.

The Raman spectra (Fig. III-11-16) of the samples showed several clear peaks. On the basis of Raman spectra of $\alpha\text{-Fe}_2\text{O}_3$ and Fe_3O_4 and also literature data, the spectra of the samples with less chromium than 9% are similar to that for $\alpha\text{-Fe}_2\text{O}_3$ plus a small amount of Fe_3O_4 and Cr_2O_3 . The ratio of the Cr_2O_3 Raman peak to those associated with the $\alpha\text{-Fe}_2\text{O}_3$ structure increases in an approximately linear manner with the Cr concentration of the alloy. This experiment shows that the Raman spectroscopy can be used as a powerful analytical tool in the field of corrosion and oxidation.

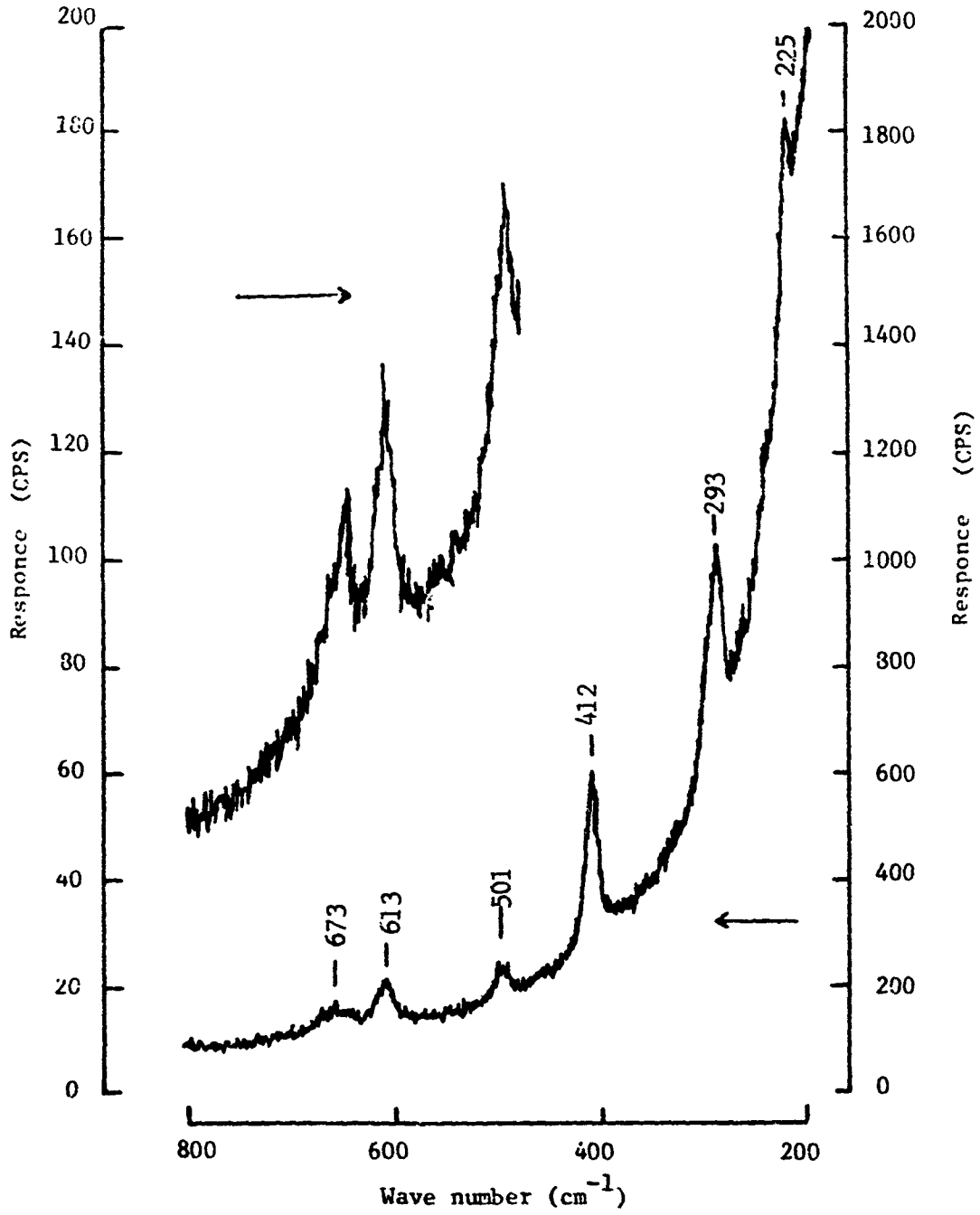


Fig. III-11. Raman signal of air oxidized Fe-0.5 cr % at 500°C for 1 hour. $\lambda = 514.5 \text{ nm}$

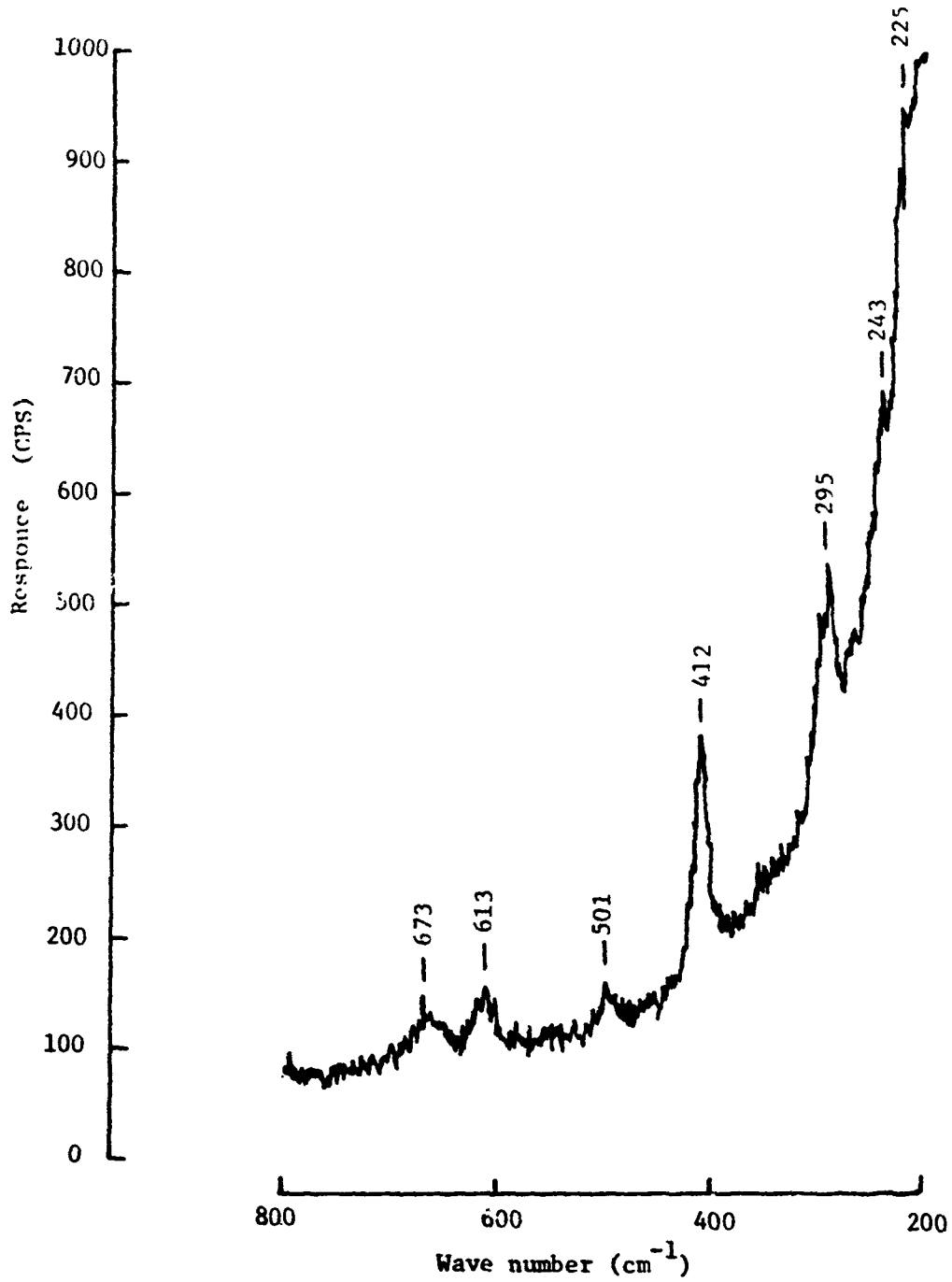


Fig. III-12. Raman signal of the air oxidized Fe 1% Cr at 500°C in air. $\lambda = 514.5$ nm

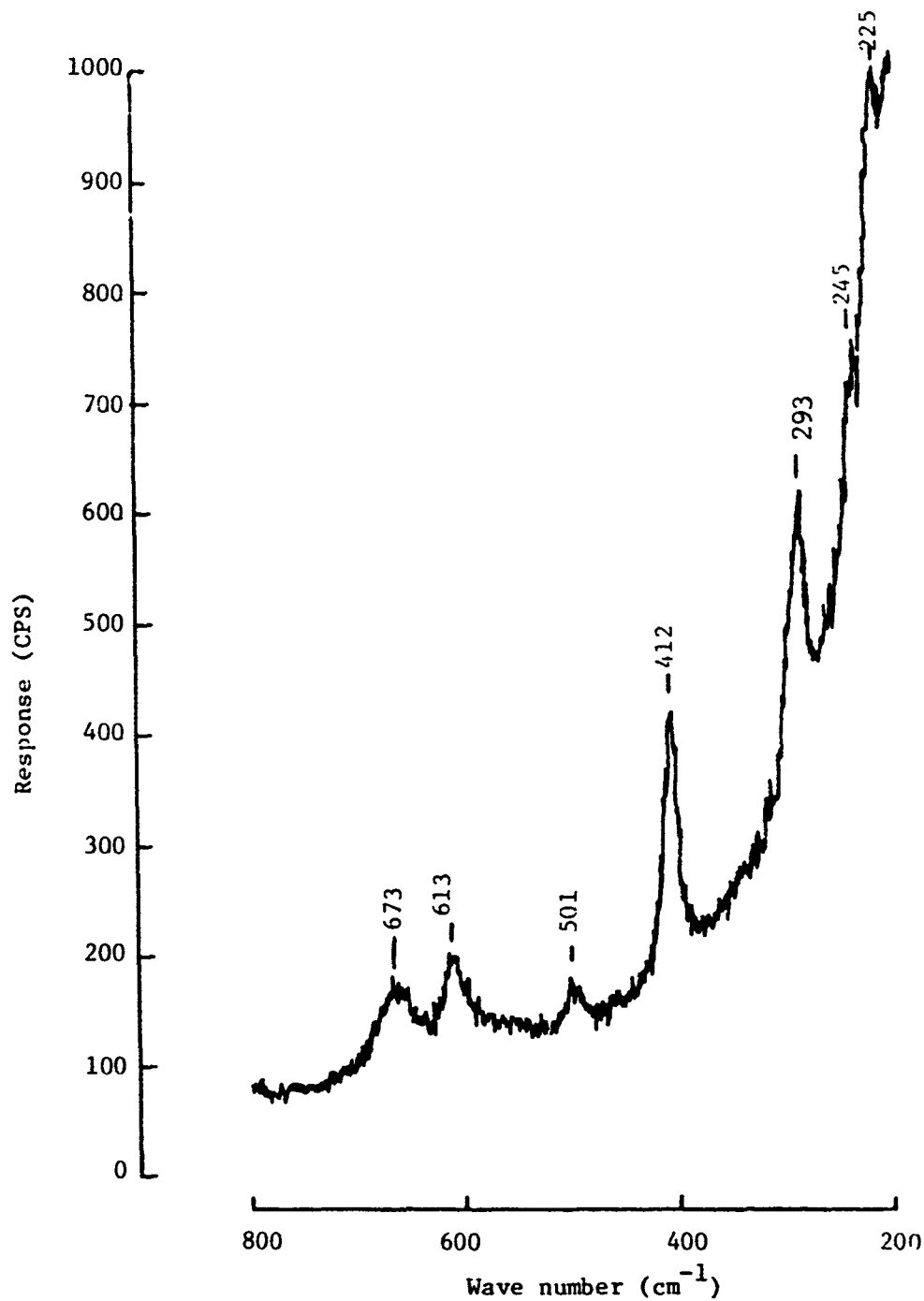


Fig. III-13. Raman signal of air oxidized Fe-2% Cr at 500°C.

$\lambda = 514.5 \text{ nm}$

PHOTO COPY FROM THE AUTHOR'S COLLECTION

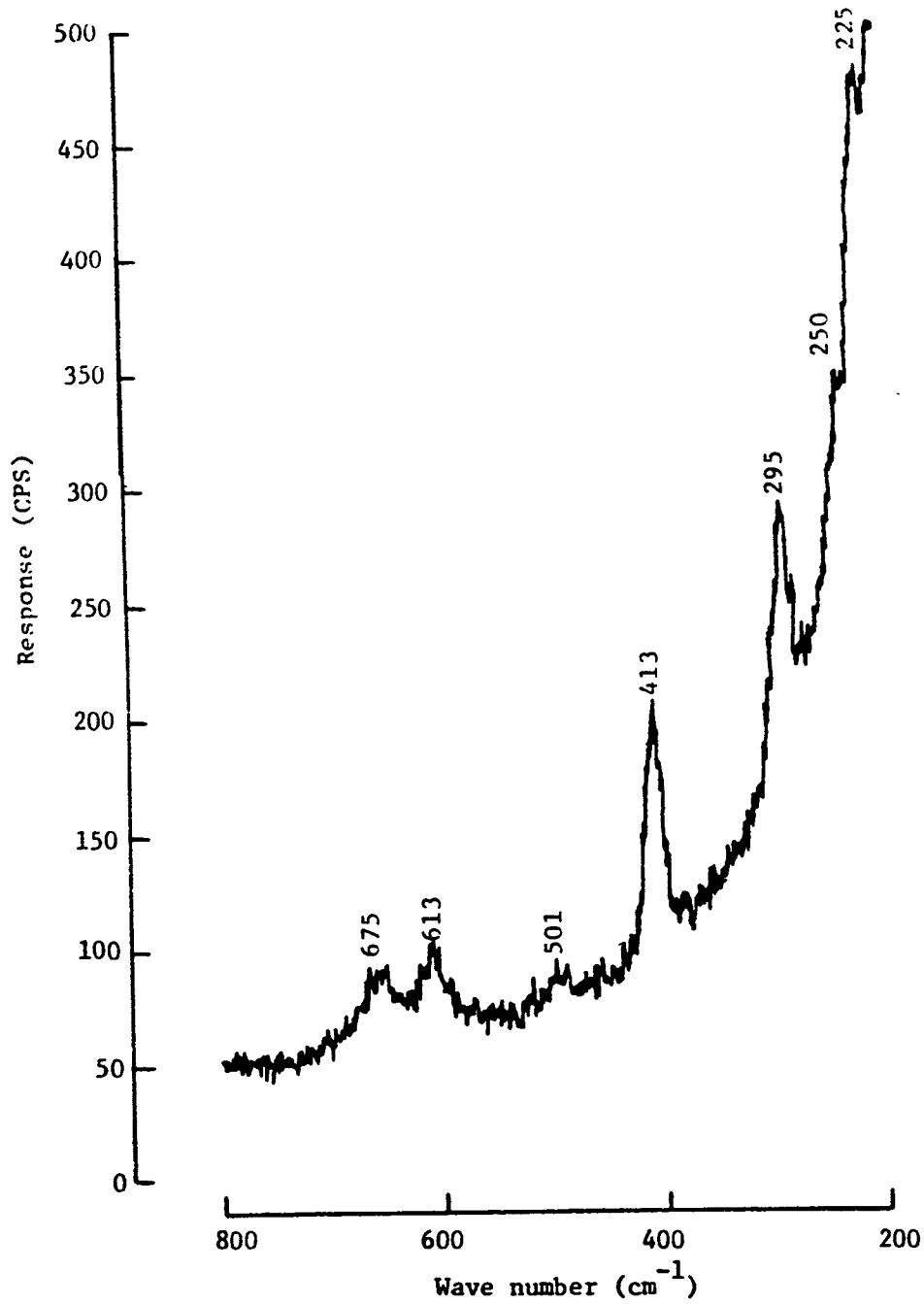


Fig. III-14. Raman signal of air oxidized Fe-8% Cr at 500°C (1 hour). $\lambda = 514.5 \text{ nm}$

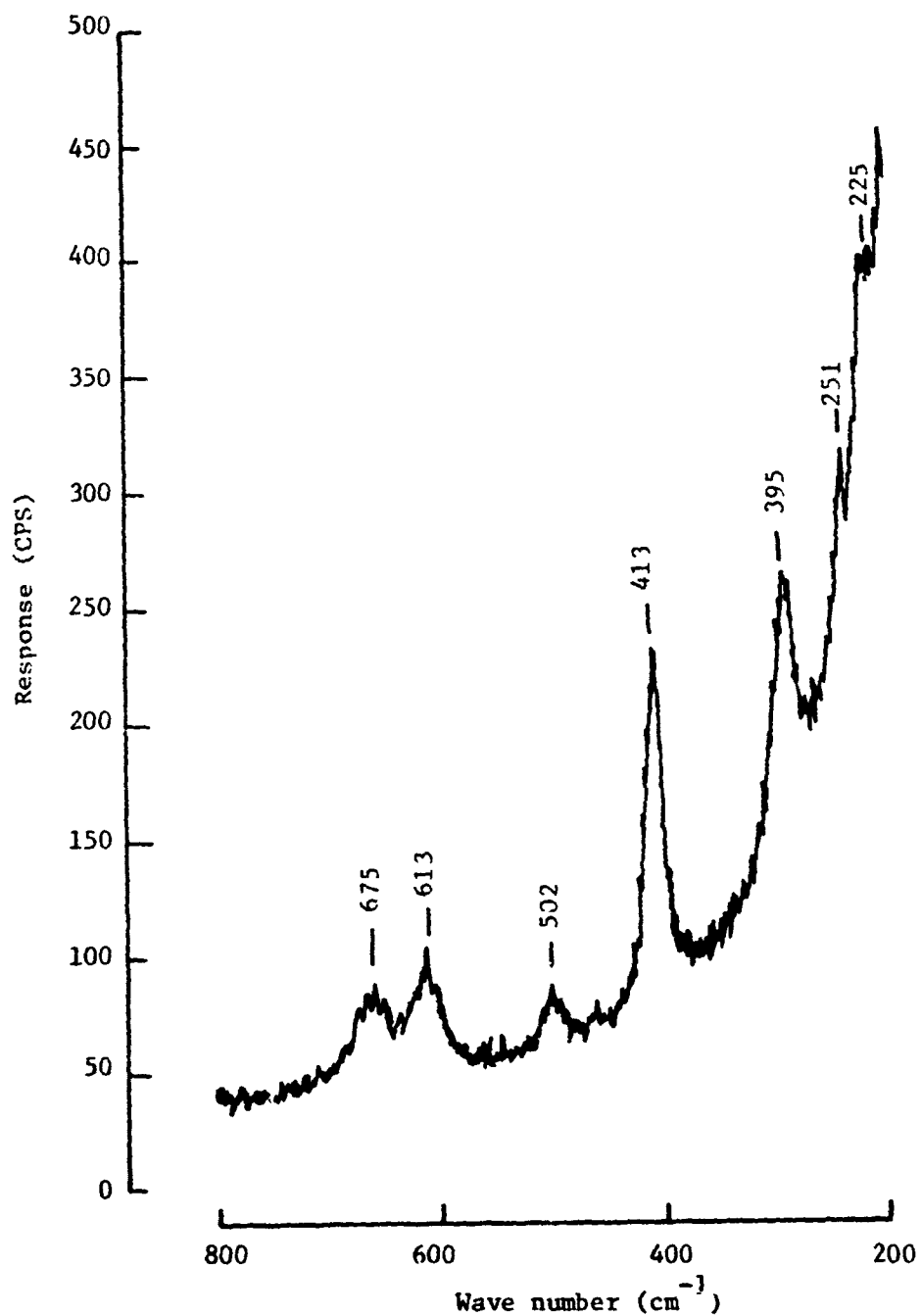


Fig. III-15. Raman signal of air oxidized Fe-11.6% Cr at 500°C (1 hour). $\lambda = 514.5 \text{ nm}$

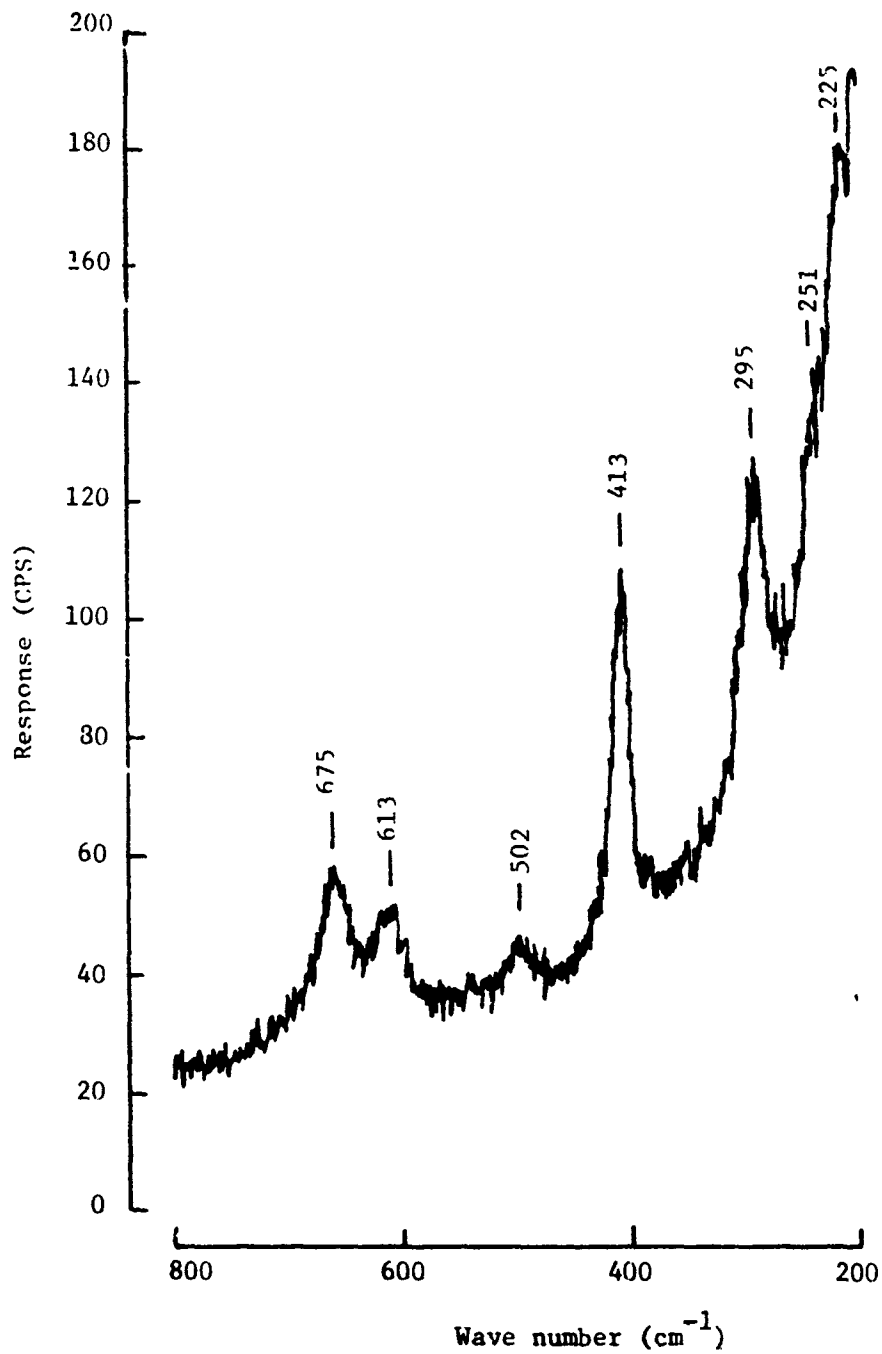


Fig. III-16. Raman signal of air oxidized Fe-24% Cr at 500°C (1 hour). $\lambda = 514.5 \text{ nm}$

REFERENCES

CHAPTER III

1. M. Fleischmann, P.J. Hendra and A.J. McQuillan, Chem. Phys. Lett. 26, 163 (1974).
2. R.P. Van Duyne, J. Physique 38, C₅-239 (1977).
3. T.E. Furtak, Solid State Commun. 28, 903 (1978).
4. F.W. King, R.D. Van Duyne and G.C. Schatz, J. Chem. Phys. 69, 4472 (1978).
5. A. Otto, Surface Sci. 75, L392 (1978).
6. S. Efirna and H. Metui, J. Chem. Phys. 70, 602 (1979); 70, 2297 (1979); and 70, 1939 (1979).
7. R. Kötz and E. Yeager, J. Electroanal. Chem. Interfacial Electrochem. 88, 269 (1978); and R. Kötz and E. Yeager, J. Electroanal Chem. Interfacial Electrochem. 111, 105 (1980).
8. R. Keisers, P. Fabis, C. Brown and R. Heidershback, Technical report No. 8, Department of the Navy, Office of Naval Research, Metallurgy Program, Code 471, Jan. 1980.

CHAPTER IV
ELECTRON DIFFRACTION STUDIES OF PASSIVE
FILM ON IRON AND IRON-CHROMIUM ALLOYS

I. INTRODUCTION

Relatively few transmission electron microscopy studies of the passive film on iron have been reported.¹⁻⁵ Two types of techniques have been used. In the first the iron is passivated in an appropriate electrolyte and the film then stripped from the iron by using appropriate chemical reactions, usually iodine. In the second, the passivated layer is produced on a very thin iron substrate and the TEM measurements on the passivation layer are carried out directly through the iron substrate. The second method has been used in this present study.

The first method has the disadvantage in that the structural and compositional changes may occur during the stripping. The second method does not have this disadvantage. The only work with this method is that by Foley *et al.*¹ and McBee and Kruger.² The passivation procedure used by these workers are not fully clear.

In the present study, the passivation film was produced by stepping the potential to various values in the passive range from the cathodic protection region. This technique minimizes the tendency to form any gel-like overlayer.

The ultra thin section of the iron specimen through which the TEM studies are carried out is polycrystalline. The individual

iron crystals are clearly evidenced by the microelectron diffraction patterns; thus the structure of passive film on different crystallographic planes has been obtained. The diffraction patterns of the passivation film in this study coincide with that for $\gamma\text{-Fe}_2\text{O}_3$ except that at low anodic potential and open circuit potential the patterns appears to correspond to the Fe_3O_4 . The structure of the passive film on the surface of the iron-chromium alloys also have been examined.

II. EXPERIMENTAL

- a. Rolling. The pure polycrystalline iron (99.998%) and iron-chromium alloys were cold-rolled to foils, 0.15 μm thickness.
- b. The sample was chemically polished with a 24% by weight H_2O_2 + 24% by weight HF prepared from Fisher chemical reagents.
- c. The sample was annealed in vacuum at 10^{-5} Torr at 800°C in a sealed quartz tube for 24 hours. After annealing the temperature of the sample decreased as it cooled in the furnace down to room temperature over a period of 3 hours. When the sample reached room temperature, it was removed from the furnace.
- d. The annealed sample was chemically cleaned in the same H_2O_2 + HF solution for 30-60 sec.
- e. The standard microscope disk specimens with 3 mm diameter
- f. Electrochemical thinning. The Tenupol apparatus (STRUERS) was used for the electrochemical thinning (jet polishing) of iron

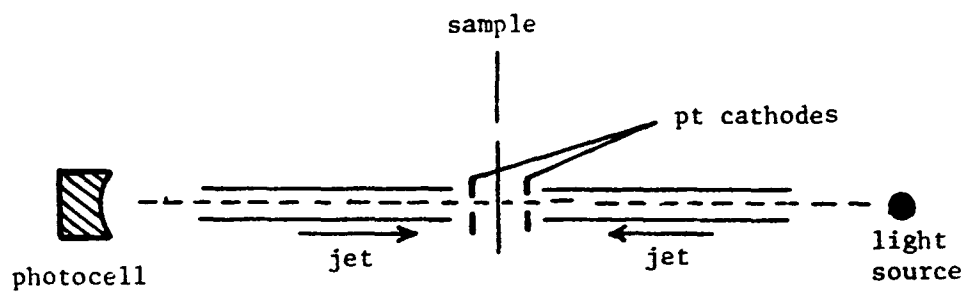


Fig. IV-1. Schematic of jet polishing apparatus

disks which had been chemical¹, polished earlier. The electrolyte for the jet polishing was 50 ml perchloric acid (70-72%) + 950 ml glacial acetic acid from Fisher Scientific Company.

The arrangement for etching away the iron is shown in Fig. IV-1. The cathodes on the two sides of the sample were platinum rings located symmetrically about the jets. A photoelectric device cut off the current when the film first perforated. The total etching current was adjusted to 0.5 A and the voltage to 80 V to ensure a proper pinhole at the center of the sample. In the subsequent TEM measurements the electron beam was passed through the ultra thin section of the iron foil adjacent to the pinhole.

g. After electrochemical thinning, the sample was removed and placed into pure methanol to stop further reaction. To further clean the sample, it was submerged in pure methanol in four successive beakers. The methanol on the surface of the sample was then removed with triple distilled water. At this stage the electrode was transferred into the electrochemical cell and cathodically reduced at controlled potential (-0.4 V). The washing procedure from the jet polishing machine to the transferring into the electrochemical cell took less than 1 min.

The electrochemical cell contained 15 ml of purified borate buffer which was saturated with ultra pure argon. The reference electrode was an α -Pd H bead and the counter electrode a platinum wire. After 15-20 min of cathodic reduction at -0.4 V the electrolyte was replaced with a fresh electrolyte to remove the ferrous

ions which was produced during the cathodic reduction. After the cathodic reduction, the electrode potential was stepped to the desired value (using a Stonehart BC 1200 potentiostat). The potential of the sample was held constant at the desired value for 1 hour. Then the sample was transferred from the electrochemical cell and submerged in distilled water for a few seconds and immediately transferred to the electron microscope which was aligned and ready to operate. The time between transference of the sample from the electrochemical cell and taking the first diffraction pattern was less than 5 min.

The sample, under 10^{-5} Torr, has been examined by electron microscopy. The diffraction patterns of the passive film on the different crystallographic plane of the iron substrate have been recorded. The bright field and dark field image of the passive film also have been obtained.

III. RESULTS AND DISCUSSION

TEM was used to examine the passive film formed on an iron specimen in borate buffer, pH 8.4. In this experiment considerable attention was focused on the procedure of passive film formation to avoid contribution of any primary oxide and deposited over-layer as discussed in Chapter II, i.e., the use of a potential step.

The results of these experiments confirm that the passive film exists as an oxide layer on the surface of iron electrodes, which is in agreement with the oxide film theory for passivation already

mentioned in Chapter I. The passive film was observed over the entire range of passivation examined from 0.4 V up to 1.6 V in the electron diffraction studies. This verifies the existence of the passive film on the surface of electrodes.

These experiments confirm that the structure and thickness of the passive film are potential dependent. Figure IV-2 shows the electron diffraction pattern of the passive film on the iron(111) plane at two different potentials (1.6 and 0.4 V). The diffraction patterns of the passive film in both cases show spots rather than rings, which indicates that the passive film formed in this condition has crystalline structures. However, it is difficult to conclude that crystallinity is an intrinsic property of the passive film since transference of the latter to the electron microscope column (10^{-5} Torr) may induce crystallization. Kruger *et al.*² concluded that the structure of passive film during this transference does not change. However, Mössbauer studies of the passive film by O'Grady⁶ showed differences between the in-situ and ex-situ Mössbauer spectra. O'Grady concluded that the passive layer is polymeric which made the interpretation of the Mössbauer spectra difficult.

The TEM studies of passive films in the present work show that the structure of the passive film on iron at different potentials is not the same. In Fig. II-2 the spots belonging to the passive film shown by (o) match with the $\gamma\text{-Fe}_2\text{O}_3$ and also Fe_3O_4 . It

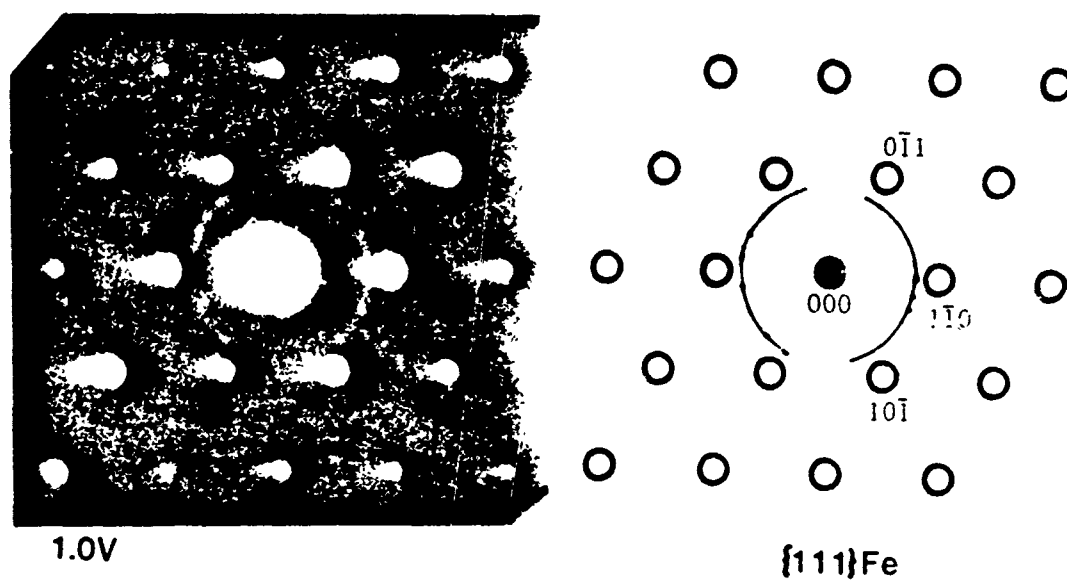
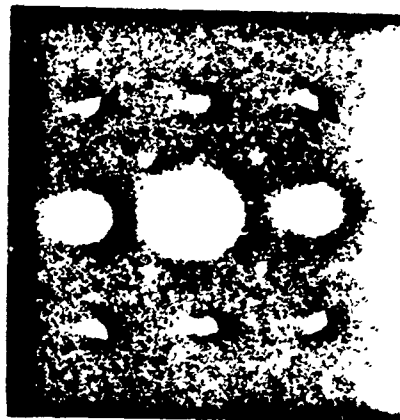
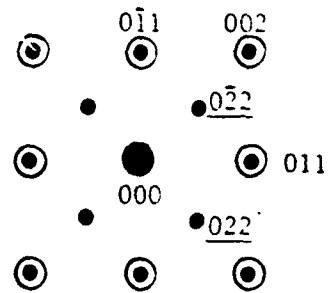


Fig. IV-2. Electron diffraction patterns of passive film formed on iron{111} plane in borate buffer (pH 8.4)



1.0V



$\{100\}Fe//\{100\}Oxide$

Fig. IV-3. Electron diffraction patterns of passive film formed on iron{111} plane in borate buffer (pH 8.4)

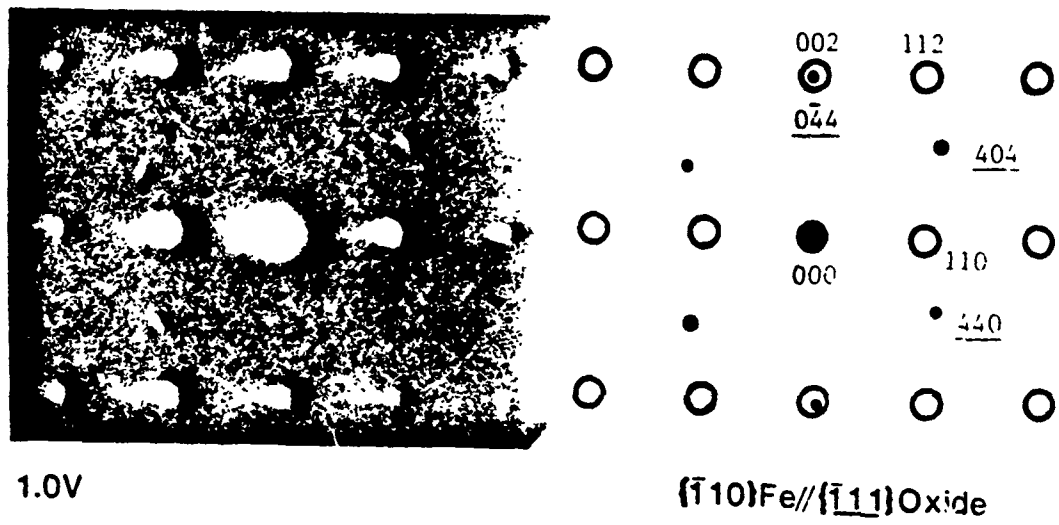


Fig. IV-4. Electron diffraction patterns of the passive film on iron{110} plane in borate buffer (pH 8.4)



0.6V

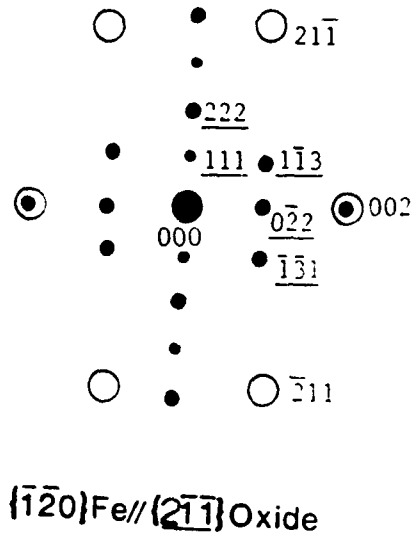


Fig. IV-5. Electron diffraction patterns of passive film formed on iron{120} plane in borate buffer (pH 8.4)

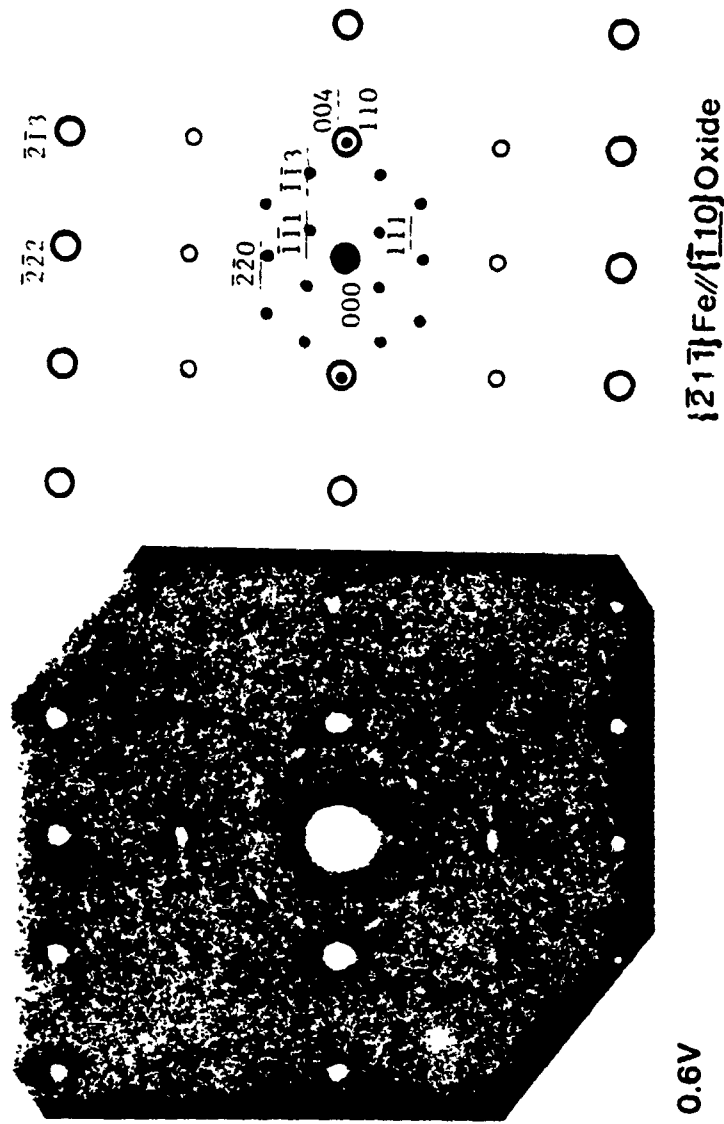


Fig. IV-6. Electron diffraction patterns of passive film formed on iron{211} plane in borate buffer (pH 8.4)

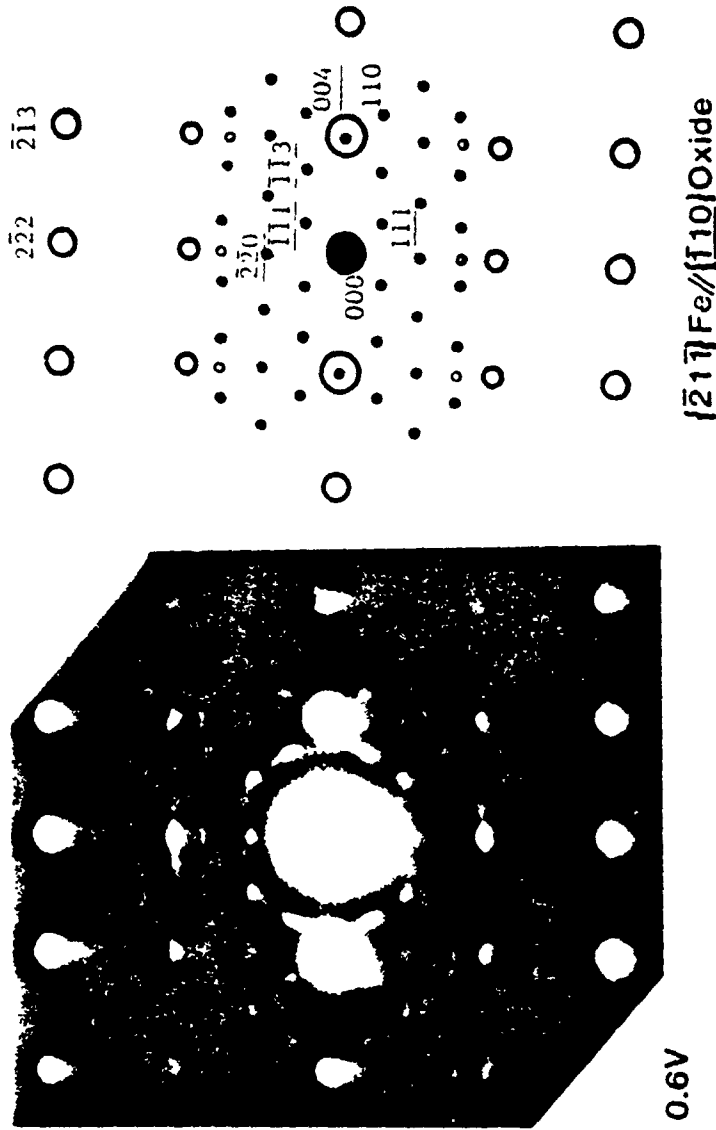


Fig. IV-7. Electron diffraction patterns of passive film formed on iron(211) plane with occurrence of relrod effect.

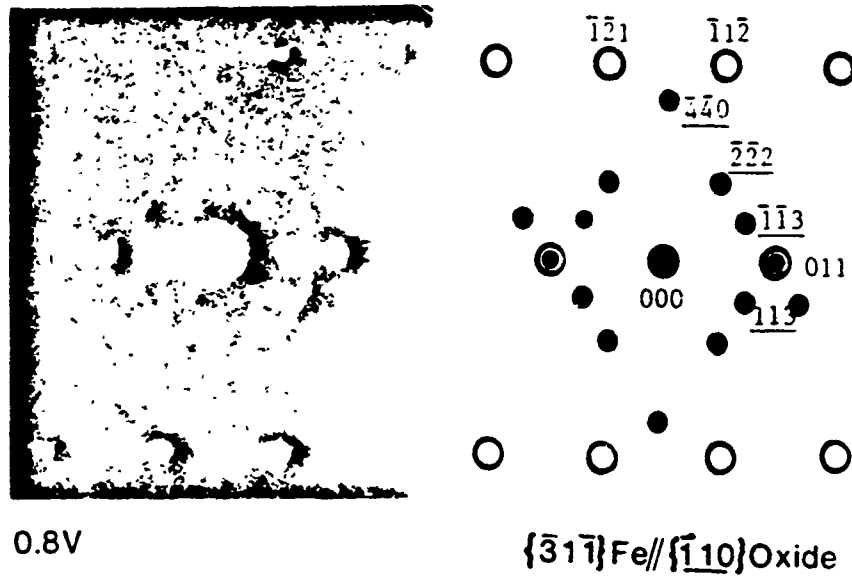


Fig. IV-8. Electron diffraction patterns of the passive film formed on iron{311} plane in borate buffer (pH 8.4)

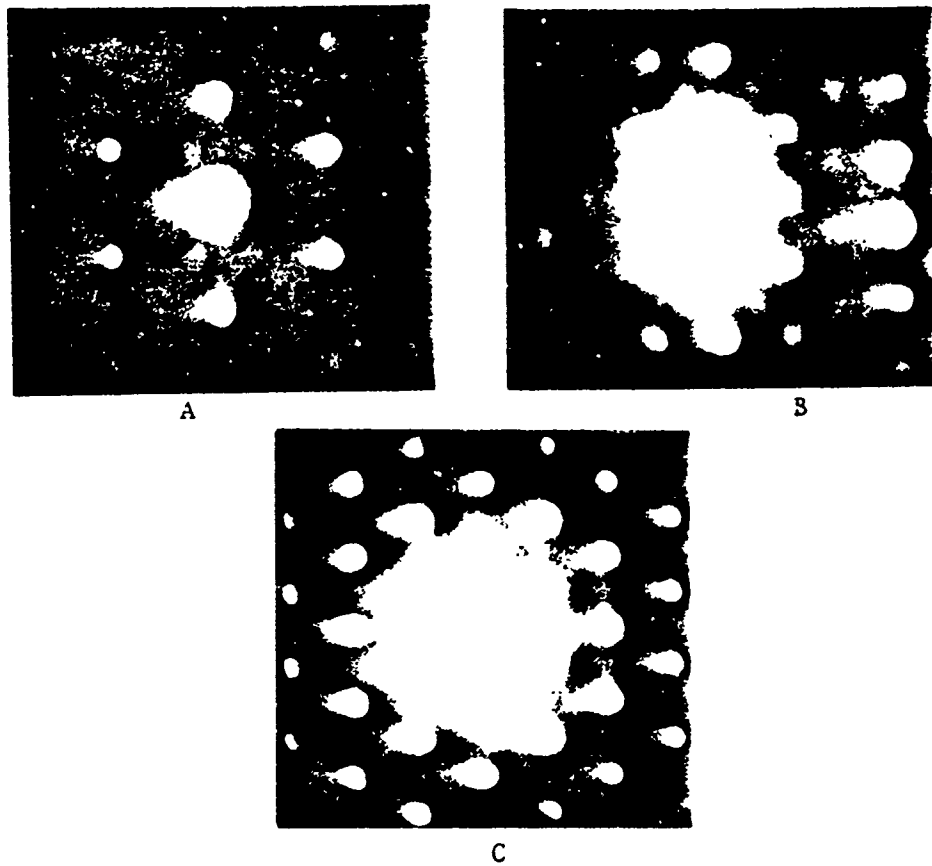


Fig. IV-9. Microdiffraction patterns of passive film formed at 1.0 V on A-113, B-012 and C-111 planes

is difficult to distinguish between these two oxides because the d spacings associated with the spots for these two oxides and their intensity ratios are very close to each other. Therefore diffraction studies of thin film such as passive film usually are not able to distinguish between Fe_3O_4 and $\gamma\text{-Fe}_2\text{O}_3$ which are so close to each other. The diffraction patterns of the passive film formed on 6 different crystallographic planes have been observed. Figures IV-2-7 show the electron diffraction patterns of the passive film on the surface of different crystallographic planes. The epitaxial relationships between metal substrate and passive film is shown in Figures IV-2-7. The passive film on the 100 plane showed Bain relation. However other planes showed Nishiyama-Wasserman relationship. This phenomena is attributable to the need to accommodate the misfit strain between the oxide and the iron substrate. Micro diffraction patterns of passive film on 113, 012 and 111 planes also showed the spot patterns due to the crystallinity of the passive film (see Fig. IV-9).

Figures IV-10,11,12 and 13 show the occurrence of the same forbidden diffraction patterns. This phenomena can be attributed to relrod effects due to the small size of the diffracting particles. For thin specimen such as passive film the relrods of the reciprocal lattice points are quite long, and there is a possibility that relrods from the next layer of reciprocal lattice intersect the reflecting sphere and give rise to forbidden reflections. In

addition, the bending of the sample or small deviations from the exact symmetrical orientation gives the occurrence of the forbidden of other lane zone diffraction spots. The oxides formed on different crystallographic planes do not have the same intensity in the diffraction spots. This probably indicates that the thickness of the passive film from one grain to another is not the same.

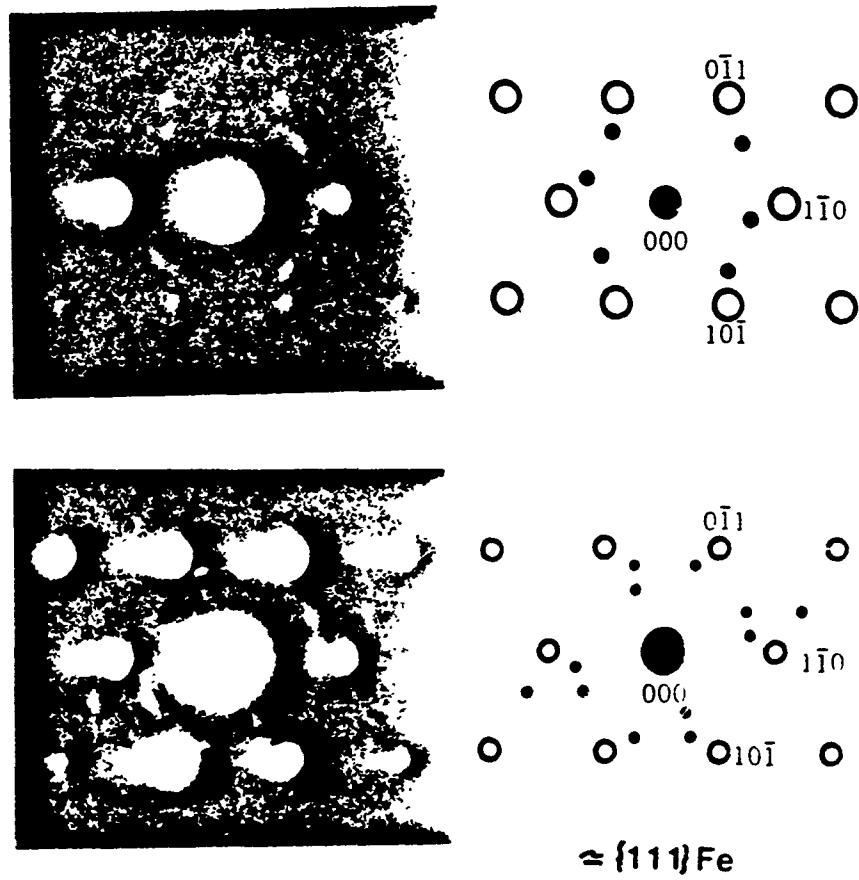


Fig. IV-10. Electron diffraction patterns of the passive film formed on iron $\sqrt{\{111\}}$ plane with relrod effects in borate buffer (pH 8.4).

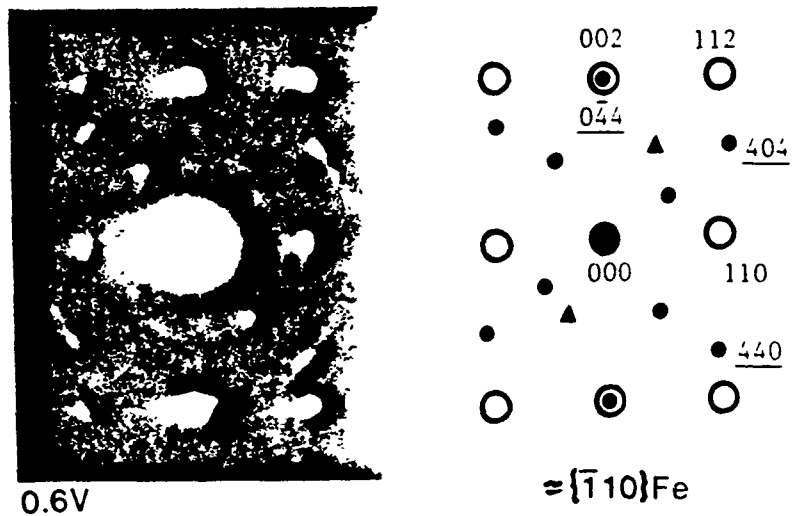


Fig. IV-11. Electron diffraction patterns of the passive film formed on iron $\{110\}$ plane with reloid effects in borate buffer (pH 8.4)

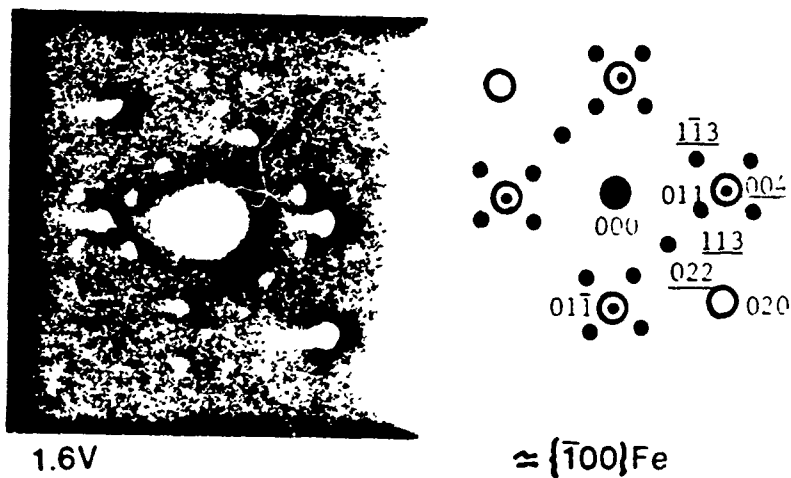


Fig. IV-12. Electron diffraction patterns of the passive film formed on iron $\{100\}$ plane with relrod effects in borate buffer (pH 8.4)

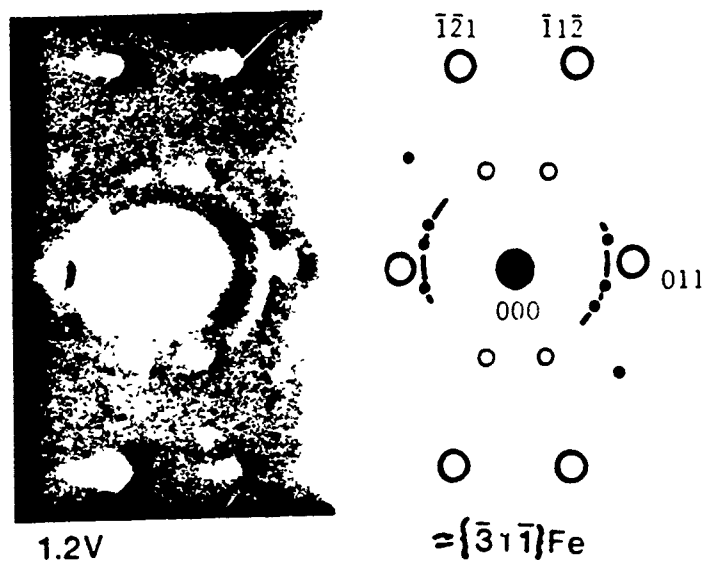


Fig. IV-13. Electron diffraction pattern of the passive film formed on iron $\{311\}$ plane with relrod effects in borate buffer (pH 8.4)

This kind of anisotropy is also reported in the literature. These differences in the thickness of the passive film from one crystallographic plane to another is not surprising because there is evidence that electrochemical behavior of the crystal planes of iron are not the same. Stockbridge *et al.*⁸ found the hydrogen overvoltage on iron is different on surfaces of different crystallographic orientation. Mieluch³ also reported that the protectiveness of the passive film on different crystallographic planes is not the same. It is well established that the dissolution rate of the different crystallographic planes are different. Therefore, passive films formed on different planes may have anisotropic structures.

On the basis of this study, the model shown in Fig. IV-14 is postulated for the structure of the passive film on the surface of iron. In this model the composition of passive film is proposed to be a single layer $\gamma\text{-Fe}_2\text{O}_3$ with different thicknesses on each grain. Due to this model, there must be some degree of strain in the film, because of the misfit at grain boundaries and also mismatch of oxide and its substrate. These differences in the thickness of the film at different grains for a film with 30 Å thickness should not be more than a few (5) Angstroms. There is not any evidence for the existence of oxide nucleation on the surface of passive film. The dark and bright field images of the passive film formed at 1.4 V did not show any nucleation of the oxide on

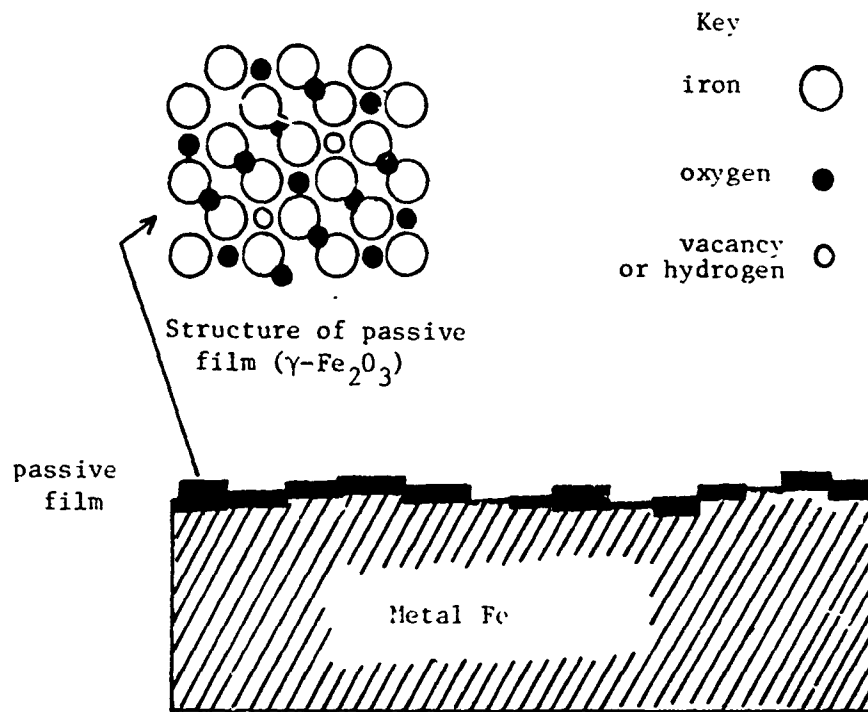


Fig. IV-13. Structure model for passive film on polycrystalline iron

the surface of passive films. Figure IV-15 shows the dark and bright field image of the passive film on iron.

The structure of the passive film formed on Fe-18%-Cr alloy at 1.0 V in borate buffer (pH 8.4) also has been examined. In this experiment the diffraction pattern of the passive film showed only a diffuse ring pattern. This indicates that the passive film on Fe-18% Cr is more amorphous like than the passive film on pure iron. Figure IV-17 shows the diffraction pattern of the passive film on Fe-18% Cr alloy.

In addition to the passivation studies by TEM the morphology of the film formed on iron in borate buffer (pH 8.4) during potential cycling was examined. The dark field image of the film formed after 100 potential cycling from -0.4 up to 1.4 V is shown in Fig. IV-16. The dark spots are probably due to the voids produced in the film formed during potential cycling.

The electron diffraction patterns of the corrosion product inside the pit which is produced electrochemically also have been obtained. The diffraction patterns show both rings and spots. In this experiment the pit was generated during jet polishing with a shorter time than is required for making a pinhole. The bright field image of the surface of this sample shows the dissolution of the iron crystal from the (111) plane (Figs. IV-18.



1 μm

Fig. IV-15. The dark and bright field image of the passive film formed on iron in borate buffer (pH 8.4)



Fig. IV-16. Electron diffraction patterns of the passive film formed on Fe-18% Cr in borate buffer (pH 8.4)



2μm

Fig. IV-9. Dark field image of the surface of iron electrode after 100 potential cycling from -0.4 up to 1.4 V (50 mV/s).

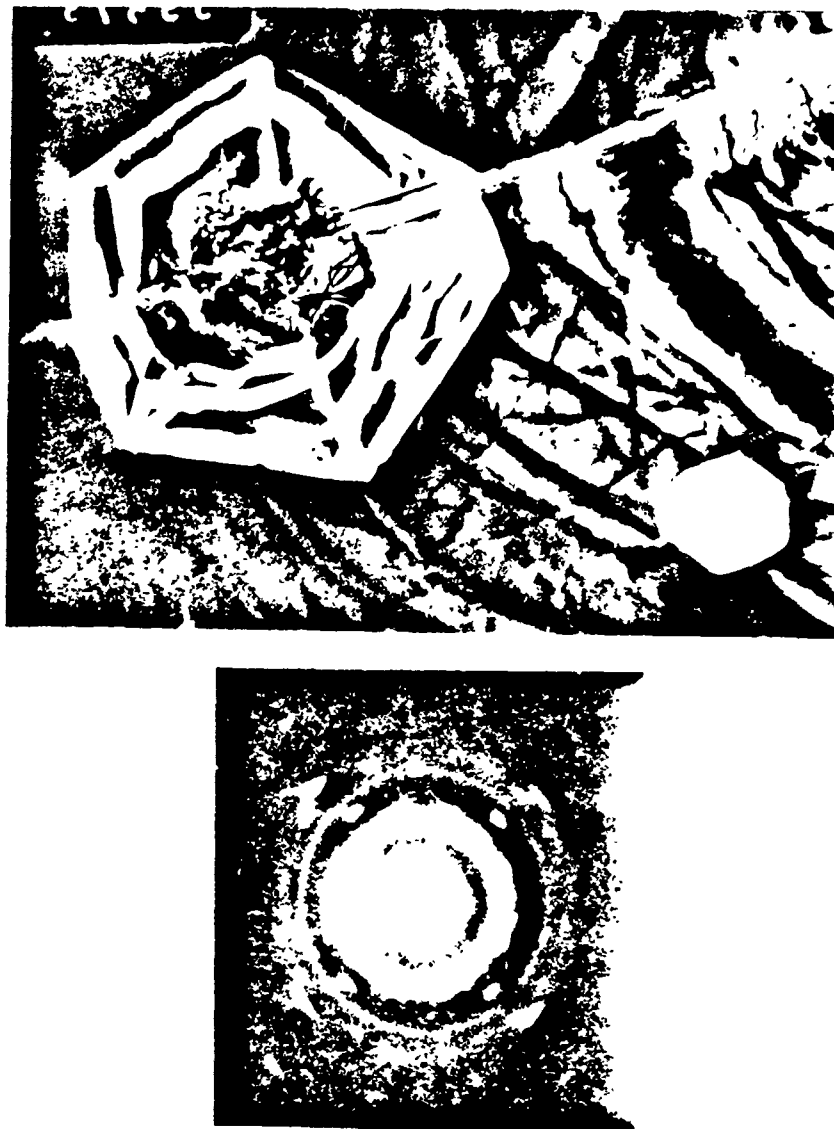


Fig. IV-18. Bright field image of the iron surface with pit and electron diffraction patterns of the corrosion products inside the pit

IV. CONCLUSION

The TEM studies of passive film showed the existence of a crystalline film. The diffraction spots of the passive film on different crystallographic planes are not the same. The diffraction spots for the film formed at potentials higher than 0.4 V vs. RHE are close to those for $\gamma\text{-Fe}_2\text{O}_3$. However, the passive film formed at lower potential has Fe_3O_4 oxide in the film. The thickness of the passive film from one grain to another is not the same. The dark field and bright field images of the passive film on iron does not give any indication of oxide nucleation. The structure and composition of the passive film is proposed to be as shown in Fig. IV-13.

REFERENCES

CHAPTER IV

1. C.L. Foley, J. Kruger and C.J. Bechtoldt, J. Electrochem. Soc. 114, 994, 1976.
2. C.L. McBee and J. Kruger, Electrochim. Acta 17, 1337 (1972).
3. J. Mieluch, Bulletin De L'Academie Polonaise des Sciences Serie des science chimiques, Vol. XV, No. 12, p. 597 (1967).
4. B. MacDougall, D.F. Mitchell and M.J. Graham, Israel J. Chem. 18, 125 (1979).
5. S.H. Chen and J.W. Morris, Metallurgica Transactions A 8A, 19 (1977).
6. W.E. O'Grady, J. Electrochem. Soc. 127, 552 (1980).
7. W.E. Boggs, R.H. Rachik and G.E. Pellissier, J. Electrochem. Soc. 114, 32 (1967).
8. C.D. Stockridge, P.B. Sewell and M. Cohen. J. Electrochem. Soc. 108, 928 (1961).

CHAPTER V

CONCLUSION AND REMARKS

1. Dissolution and Passivation of Iron

The potential sweep and potential pulse measurements recorded during passivation indicated the introduction of the ferrous ion into solution. These dissolved ferrous ion at the interface can be deposited on the surface of the passive film to form an oxy-hydroxide gel-layer structure. Such an overlayer is particularly likely to be formed when the potential of the passive film is slowly swept from the cathode protection region into the passive range but may also be formed even with a potential step function under some conditions. It is possible that many of the apparent conflicts in previous works in this field may be related to this deposited gel-layer on the surface of the passive film. The structure of this deposited layer is proposed to be close to FeOOH with an open structure which acts as a trap for water molecules and also anions from solution.

In an effort to overcome some of the ambiguities which still exist after 100 years of research effort in this field, a model for the passive film and deposited over-layer is suggested in Fig. II-14. Much of the work on electrochemical passivation by corrosion scientists reported in the literature has been done for this kind of film. In this model the passive film is covered by the deposited Fe(III) overlayer. However, the real passive film is in contact with iron and is proposed to have a compact mosaic type struc-

ture which is different from the structure of this overlayer. The structure of the passive film is highly defective and nonstoichiometric and the conductivity of the passive film is highly related to the concentration of defects. The concentration and nature of these defects are potential dependent. At the initiation of passivation the oxygen containing species (H_2O , OH^-) adsorbs on the surface of the passive film. As one goes to more anodic potential the passive film changes from having an excess of anionic vacancies toward an excess of cationic vacancies. In this case anionic and cationic vacancies can behave as electron acceptors and electron donors, respectively, in the oxide film. The conductivity of the passive films at low and high anodic potential can be related to changes in the concentration of vacancies and defects in the film. In this transition from anionic vacant to cationic vacant, the passive film may approach to the stoichiometric and rather defect free structure. In this case the passive film has maximum resistance and behaves as an insulator. However, the passive film at potentials lower and higher than this potential behaves as a p and n type semiconductor, respectively.

In the initial phase of passive film reduction a stirring insensitive reaction is obtained (peak C_I , Fig. II-). The broadness of the first cathodic peak (C_I) however is probably due to the defect structure of the passive film, and also overlap of the two reduction peaks (C_I and C_{II}). The passive film which is partially

reduced at C_I undergoes further reduction as the potential changes to more cathodic values. At peak C_I the ferrous ion which enters into the solution due to the solubility of ferrous oxide can be reduced to a metallic state at higher cathodic potential. The splitting of peak C_{II} corresponds to the reduction of ferrous ion from the oxide on the surface of the electrode and reduction of the ferrous ion from the solution phase.

2. In-Situ Raman Spectroscopy of Passive Film

The in-situ Raman spectra of passive film shows several Raman bands at low frequency range ($200-800 \text{ cm}^{-1}$). However, this in-situ spectrum does not match well with any Raman spectrum of a known iron oxide or oxy-hydroxide. Further experimental and theoretical calculations have to be done to analyze the Raman spectrum of these films. In addition to the in-situ spectrum of the passive film, we show the capability of Raman spectroscopy for dry corrosion studies. It is strongly believed that this in-situ technique will be widely used in the future for in-situ corrosion studies.

3. Electron Microscopy of the Passive Film on Iron

This work shows that the thickness of passive film on each crystallographic plane is different from that of others. The composition of the passive film formed on iron at potentials higher than 0.4 V has $\gamma\text{-Fe}_2\text{O}_3$ spots. However, the spot due to the spinel

structure of Fe_3O_4 at low anodic potential is also clear. The changes in lattice parameters of the oxide at each plane reflects the misfit of the oxide and its substrate structure. This work confirmed that the passive film has a crystalline structure on pure iron in the electron microscope. One possibility that the passivation film is amorphous in the electrolyte and then crystallizes in the electron microscope cannot be ruled out but appears unlikely. There is no evidence for oxide nucleation on the surface. It is believed that the passive film has a compact mosaic type structure.

TECHNICAL REPORT DISTRIBUTION LIST

	<u>No. Copies</u>		<u>No. Copies</u>
Office of Naval Research Attn: Code 472 800 North Quincy Street Arlington, Virginia 22217	2	U. S. Army Research Office Attn: CRD-AA-IP P.O. Box 1211 Research Triangle Park, N.C. 27709	1
ONR Branch Office Attn: Dr. George Sandoz 536 S. Clark Street Chicago, Illinois 60605	1	Naval Ocean Systems Center Attn: Mr. Joe McCartney San Diego, California 92152	1
ONR Area Office Attn: Scientific Dept. 715 Broadway New York, New York 1003	1	Naval Weapons Center Attn: Dr. A.B. Amster, Chemistry Division China Lake, California 93555	1
ONR Western Regional Office 1030 East Green Street Pasadena, California 91106	1	Naval Civil Engineering Laboratory Attn: Dr. R.W. Drisko Port Hueneme, California 93401	1
ONR Eastern/Central Regional Office Attn: Dr. L. H. Peebles Building 114, Section D 666 Summer Street Boston, Massachusetts 02210	1	Department of Physics & Chemistry Naval Postgraduate School Monterey, California 93940	1
Director, Naval Research Laboratory Attn: Code 6100 Washington, D.C. 20350	1	Dr. A.L. Slafkosky Scientific Advisor Commandant of the Marine Corps (Code RD-1) Washington, D.C. 20380	1
Commander, Naval Air Systems Command Attn: Code 310C (H. Rosenwasser) Department of the Navy Washington, D.C. 20360	1	Office of Naval Research Attn: Dr. Richard S. Miller 800 N. Quincy Street Arlington, Virginia 22217	1
Defense Technical Information Center Building 5, Cameron Station Alexandria, Virginia 22314	12	Naval Ship Research and Development Center Attn: Dr. G. Bosmajiar, Applied Chemistry Division Annapolis, Maryland 21401	1
Dr. Fred Saalfeld Chemistry Division, Code 6100 Naval Research Laboratory Washington, D.C. 20375	1	Naval Ocean Systems Center Attn: Dr. S. Yamamoto, Marine Sciences Division San Diego, California 91232	1
The Assistant Secretary of the Navy (RE&S) Department of the Navy Room 4E736, Pentagon Washington, D.C. 20350	1	Mr. John Boyle Material Branch Naval Ship Engineering Center Philadelphia, Pennsylvania 19112	1

DISTRIBUTION LIST, GEN

No.
Copies

Dr. Rudolph J. Marcus
Office of Naval Research
Scientific Liaison Group
American Embassy
APO San Francisco 96503 1

Office of Naval Research
Materials Division
Attn: Ed McCafferty
800 North Quincy Street
Arlington, Virginia 22217 1

Mr. James Kelley
DTNSRDC Code 2803
Annapolis, Maryland 21402 1

Dept. of the Navy
ONR Resident Representative
The Ohio State University Res. Center
1314 Kinnear Road
Columbus, OH 43212 1